MODELLING ANTARCTIC LAKE ICE RESPONSES TO METEOROLOGICAL VARIABLES

Timothy Drummond Reid

Thesis submitted to The University of Nottingham
for the degree of Doctor of Philosophy

July 2005

Contents

List of Figures

List of Tables

List of Symbols

AIC	Akaike Information Criterion
BIC	Bayesian Information Criterion
C	Cloud cover fraction
C_D	Drag coefficient
C_{DN}	Drag coefficient under neutral stratification
C_E	Bulk transfer coefficient for latent heat
C_H	Bulk transfer coefficient for sensible heat
C_{HW}	Heat exchange coefficient between ice and water
CV	Cross-validation index
$\bar{D}$, D_i	Model data
E_0	Scalar irradiance (W m^{-2})
E_d	Downwelling irradiance (W m^{-2})
F_b	Conductive heat at bottom of ice layer (W m^{-2})
F_i	Conductive heat at top of ice layer (W m^{-2})
F_w	Sensible heat flux from water (W m^{-2})
H	Hessian curvature matrix of parameter estimates
HA	Hour angle
H_i	Ice thickness (m)
$ICOMP$	Information-theoretic measure of complexity
J	Julian day
L_f	Latent heat of freezing for water (= 0.33×10^6 J kg^{-1})
$\bar{M}$, M_i	Model outputs
M_a	Average molar mass of air (= 0.029 kg mol^{-1})
MDL	Minimum Description Length
ML	Maximum likelihood
MS_{mod}	Model mean sum of squares
MS_{res}	Residual mean sum of squares
N	Number of internal ice layers defined for calculations
PAR	Photosynthetically active radiation (W m^{-2})

Q_b	Upwelling terrestrial longwave radiation at surface (W m^{-2})
Q_d	Downwelling atmospheric longwave radiation at surface (W m^{-2})
Q_h	Sensible heat flux at surface (W m^{-2})
Q_l	Latent heat flux at surface (W m^{-2})
Q_s	Solar shortwave radiation at surface (W m^{-2})
R_c	Critical Bulk Richardson number
R_e	Roughness Reynolds number
R_g	Universal gas constant (= 8.51 J mol^{-1} K^{-1})
RH	Relative humidity (%)
R_l	Enthalpy of vaporization of water (J kg^{-1})
$RMSD$	Root Mean Squared Deviation
R_z	Bulk Richardson number
S	Solar constant (= 1367 W m^{-2})
T_a	Air temperature (K)
T_f	Freezing point of water (= 273.15 K)
T_i	Ice temperature (K)
T_s	Ice surface temperature (K)
T_w	Water temperature (K)
UVB	Ultraviolet-B radiation (W m^{-2})
V	Wind speed (m s^{-1})
V_a	Volume of an air parcel (m^3)
WSS_{mod}	Weighted model sum of squares
WSS_{res}	Weighted residual sum of squares
WSS_{tot}	Weighted total sum of squares
Z	Solar zenith angle
c	Speed of light (= 3×10^8 m s^{-1})
$\bar{c}$, c_i	Model constants
c_a	Specific heat capacity of air (= 1004 J kg^{-1} K^{-1})
c_i	Specific heat capacity of ice (= 2093 J kg^{-1} K^{-1})
c_w	Specific heat capacity of water (= 4190 J kg^{-1} K^{-1})
df_{mod}	Model degrees of freedom
df_{res}	Residual degrees of freedom
df_{tot}	Total degrees of freedom
dt	Infinitesimal timestep (s)
e_a	Actual vapour pressure (Pa)
e_s	Saturation vapour pressure (Pa)
g	Acceleration due to gravity at the earth's surface (= 9.8 m s^{-2})
h	Thickness of internal ice layers defined for calculations (m)
h_p	Planck constant (= 6.63×10^{-34} J s)

h_t	Solar time
k	Von Karman constant (= 0.41)
k_i	Thermal conductivity of ice (= 2.03 W m^{-1} K^{-1})
k_w	Thermal conductivity of water (W m^{-1} K^{-1})
n_a	Number of moles in an air parcel
n_c	Number of model constants
n_d	Number of model datapoints
n_p	Number of model parameters
n_x	Number of model input variables
n_y	Number of intermediate model variables
$\bar{p}$, p_i	Model parameters
p_a	Air pressure (Pa)
q_*	Fundamental humidity scale (kg kg^{-1})
q_a	Specific humidity of air (kg kg^{-1})
q_s	Specific humidity of surface (kg kg^{-1})
r	Correlation coefficient
t	Model time (s)
t_*	Fundamental temperature scale (K)
u_*	Friction velocity (m s^{-1})
$\bar{x}$, x_i	Model input variables
$\bar{y}$, y_i	Intermediate model variables
z	Depth in ice layer (m)
z_0	Aerodynamic roughness length (m)
z_a	Height of measurements (m)
z_q	Roughness length for humidity (m)
z_T	Roughness length for temperature (m)
α	Ice albedo
γ	Kinematic viscosity of air (m^2 s^{-1})
δ	Solar declination angle
Δt	Finite timestep (s)
ϵ_i	Ice surface emissivity (= 0.96)
ϵ_*	Effective emissivity of the atmosphere
ζ	Monin-Obukhov stability parameter
κ_i	Ice extinction coefficient (m^{-1})
κ_w	Water extinction coefficient (m^{-1})
λ	Wavelength of radiation (m)
μ	Mean
ν	Residual degrees of freedom
ξ	Geometric surface roughness (m)

ρ_a	Air density (kg m^{-3})
ρ_i	Ice density (= 915 kg m^{-3})
ρ_w	Density of water (= 1000 kg m^{-3})
σ	Standard deviation
σ_s	Stefan-Boltzmann constant (= 5.67×10^{-8} W m^{-2} K^{-4})
ϕ	Latitude
χ^2	Weighted residual sum of squares
Ψ_E	Integrated universal function for moisture
Ψ_H	Integrated universal function for heat
Ψ_M	Integrated universal function for momentum
Ω	Covariance matrix of parameter estimates

Acknowledgements

This project was funded by the Engineering and Physical Sciences Research Council (EPSRC) as part of the UK E-science initiative. I am indebted to my supervisor Neil Crout for his support and guidance throughout.

The device which provided most of the data for this thesis was designed and deployed by Ben Palethorpe and Malcom Foster. Meteorological data was supplied by the Australian Bureau of Meteorology and the British Antarctic Survey READER project. Biological data was provided by Johanna Laybourn-Parry and Peter Bayliss. E-mail correspondence with Bin Cheng was particularly helpful for ice physics work.

My fieldwork was made possible by the Australian Antarctic Division. I was greatly helped by Trevor Bailey, Chad Marshall and Nanette Madan among others. Thanks to station leader Bob Jones and everyone else who was at Davis station in summer 2003-04 for making it a hugely enjoyable time. The Dirty Skuas will ride again!

I've enjoyed many stimulating coffee or pub breaks with my fellow PhD students and staff in Nottingham over the last three years, to name a few: Christin Sawström, Lee Stapleton, Catherine Morris, Ed Adams, Glen Cox, Davide Tarsitano, Jess Lenham, Darren Hepworth, Matt Beardsley and John Corrie. Thanks also to Dave Wills, Dave Kiwuwa, Sung-Il Lee and John Stephens for providing much-needed non-science chat at lunchtimes.

Thanks to my family for their support, and last but most to Lara for always managing take my mind off it.

Abstract

Inland Antarctic lakes are among the harshest environments in the world for life to inhabit. Ice cover causes low levels of light and temperature, and prevents mixing by wind, resulting in low nutrient levels and truncated food chains. Such ecosystems are widely regarded as sensitive indicators of climate change, and it is therefore useful to build up a strong physical and biological understanding of them. In 2003 an automatic probe (Palethorpe et al. 2004) was deployed on Crooked Lake (68^o25' to 68^o40'S, 77^o55' to 78^o35'E), an ultra-oligotrophic freshwater lake in Eastern Antarctica which has been the subject of limnological studies since 1990. The probe measured several physical parameters in, above, and below the ice layer at temporal resolutions of up to one measurement every five minutes.

A physics-based model was developed to simulate the growth and melt of the lake ice over time, considering all heat and radiation fluxes. Meteorological data were used as inputs to the model, with ice thickness the main output. The model fitted Crooked Lake ice thickness well, despite having narrow mechanistic constraints on parameter values. A number of simpler models were also developed which provided comparable goodness of fit, and illustrated that air temperature is the dominant variable in such systems. The issue of optimum complexity was addressed using model selection criteria, and some criteria selected a simple model over the physics-based model. However when both were subjected to long-term model runs with superimposed global warming scenarios, the simple model was shown to be unstable.

In addition, a 1992-93 biological dataset was analysed. Populations were shown to exhibit a significant annual cycle, but no significant smaller-scale population oscillations, suggesting that higher sample rates were required to identify such phenomena. A prototype procedure was developed using simulated data to inform field sampling strategies, in the aim of identifying the population dynamics that are predicted by many plankton models.

And now there came both mist and snow,
And it grew wondrous cold:
And ice, mast-high, came floating by,
As green as emerald.

- from "The Rime of the Ancient Mariner"
by Samuel Taylor Coleridge

Chapter 1

Introduction

1.1 Antarctica and climate change

Antarctica has been a site of great scientific interest over the last century. The continent is not only a place of unrivalled natural beauty but is also uniquely remote and largely unaffected by direct human impact. Antarctica is the highest, coldest, windiest and driest (yearly snowfall is only one to three inches) of all continents, yet paradoxically the immense continental ice sheet holds over 70% of the world's freshwater (ASOC 1998). The continent and the changing fields of sea ice around it provide the majority of the Earth's cryosphere, defined as the part of the Earth's surface that remains perenially frozen or near/below freezing point, or all forms of frozen water on land or sea (National Research Council 1999). The cryosphere enhances the thermal gradient between the equator and the poles by increasing the surface albedo, thus further reducing polar net surface radiation and temperatures. It also has a predominant role in global sea level, for example the West Antarctic ice sheet is considered highly vulnerable to temperature increases, and could raise sea level by 18 m if it melted. Snow and ice boundaries appear to be preferred areas for cloud formation, and the extent of sea ice each year has been linked to global amounts of cyclogenesis (formation of atmospheric depressions) and the El Nino southern oscillation (Drake 2000). Polar research in recent years has therefore been commonly focussed on increasing our understanding of how such areas may be affected by, and thus be indicators of, global climate change.

The response times of the Antarctic ice sheet as a whole to climate change may be several thousands of years (Drake 2000), and changes are hard to measure, so

the most striking signs of change are around the edges of the continent. Sea ice extent has only been accurately measured (via satellite images) since the 1970s, and shows no significant decline to 2000 (IPCC 2001), although studies of whaling records suggest an abrupt mid-twentieth-century decline in sea-ice extent (de la Mare 1997). Glaciers give greater evidence of change, with 87 % of 244 marine glacier fronts on the Antarctic peninsula seen to be retreating over the past 61 years (Cook et al. 2005).

Antarctic waters support a diverse biota (Shirihai 2002), and the broader effects of climate change can be inferred from observations of, for example, penguin migration in relation to sea ice distribution (Trathan et al. 1996). In addition, human impact on the continent has introduced alien species of both plants and animals, which flourish in higher temperatures (Frenot et al. 2005). In recent years the importance of inland lakes has been recognised. These may be covered with ice the whole year round, yet support plankton in truncated food webs (Roberts et al. 2000, Laybourn-Parry and Bayliss 1996).

Historic lake ice data are limited, and not particularly useful for assessing climate effects due to differing protocols for identifying 'ice on' and 'ice off' dates. However, 39 records of northern hemisphere lake and river ice showed an average spring ice break-up 9 days earlier, and autumn freezing 10 days later, than at the start of records (Magnuson et al. 2000). Larger lakes have the best records, but are often near human settlements which act as 'heat islands' and skew results, so The Intergovernmental Panel on Climate Change suggests that "care is needed to select suitable lakes" as indices of climate variability and change (IPCC 2001). Antarctic lakes are isolated from direct human (and in many cases even animal) impact, and are therefore ideal candidates to be sensitive indicators of global change (Vincent et al. 1998, Wharton Jr. et al. 1992).

1.2 The lakes of the Vestfold Hills

The Vestfold Hills (Figure 1.1) lie in Princess Elizabeth Land, Eastern Antarctica and cover around 400 km^2 at 68^{o}25' to 68^{o}40'S, 77^{o}55' to 78^{o}35'E. They form one of the few low-lying, ice-free areas on the coast of Antarctica where the ice plateau has receded and isostatic uplift of the ocean floor has created an arid, desert landscape with lakes formed by the trapping of seawater (Henshaw 2001). Some of the lakes remain saline, while others have been continually flushed with meltwater from the plateau and the nearby Sorsdal Glacier to become some of

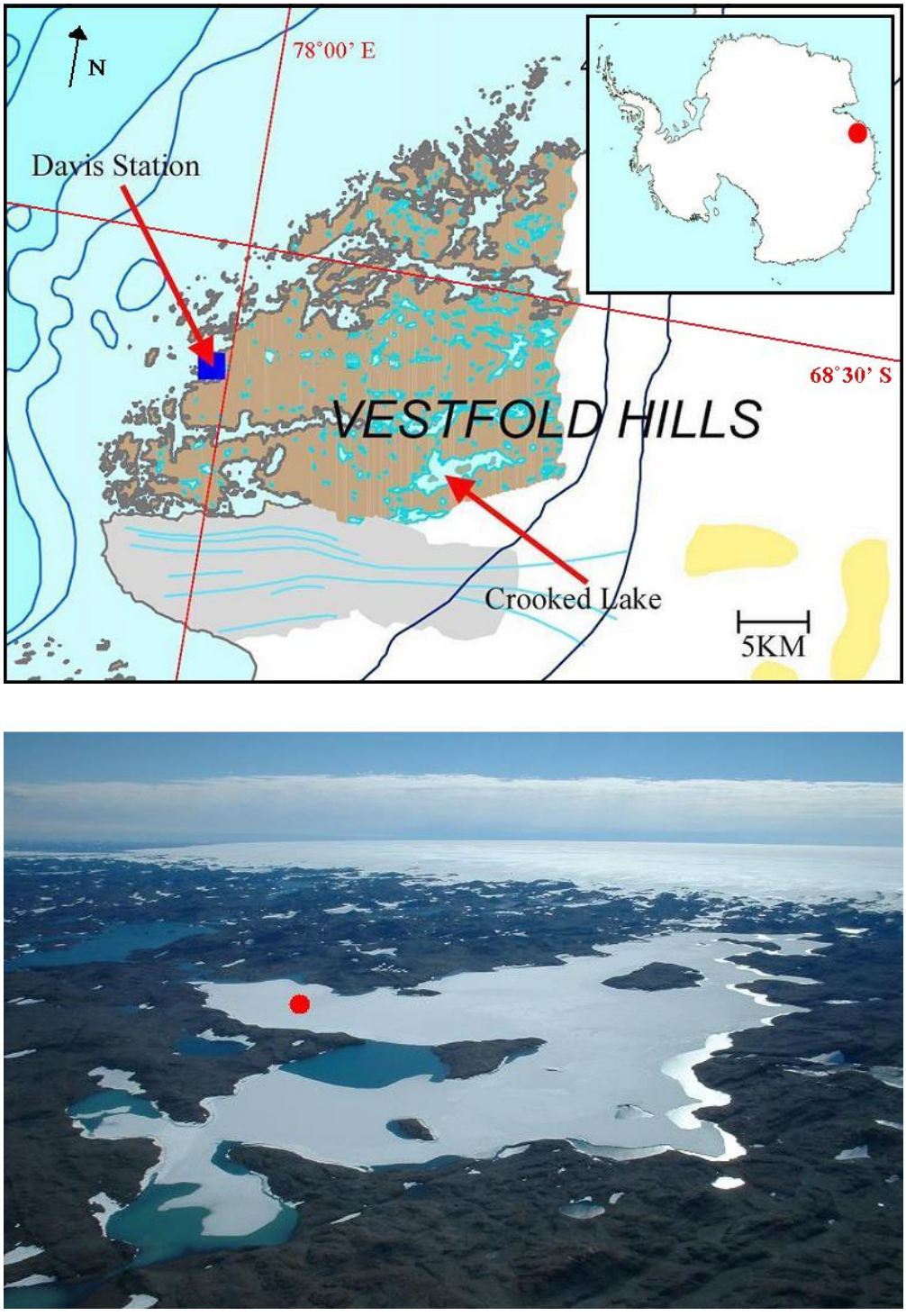

Figure 1.1: Map of the Vestfold Hills, showing Crooked Lake and Davis station and, inset, the position on the Antarctic continent (top). Aerial photograph of Crooked Lake in summer, with red circle indicating the bay in which measurements were taken (bottom).

the freshest lakes in the world.

The study site for this project is Crooked Lake, which lies in the southeast corner of the Vestfold Hills, and is one of the largest and deepest freshwater lakes in Antarctica (Laybourn-Parry et al. 1992). It contains a sparse community of plankton in some of the most oligotrophic conditions in the world (Bayliss et al. 1997). The lake receives negligible inputs of carbon and inorganic nutrients from the catchment area, and there are no fish, only a few rotifers and one cladoceran, *Daphniopsis studerii* (Laybourn-Parry and Marchant 1992). Therefore the trophic dynamics are driven by the 'bottom-up' forces of inorganic nutrient dynamics and primary production, and dominated by the microbial loop (Laybourn-Parry and Parry 2000). This provides a unique environment to study the interactions of micro-organisms such as nanoflagellates, bacteria and viruses, and the lake has been part of several microbiological studies since 1990 (Laybourn-Parry et al. 1991, Laybourn-Parry et al. 1992, Laybourn-Parry and Marchant 1992, Laybourn-Parry et al. 1995, Bayliss et al. 1997, Laybourn-Parry et al. 2001, Henshaw and Laybourn-Parry 2002, Laybourn-Parry et al. 2004).

The availability of Photosynthetically Active Radiation (PAR) for fixation of carbon by phytoplankton is a key factor in the functioning of such an ecosystem. At such high latitudes the low solar elevations, high reflectance of the ice surface, and an apparent spectral shift towards the blue end of the spectrum (Howard-Williams et al. 1998, Campbell and Aarup 1989), can result in very little PAR reaching the water column. In addition, photosynthesis rates are considerably reduced by high levels of ultraviolet (UV-B) radiation (Wangberg et al. 1998, Karentz and Bosch 2001) or low temperatures (Rae and Vincent 1998). Both of these are common conditions in the Antarctic. Therefore, temporal variation in the thickness and optical properties of polar lake ice-covers can have profound effects on the process of photosynthesis in the water column and on carbon cycling (Fritsen and Priscu, 1999). It is worthwhile to accumulate data and formulate models of the physical characteristics of such an ecosystem to support understanding of biological processes.

Previous studies of Crooked Lake consisted of manual sampling, restricted to days when travel to the lake was possible in the harsh environmental conditions of the Antarctic, and were often part of studies comparing several lakes. There are also limitations on how much equipment and sampled water can be carried in a helicopter or on a quad bike. Therefore both physical and biological data are limited to around one or two datapoints per month. Higher temporal resolution of data is preferable for model formulation.

Figure 1.2: The automatic measuring device and sensors embedded in the ice on Crooked Lake, which provided the majority of data used in this thesis.

For this reason, an automatic sensing probe (Figure 1.2) was designed and deployed on Crooked Lake in 2003 as part of a multi-disciplinary research project (Palethorpe et al. 2004). The system recorded ice thickness as well as PAR, UV-B and temperature at a range of depths in the water column, and weather variables at the surface. A satellite telemetry system allowed data of temporal resolution as high as one datapoint per minute to be accessed at Davis Station (16 km distant). The data has been utilised in this thesis for the development of models of the ice layer.

1.3 Ice modelling

There are many reasons why a good understanding of ice is crucial to any assessment of climate change. The melt and freeze of sea ice influences sea-surface salinity and deep water formation, initiating the global thermohaline circulation (IPCC 2001). Ice adds great complexity to surface energy and water balance calculations. The albedo of an ice surface is greater than water, and is dependent on its age, temperature and depth. This provides a potential positive feedback for climate change, whereby higher temperatures lead to less ice, therefore a lower

average surface albedo, and less reflection of heat back to space (a potential counterpoint to this is that more areas of open ocean will lead to more evaporation, forming low clouds that increase overall albedo) (IPCC 2001).

Research into the nature and dynamics of sea ice is far more extensive than into freshwater lake ice, but many of the basic concepts are transferrable. The main difference is that the freezing point of seawater is lower than for freshwater, but this is somewhat compensated for by ocean swell; waves increase the number of collisions amongst small ice crystals and larger 'pancake ice' which form extensive ice floes (Wadhams 1991).

New ice forms from the bottom of an ice layer, so ice thickness is limited by the temperature at the bottom. Thin ice grows faster than thick ice because it doesn't insulate the water from heat loss so well. Strong winds can also increase ice cover, by carrying heat away from the surface, or by creating ridges in the ice which increase drag, producing more areas of open water which lose their heat faster (Drake 2000).

In some ways lake ice provides a useful analogous system that is simpler to model than sea ice. Wadhams (1991) defines four major factors that affect sea ice: oceanic heat flux, wind-driven/thermohaline circulation, waves and atmospheric temperature. Apart from the latter, each of these factors are considerably less significant in a lake, and may be negligible. Air temperature is influential on the other three factors. A well-formulated model of lake ice may therefore be expected to be more sensitive to air temperature than any other variable. This may provide a useful 'control' model for investigating the responses of sea ice to atmospheric variables, and if shown to fit sea ice data, would imply that other phenomena are either negligible or cancel each other out.

In modelling lake ice, it is important to consider the interactions with the surrounding environment, and the boundary surfaces become crucial. Under realistic environmental conditions, a lake can be considered a closed system, as it exchanges energy with its surroundings but no significant amount of mass. The ice layer, however, is an open system if we consider that it exchanges mass with the water. The atmosphere can be considered a heat sink for the ice layer, as can the water if the lake is significantly deep.

Over a large body of water, vertical processes tend to dominate, except in the vicinity of cracks and leads (Cheng 2002). For a lake such as Crooked Lake, which has 100% ice cover for the majority of the year, this is particularly true; horizontal processes may be negligible except during partial break-up of ice in

summer. The laws of thermodynamics allow realistic parameterisations of all the heat fluxes that may affect an ice layer, and the resulting growth or melt of the layer can be calculated by considering the boundary conditions at the air-ice and ice-water interfaces. Launiainen and Cheng (1998) present a thermodynamic model for ice-covered water, which according to their assessment of past literature is the most advanced one-dimensional model formulated to date. Their model is driven by radiative and conductive heat fluxes, and predicts ice temperature, ice thickness and air-ice interactions. They found the state of the atmospheric boundary layer (wind, humidity and temperature) to be the primary controlling factor in ice growth processes, while solar shortwave radiation becomes important in controlling melting in the spring. Their model has been validated with data from the Baltic Sea and shown to give good agreement with mild-weather measurements (Cheng et al. 2001). Several other models have been developed for ice modelling in various environments (Fang et al. 1996, Fang and Stefan 1996, Bitz and Lipscomb 1999, Peeters et al. 2002). The basic approach, considering heat-balance equations and atmospheric variables, is common throughout.

Many heat balance models use constants to represent certain physical properties of the environment. Such an approach is suitable for short-term simulations, but on longer timescales the physical characteristics of ice, such as aerodynamic roughness lengths, albedo and attenuation of radiation may be indeterminately affected by factors such as temperature, salinity, meltwater or snow on the ice surface, stresses and curvature, air bubbles and radiatively-induced internal melt structures known as Tyndall figures (Wettlaufer 1999, Henneman and Stefan 1999, McKay et al. 1985, McKay et al. 1994, Vincent et al. 1998). Climate models incorporating the whole continent also identify the importance of the roughness lengths for momentum and heat in the stability of the atmosphere and the resulting surface heat fluxes (Reijmer et al. 2004). The equations relating atmospheric variables to ice growth may be complicated by circumstances, for example Andreas and Makshtas (1985) found that wind from the ocean resulted in heat transfer to sea ice, while wind from the continent took heat away.

It is apparent from a visual inspection of lake ice cover over the course of a whole year that the physical appearance of an ice layer changes considerably as it grows and melts. On Crooked Lake, the midwinter ice cover is clear, blue, flat and smooth, whereas in summer it becomes considerably more opaque, and the surface becomes rough and broken, with ridges and troughs up to a few centimetres in height. Therefore it is worthwhile using long-term data to estimate how the values of such parameters change over a year, and how ice cover is affected.

1.4 Plankton population modelling

Models of plankton ecosystems are often developed from generic models for any type of population. The simplest population model consists of the Lotka-Volterra differential equations, giving rise to predator-prey oscillations which have been observed in real populations of several animal species (Elton and Nicholson 1942, Bety et al. 2001, Blomqvist et al. 2002, McLaughlin et al. 2002, Norrdahl and Korpimaki 2000, Hanski et al. 2001, Norrdahl and Korpimaki 2002, Jensen and Miller 2001). With specific relevance to this project, Laybourn-Parry et al. (1991) found a suggestion of a predator-prey oscillation between bacteria and flagellates in Crooked Lake over January-February 1990. A number of more detailed models (Steele and Henderson 1981, Edwards and Brindley 1999, Gamarra and Sole 2000, Edwards 2001, Edwards and Bees 2001, Huisman and Weissing 2001, Kendall 2001, Petrovskii and Malchow 2001, Letellier et al. 2002, Malchow et al. 2001) find that populations may settle to steady-state values, adopt a chaotic state, or, in an intermediate range of parameter values, reach stable cycles in which the populations can evolve and change (Turchin et al. 2000, Turchin and Hanski 2001). Oscillations may thus allow populations to exist at the 'self-organised critical (SOC) state' between the unchanging steady state and pure chaos (Bak 1997, Pascual et al. 2002) and may contribute to biodiversity (Huisman and Weissing 1999, Figure 1.3). It is believed that the atmosphere and some populations may exist at the SOC state (Sole et al. 1999), so it is worth investigating both physical and biological data and model outputs for evidence of this phenomenon.

Another mechanism by which populations may maintain a far greater degree of community persistence and stability (McCann et al. 1998) is 'intraguild predation' (Polis and Holt 1992, Holt and Polis 1997, Morin 1999, Hart 2002, Revilla 2002), whereby predators may exploit more than one resource, resulting in food chains with numerous weak interactions (as opposed to few strong interactions).

However, microbial data is limited, often from short, detailed studies involving lengthy lab analysis, and typical Antarctica logistics allow sampling at most once or twice a week. Quantifying the errors involved in sampling and counting plankton is not easy, even when one is not concerned with the differences between depths or sites on a lake and is interested only in lake populations as a whole. The volume of water that can be analysed in practice is small. Also it is only possible to sample at discrete depths (the sample is not continuous with depth), and usually at only one or two sites (in the horizontal), given the time it takes

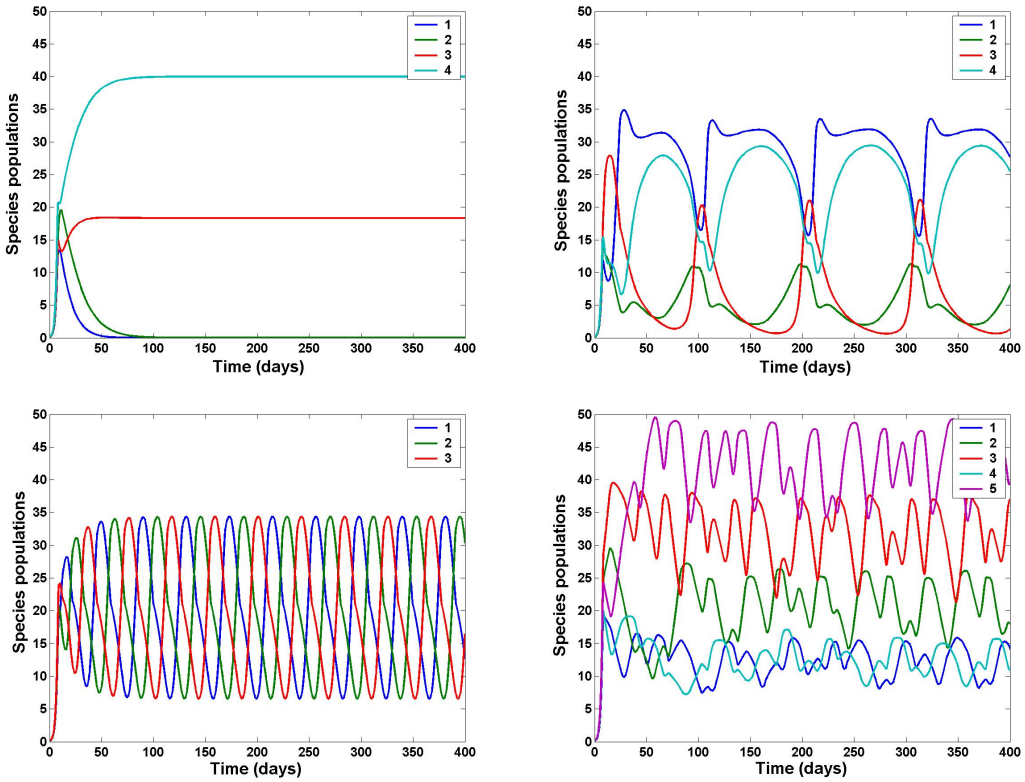

Figure 1.3: Some predictions from the plankton population model of Huisman and Weissing (1999), calculated by the author. Clockwise from top left: competitive exclusion of 4 species on 4 resources, oscillations of 4 species on 3 resources, chaotic dynamics of 5 species on 5 resources, stable oscillations of 3 species on 3 resources.

to drill holes in the ice. Therefore the numbers obtained for any site are just samples of the true populations, and one must use careful statistical analysis to make any inferences about the true population.

Biologists often assume that natural variability is so great they need not be concerned about measurement uncertainties (Quinn and Keough 2002), and with good lab practice these should be low. However it may not be sufficient to rely solely on the standard error across different replicates. Modelling studies of count uncertainties have been undertaken for many types of microbial counts (e.g. Bohmer and Hildebrandt 1998, Niemela 2003), and report common problems. Unavoidable random sampling errors can be compounded by clustering and the partly subjective nature of microscope counts, such that a non-homogeneous distribution should always be expected at microbial counts close to the detection limit. Models based on short-term 'noisy' data may exhibit changes in qualitative behaviour when expanded to longer timescales for the investigation of, for example, climate change (Fleming et al. 2002). This problem becomes worse as data gets sparser and noisier, so is an important issue in ecological modelling. It

may be useful to estimate how much data, and what accuracy of data, is required to test the population hypotheses in the above models for the case of Antarctic plankton, and assess if acquiring such data is feasible.

1.5 Modelling philosophy

The main method of thinking in the scientific community since its inception can broadly be put under the heading of 'reductionism'. The term stems from a number of related but contentious philosophical theories which roughly say that 'the nature of complex things can always be reduced to (explained by) simpler or more fundamental things'. The computer scientist John Holland, who invented the 'genetic algorithm', puts it like this:

"For the last 400 years science has advanced by reductionism... The idea is that you could understand the world, all of nature, by examining smaller and smaller pieces of it. When assembled, the small pieces would explain the whole" (Holland 1999)

The opposite of reductionism is 'holism', the concept that all of nature is made up of organic or unified wholes that are greater than the simple sum of their parts. This is becoming more common across science in cases where an explanation of a system's behaviour is not readily apparent on examining the individual interactions between its constituent parts. Holism is, not surprisingly, popular in many religions, as it may support the belief in higher powers.

However many real problems cannot be practically solved by either reductionism or holism. One has a limited amount of time for the job in hand, and it is therefore more common for scientists to employ what the eminent biologist Richard Dawkins calls 'hierarchical reductionism' (Dawkins 1986). For example, to explain the movement of a spider one need not examine the quantum physics effects occuring in the atoms of the spider's legs, but at the same time a scientist is unlikely to accept the explanation that 'God made it walk'.

In scientific modelling, a rough working definition of hierarchical reductionism may be 'the inclusion of as much detail as *reasonably* possible'. Development of a model has to stop at some point, and it is important to identify which aspects of a model will significantly affect the output to a greater extent than the intrinsic errors in measurements. Many equations are, by the very nature of research, selected on a partly subjective basis, since many scientists have taken different

approaches and calibrated their equations for different datasets. Trying them all may be a waste of time and effort when the difference between two approaches may be no more than the error that already exists.

In recent years, therefore, there has been considerable discussion of modelling via the 'principle of parsimony'. This is rooted in the famous 'Occam's razor', which states that "entities are not to be multiplied beyond necessity". In modelling this can be translated as a preference for the simplest model that adequately accounts for the data, and comes into practice when a sufficient model has something added to it which does not improve its predictive power. For example, when choosing from a number of models to describe some data, the most complex model will usually provide the best fit. Such a fit can be misleading because it results from extraneous properties of the model that have nothing to do with the underlying processes of interest (Pitt and Myung 2002). If one has several datasets arising from the same underlying process, the parameter estimates for more complex models may show large variation across the datasets, rendering their values theoretically meaningless. Also a large amount of data may be required to calibrate and validate large and complex models in the first place (Young 1998).

Occam's razor cannot account for the fact that there may be several models which explain the data equally well, while having no relation to one another. This problem can only be combatted with subjectivity and 'common sense', but a number of techniques have been developed in recent years which mathematically formalise Occam's razor and make the task simpler. These include Monte-Carlo methods to identify key areas of uncertainty in a model (e.g. Hornberger and Spear 1981), simple criteria that balance a model's goodness of fit against the number and accuracy of parameters (e.g. Kadane and Lazar 2004, Myung 2000), and Bayesian model averaging methods (e.g. Wasserman 2000, Raftery and Zheng 2003).

To date most model selection techniques have been developed in the world of statistical modelling and cognitive psychology, with few examples of application to real data. It is worthwhile testing these techniques for some real environmental situations. To what extent can they complement a researcher's informed subjectivity?

1.6 Objectives

The principal objectives of this thesis are:

- To develop both complex mechanistic and simple empirical models of freshwater lake ice using suitable parameterisations from the literature and basic regression techniques.
- To parameterise the models using data collected on Crooked Lake, Antarctica.
- To assess the relative importance of meteorological variables in lake ice dynamics.
- To spectrally analyse plankton data from Crooked Lake, and assess how much data is required to identify theoretical phenomena such as population oscillations.
- To employ a number of new and emerging model selection techniques in choosing the best models for Crooked Lake ice dynamics, and thus test their suitability for a real environmental system.
- To predict responses of Crooked Lake to potential climate change.

1.7 Thesis overview

- **Chapter 2** outlines the generic modelling and analysis techniques that were used and developed.
- **Chapter 3** describes the development of a physics-based model of freshwater lake ice, using selected approaches from the literature.
- **Chapter 4** describes the parameterisation, sensitivity analysis and outputs of the physics-based model developed in Chapter 3, against automatically-collected data from Crooked Lake.
- **Chapter 5** discusses the merits of some simple empirical models of lake ice and the use of model selection criteria to inform a choice of model for Crooked Lake.

- **Chapter 6** employs both the physics-based model and a simple empirical model in long-term model runs subject to air temperature perturbations, and discusses which is more reliable for predicting future responses to climate change.
- **Chapter 7** describes a modelling assessment of population oscillations in plankton data from Crooked Lake, and introduces a prototype method for predicting how much data would be necessary to significantly observe such behaviour.
- **Chapter 8** provides a summary and discussion of the key results, outlining applications, limitations and potential future work.

Chapter 2

Methods

2.1 Overview

This chapter outlines the generic modelling and analysis techniques that were used and developed in this thesis. It describes the software, notation and conventions employed and defines the quantities involved in model structure. Some basic statistics and a number of 'merit functions' for a model are defined, which form the first step in analysing a model's performance with respect to data.

The concept of model optimisation is introduced. An iterative procedure written by the author to implement the Levenberg-Marquardt method of optimisation for the given system is fully described. A new method for assessing the importance of individual model input variables is introduced. This is termed 'model trimming' and is intended to inform the development of parsimonious models from complex models, where some of the input variables or equations may have a negligible or adverse effect on model behaviour. A number of model selection criteria are described, which weigh a model's goodness of fit against it's complexity, to assess the generalisability and predictive power of the model.

Note: As this is a modelling-centred thesis, and much of the data used and discussed was not collected by the author, this chapter does not include any descriptions of fieldwork methods. Where data is introduced later, a brief description of methods is given and relevant publications are cited.

2.2 Software

The following software was used for modelling work in this thesis:

- **MatLab version 6.1** (©1984-2001 The MathWorks Inc.) - a high-performance computing language based largely on matrix notation, which proved particularly useful for handling large amounts of data in matrix form. It integrates computation, visualization, and programming, and thus allowed models to be run and analysed using interactive scripts.
- **ModelMaker 3** (©1993-1997 Cherwell Scientific Publishing Ltd.) - a Windows-based program developed for compartment flow type models. It is particularly useful for small-scale, one-dimensional real-time models, providing a number of numerical integration methods and optimisation procedures.

Data was mainly provided in spreadsheet form using Microsoft Excel (©1985-1999 Microsoft Corporation), then edited and converted to ASCII text form for input to MatLab and ModelMaker.

2.3 Model structure, notation and conventions

Real-time model calculations depend on several quantities from field, lab or modelling studies, which may be used as inputs to mathematical equations or kept for comparison with model outputs. Each quantity may be known to a different degree of accuracy, and it is important to identify their roles in model operation. The classifications and notation of these quantities as used in describing generic modelling techniques for this thesis are described below, and summarised in Figure 2.1 as a flowchart.

- **Input variables** - quantities which may change over time, from recorded field or lab datasets with associated errors. In cases of data over time, datapoints are linearly interpolated to give values of the input variable at times when data were not measured (see Figure 2.2). Notation: x_i where $i = 1, 2...n_x$.
- **Constants** - quantities which do not change with time (for the purposes of the model) and are known to a high degree of accuracy from measurements

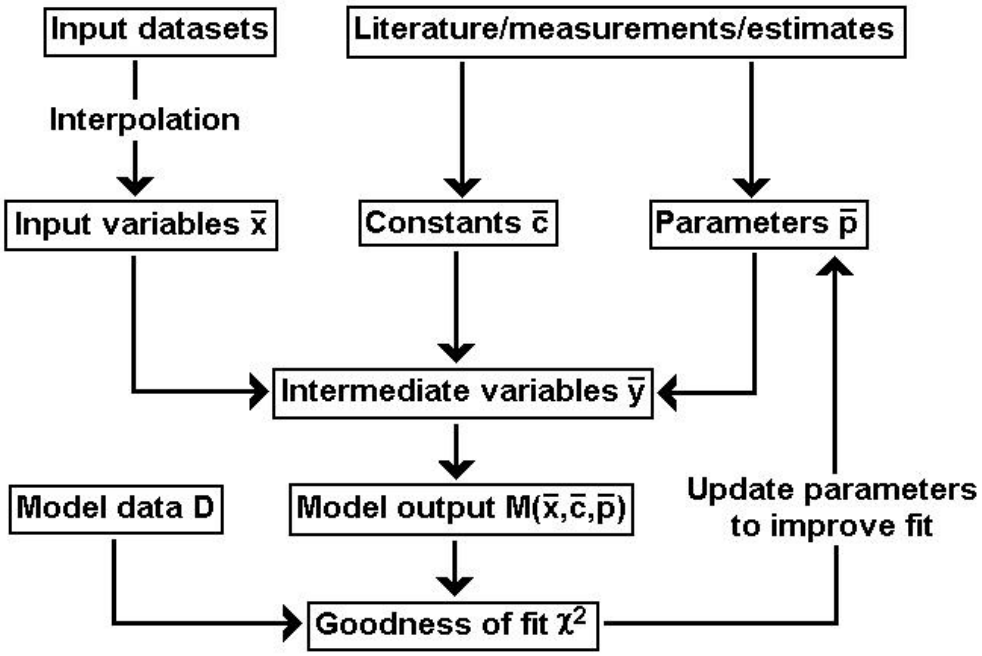

Figure 2.1: Flowchart illustrating the conventions and notation used for the quantities involved in model structure for this thesis.

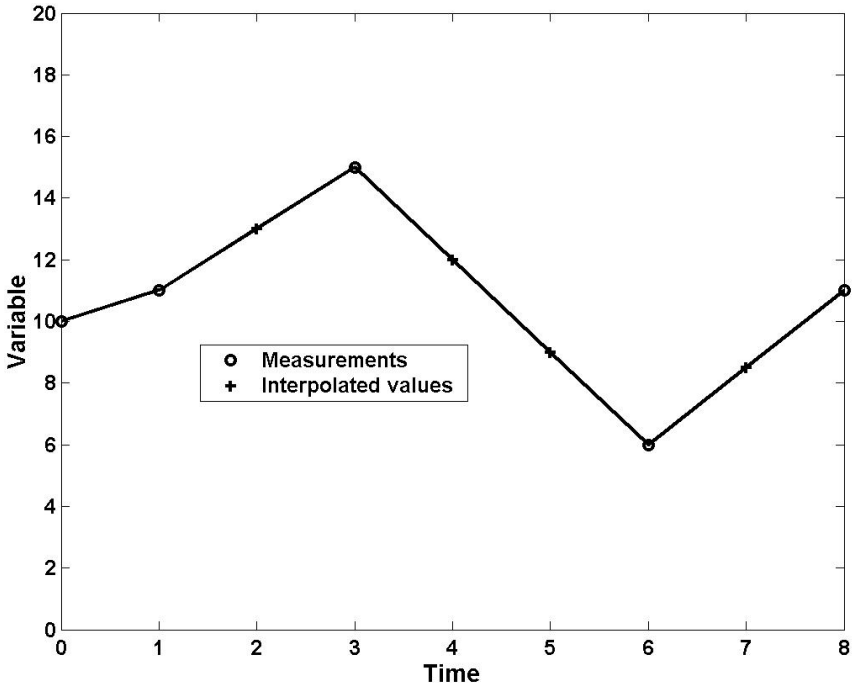

Figure 2.2: Linear interpolation of a dataset to provide an input variable. The circles are real measurements and crosses are interpolated values of the variable, allowing a timestep of 1.

or the literature. For example, the acceleration due to gravity at the earth's surface is very close to g =9.8 m s^{-2}. Notation: c_i where $i = 1, 2...n_c$.

- **Parameters** - quantities which do not change over time, but are not known well, and are therefore adjusted or 'optimised' to search for the best model fit to data. Gaining information on parameter values may often be the main aim of a modelling exercise. Notation: p_i where $i = 1, 2...n_p$, or a vector of parameters $\bar{p}$.

- **Intermediate variables** - quantities which are calculated from input variables, constants and parameters during model execution. They may be an intermediary step in the calculation of the main model output, or a real physical quantity of interest. Notation: y_i where $i = 1, 2...n_y$.

- **Model data** - a collection of n_d datapoints, representing a quantity measured during the same time period as the input variables, which we are interested in modelling. Notation: D_i where $i = 1, 2...n_d$, or a vector $\bar{D}$.

- **Model output** - the calculated quantity which is directly comparable to the model data, i.e. it is the model-predicted value of D_i. If we consider only the predicted values at times when a datapoint D_i was recorded, this is a vector of size n_d. Notation: M_i where $i = 1, 2...n_d$, or a vector $\bar{M}(\bar{p})$.

It should be noted that there may be more than one 'model output' quantity representing more than one collection of 'model data' measurements. For each finished model the only quantities that are considered 'adjustable' are the parameters $\bar{p}$, and so in each case the model output can be expressed as a function of $\bar{p}$. If any other aspects of a model are changed, it is considered a new model.

2.4 Integration methods

At the core of most real-time models is a differential equation of the form $\frac{dM}{dt} =$ (maths). In most cases such an equation cannot be solved analytically and numerical methods must be employed. This involves replacing the infinitesimal time dt with a finite timestep Δt. Several methods of numerical integration are commonly used and are readily available for easy computation in many software packages. The most simple is the Euler method, which takes a finite user-defined timestep and simply calculates the model output based on the values at the previous timestep. However this method may lead to the propagation of errors if the

system undergoes large changes in the course of one timestep. The Runge-Kutta method is among the most popular of more complex methods and can use an adaptive step size to control accuracy, but takes a considerably longer time to evaluate a model.

In models with considerable amounts of input data, the timestep of the data must also be taken into consideration when choosing a method of integration. It is simple to linearly interpolate data for times when data is unavailable, but if the model timestep is considerably shorter than the time between datapoints, one may make incorrect assumptions about the behaviour of the system. Such a technique may for example lead to the conclusion that a system is more constant than it really is, since we have calculated the model output by assuming the input variables either stay constant or change steadily between real datapoints, while in reality they may exhibit anomalistic behaviour. Therefore if one chooses a timestep shorter than the available input data provides, one must ensure the output is only considered valid at the same times as data was recorded.

In this thesis both the Euler and Runge-Kutta methods of integration were used, but care was taken only to use Euler when it had been shown to give the same results as Runge-Kutta. This was common when the model timestep was short enough to avoid large changes in the model output in one timestep.

2.5 Basic model analysis tools

2.5.1 Merit functions

A number of 'merit functions' exist for assessing the the performance of a model with respect to observed data - specifically, the 'goodness of fit' of the model. In this thesis all model analysis functions are used on the assumption that every datapoint D_i lies in a normal probability distribution with mean μ_i and variance σ_i^2:

$$P(D_i) = \frac{1}{\sigma_i\sqrt{2\pi}} \exp\left(\frac{-(D_i - \mu_i)^2}{2\sigma_i^2}\right) \tag{2.1}$$

Note that Equation 2.1 applies to a single datapoint. The dataset as a whole has a certain amount of intrinsic variation about its mean, which can be measured using the 'weighted total sum of squares', WSS_{tot}, defined as the sum over all

datapoints of the difference between the datapoint and the mean:

$$WSS_{tot} = \sum_{i=1}^{n_d} \left(\frac{D_i - \mu(D_i)}{\sigma_i} \right)^2 \tag{2.2}$$

where $\mu(D_i)$ is the mean of all the data over the time period under consideration. The difference is 'weighted' for each individual datapoint by dividing by the error on the datapoint, σ_i; hence for datapoints with lower errors, any variation from the mean is deemed more important. In a similar way, the amount of variation from the mean that is explained by a model may be assessed using the 'model sum of squares' merit function:

$$WSS_{mod} = \sum_{i=1}^{n_d} \left(\frac{M_i - \mu(D_i)}{\sigma_i} \right)^2 \tag{2.3}$$

The higher the value of WSS_{mod}, the better the fit of the model. However in practice the most useful merit function is the 'weighted residual sum of squares', WSS_{res}, which represents the variation that is *not* explained by the model. WSS_{res} is more commonly denoted by χ^2, and for the purposes of assessing the performance of a model output vector $\bar{M}$ which arises from various adjustable parameters, χ^2 is best written as a function of the parameters ($\bar{p}$):

$$\chi^2(\bar{p}) = \sum_{i=1}^{n_d} \left(\frac{D_i - M_i}{\sigma_i} \right)^2 \tag{2.4}$$

The three sums of squares quantities are related according to:

$$WSS_{tot} = WSS_{mod} + \chi^2 \tag{2.5}$$

The lower the value of χ^2, the better the fit of the model, and therefore it is often the quantity which is minimised in model optimisation. The value of χ^2 is somewhat meaningless in isolation, so in many studies, the dimensionless quantity r^2 is used. r^2 represents the fraction of the intrinsic data variation that is captured by the model:

$$r^2(\bar{p}) = \frac{WSS_{mod}}{WSS_{tot}} \tag{2.6}$$

A value of $r^2 = 1$ indicates a perfect fit, with the model output predicting all the datapoints exactly.

It is also useful to consider the true probabilistic nature of the model. This can be indicated by the maximum likelihood function, which is a measure of the probability of the model data when we assume the model predictions are true. For a normal distribution, this is:

$$\begin{aligned} ML = P(D|M,\sigma) &= \prod_{i=1}^{i=n_d} \frac{1}{\sigma_i\sqrt{2\pi}} \exp\left(\frac{-(M_i - D_i)^2}{2\sigma_i^2}\right) \\ &\approx \frac{2\pi^{-\frac{n_d}{2}}}{\sigma_d^n} \exp\left(-\sum_{i=1}^{i=n_d} \frac{(M_i - D_i)^2}{2\sigma_i^2}\right) \end{aligned} \tag{2.7}$$

In practice, with a large amount of data Equation 2.7 may give a vanishingly small number, and it more useful to consider the 'log-likelihood'. Noting that the last term is equivalent to $\exp\left(\frac{-\chi^2}{2}\right)$, this is expressed as:

$$\ln(ML) = -\frac{n_d}{2}\ln 2\pi - n_d \ln\sigma - \frac{\chi^2}{2} \tag{2.8}$$

It should be noted that Equations 2.7 and 2.8 are only valid if we make the assumption that every individual datapoint has the same standard deviation ($\sigma_i \approx \sigma$ for all i). However for the purposes of comparing two models, the relative values of $\ln(ML)$ for the two models are more relevant than the absolute values. It was therefore deemed sufficient to set $\sigma = 1$ in the second term of Equation 2.8 for all calculations.

2.5.2 Model significance

When a reasonable model fit to data has been obtained, it is important to assess whether the model fit is significant, or has simply arisen by chance. This requires statistical hypothesis testing, which is common across all scientific disciplines. In modelling, the most important concept is the 'degrees of freedom' of a model, which refers to the balance of complexity in the model (the number of parameters) with the amount of available information on the real world (the number of datapoints). There is little justification for using a highly complex model to

explain only a few observations.

The degrees of freedom of a dataset can be loosely defined as the number of opportunities the data has to change 'relative to itself' - for n_d datapoints this is $df_{tot} = n_d - 1$. In a model, the degrees of freedom are the number of opportunities the model has to change 'relative to itself' - for n_p adjustable parameters the model degrees of freedom are therefore $df_{mod} = n_p - 1$. In model fitting, however, the residual degrees of freedom are most important in terms of model significance, and are equal to $df_{res} = df_{tot} - df_{mod} = n_d - n_p$. This is the term usually referred to when discussing the degrees of freedom of a modelling exercise, and is denoted by ν. In general, a model must have positive degrees of freedom to have a chance of being statistically significant. Therefore in this thesis the goodness of fit of each model is presented in terms of the three quantities χ^2, r^2 and ν, to represent the unaccounted variability in the data, the dimensionless goodness of fit, and the number of 'free elements' used in calculating them.

To calculate the probability of the model fit occuring at random, the sum of squares of the model and the residual must be scaled using the degrees of freedom to give the 'mean sum of squares' for each:

$$MS_{mod} = \frac{WSS_{mod}}{df_{mod}} \tag{2.9}$$

$$MS_{res} = \frac{\chi^2}{\nu} \tag{2.10}$$

The model's 'F-ratio' is a statistic which follows different distributions for different values of ν (see e.g. Mason et al. 2003), and the higher it is, the more significant the model fit. It can be calculated as the ratio of the mean sums of squares for the model to the residual:

$$F = \frac{MS_{mod}}{MS_{res}} = \frac{WSS_{mod}/(n_p - 1)}{\chi^2/\nu} \tag{2.11}$$

The ModelMaker software provides the F-ratio for any model, and the associated probability P that the model output arose by chance (e.g. if P is 0.05 or less then the model is significant to the 95% confidence level). All the model statistics are commonly displayed in a standard ANOVA table (see e.g. Mooney and Swift 1999).

The significance of any improvement in model fit may be assessed in a similar way. In general model fit is improved by the addition of more adjustable parameters, which reduces the degrees of freedom in the model. The F-ratio for the model *improvement*, and the associated P-value, give information on whether the change is worthwhile, or the improvement in model fit has arisen by chance. Table 2.1 gives an example for an imaginary dataset with 100 datapoints and $WSS_{tot} = 100$, and a model of the data in which the number of parameters has been increased from 3 to 6. The extra parameters account for more of the data variation (WSS_{mod} is increased by 1), but in this case the improvement is not enough to be deemed significant to the 95% confidence level, and the improvement may have occurred by chance.

	n_p	df	WSS	MS	F	P
Original model	3	2	80	40	200	< 0.001
Improvement	+3	+3	1	0.33	1.65	0.183
Residual		94	19	0.20		
Total		99	100			

Table 2.1: ANOVA table for an imaginary model, where increasing the number of parameters from 3 to 6 has improved the model fit from $\chi^2 = 20$ to $\chi^2 = 19$. The P-value of 0.183 suggests there is an 18% chance that the improvement in fit happened by chance, so for most purposes the increased complexity may be deemed to be not worthwhile.

2.6 Optimising model performance

2.6.1 The purpose of optimisation

Model optimisation is the process of searching for a set of model parameters that provide a good fit to data for a given model. This amounts to minimising the value of $\chi^2(\bar{p})$, for example by following it's gradient with respect to the parameters $\bar{p}$. However, a number of difficulties may arise in this process, as has been found in the work towards this thesis.

Figure 2.3 shows the simple case of a one-parameter model. If the search for an optimum value begins at the point marked 1, and is confined to the area between $p = A$ and $p = B$, we conclude that the best value for our parameter is at point 2. However, the shallow slope around point 2 shows that the fit is not considerably better than anywhere else near to point 2, and there is therefore a large error on our estimate of p. On searching the whole area between $p = A$ and $p = C$, we

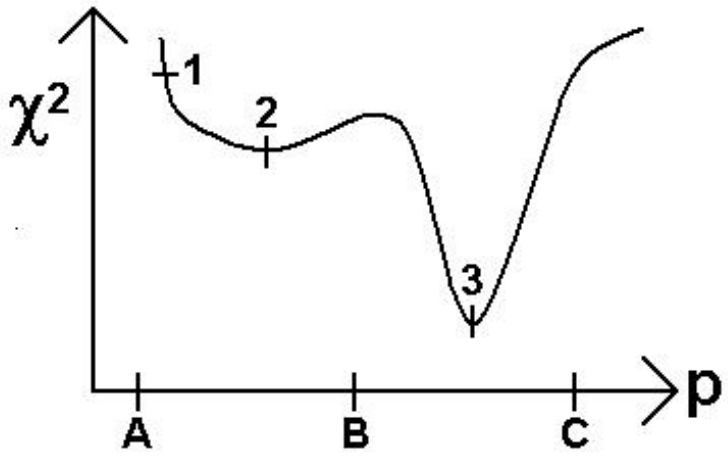

Figure 2.3: Residual sum of squares χ^2 as a function of an arbitrary parameter p. Point 2 is a 'local minimum', and the shallow well indicates a high error in using this value. The steep well at point 3 gives a better model fit, and a more accurate parameter value.

would find that there is a better-fitting value for our parameter at point 3, which lies in a steep well and is therefore more accurate. For an empirical model, where goodness of fit and 'usefulness' of the model are the primary concerns, such an approach may be very successful, and the only possible pitfall is in accepting a 'local minima' like point 2 without exploring further. However if the parameter represents a real physical quantity in a model built up from a combination of established physical equations, some subjectivity is necessary. The value of p at point 3 may just be a 'fluke' of the datasets and equations involved, which is far away from realistic values of the parameter, for example a pH of 106. In such a case one may have to accept point 2 as the best value of p to use, so concluding that the model is not highly sensitive to p, and we can't, in this instance, learn as much about the best value of p as we might have hoped. It could also be that the model structure is such that it would unwise to accept the physical interpretation of p.

On introducing more parameters, problems are magnified, but goodness of fit may be improved. A change in a second parameter may cause Figure 2.3 to look completely different - the minimum may no longer be at point 3. This gives another dimension of freedom to search for an even better minimum, but at the same time may introduce more local minima to deceive the searcher. With an arbitrary number of parameters n_p, there exists an 'n_p-dimensional parameter space' within which it is very easy to get lost.

Optimisation is therefore a non-trivial process, and it would be foolish to blindly rely on it to provide the best answer. One must have a reasonable initial estimate of all parameter values, with realistic constraints and good control over the procedure, to avoid landing at local minima or accepting deceptively good parameter values which may in fact be physically meaningless.

2.6.2 Levenberg-Marquardt optimisation

The Levenberg-Marquardt method is a standard method of nonlinear least-squares routines. ModelMaker has a built-in Marquardt algorithm and MatLab has a command for optimising a specific model in the form of a differential equation. However the usefulness of each procedure is limited by the application - the complex non-linear models with internal loops that are developed in this thesis are beyond the scope of ModelMaker, and it was found they could not be expressed in the required form for the MatLab algorithms without being simplified. Also different applications require different settings in the optimisation, and where these settings cannot be changed it is sometimes impossible to tell exactly what the command may be doing. For the purpose of this thesis a program was written in MatLab which allowed the manual adjustment of the procedure for the model in hand, ensuring robust optimisation. The development of this procedure was based mainly on the description of the Levenberg-Marquardt method given in Press et al. (2002), and is described below.

Close to the minimum of a successful model, the $\chi^2(\bar{p})$ merit function will be approximated by a quadratic form, and at the true minimum, the gradient $\frac{\partial \chi^2}{\partial p_k}$ will tend to zero for all $k = 1...n_p$. The method therefore should follow the second derivatives of χ^2 to points where it will be a constant, suggesting a quadratic form. This requires the Hessian 'curvature' matrix, which is the matrix of second derivatives of the model fit with respect to it's parameters. For n_p parameters, this is an $n_p \times n_p$ matrix defined as follows:

$$\alpha_{kl} = \frac{1}{2} \frac{\partial^2 \chi^2}{\partial p_k \partial p_l} \tag{2.12}$$

Press et al. (2002) argue that second derivatives of χ^2 can be approximated in practice, and introducing the random measurement error σ_i enables Equation 2.12 to be approximated using the first derivatives of the model output with respect to each parameter:

$$\alpha_{kl} = \sum_{i=1}^{n_d} \frac{1}{\sigma_i^2} \left(\frac{\partial M(x_i, \bar{p})}{\partial p_k} \frac{\partial M(x_i, \bar{p})}{\partial p_l} \right) \tag{2.13}$$

A vector of the first derivatives of χ^2 with respect to the parameters must also be defined:

$$\beta_k = -\frac{1}{2} \frac{\partial \chi^2}{\partial p_k} = \sum_{i=1}^{N} \left(\frac{D_i - M(x_i, \bar{p})}{\sigma_i^2} \right) \frac{\partial M(x_i, \bar{p})}{\partial p_k} \tag{2.14}$$

The desirable changes in parameters which may lead to a better goodness of fit, $\delta\bar{p}$, can be calculated from the set of linear equations:

$$\sum_{l=1}^{n_p} \alpha_{kl} \delta p_l = \beta_k \tag{2.15}$$

In practice, the changes computed from Equation 2.15 are only useful when we are already close to the minimum. The Marquardt method introduces a 'fudge factor' λ to allow smooth switching between the 'inverse Hessian' method represented by Equation 2.13 and the 'steepest descent' method, where α_{kl} is effectively replaced by a constant. To do this, α_{kl} is replaced by:

$$\begin{aligned} \alpha'_{jj} &= \alpha_{jj}(1 + \lambda) \\ \alpha'_{jk} &= \alpha_{jk} \text{ when } j \neq k \end{aligned} \tag{2.16}$$

The procedure written for MatLab runs as follows:

1. The user provides initial estimates of each parameter, and upper and lower constraint values for each parameter. The user also provides values for two accuracy settings called $brake$ and $stopfraction$.

2. λ is given an initial value of 0.001.

3. The model is executed with the initial parameter values $\bar{p}$ and $\chi^2(\bar{p})$ is calculated.

4. The matrices α and β are calculated, finding the necessary derivatives numerically.

5. The matrix α is changed to α' according to Equation 2.16, and the linear equations (Equation 2.15) are solved for $\delta\bar{p}$ using left matrix division.

6. The model is executed with parameter values $\bar{p} + brake * \delta\bar{p}$ and $\chi^2(\bar{p} + brake * \delta\bar{p})$ is calculated.

7. If $\chi^2(\bar{p} + brake * \delta\bar{p}) \geq \chi^2(\bar{p})$, λ is increased by a factor of 10, and the program goes back to step 5.

8. If $\chi^2(\bar{p} + brake * \delta\bar{p}) < \chi^2(\bar{p})$, λ is decreased by a factor of 10, the trial solution is updated ($\bar{p} \rightarrow \bar{p} + brake * \delta\bar{p}$) and the program goes back to step 4.

9. The program is stopped when the decrease in χ^2 is a negligible amount: $(\chi^2_{old} - \chi^2_{new})/\chi^2_{old} < stopfraction$.

The user-defined setting *brake* is a stability precaution, limiting the size of parameter change for a sensitive model. The smaller the value of *brake*, the longer the optimisation will take, but large moves which could force the parameter values past their constraints become less likely. A default value of $brake = 0.1$ was used in this thesis ($brake = 1$ gives the usual Marquardt procedure). The value of $stopfraction$ provides a choice of accuracy for the model, which the user may wish to vary depending on the accuracy of their data. A default value for most problems is $stopfraction = 0.001$. For data with a high degree of noise, a small change in χ^2 may be meaningless, representing a 'flat valley' of parameter values which are all equally accurate, and $stopfraction$ should then be set to something higher.

The procedure was found to provide the same parameter values as the Marquardt optimisation algorithms in ModelMaker and MatLab, for a number of simple models. It also proved capable of optimising more complex models with stable results, and so is the default optimisation procedure used throughout this thesis.

A further application of the above calculations is that the inverse of the matrix α can be used as an approximation of the covariance matrix of parameter estimates, $\Omega(\bar{p}) \approx \alpha^{-1}(\bar{p})$. The standard errors on parameter estimates can be calculated using the diagonal elements of $\Omega(\bar{p})$:

$$\Delta p_i = \sqrt{\frac{\Omega_{ii}\chi^2}{\nu}} \tag{2.17}$$

where ν is the number of degrees of freedom in the model. The errors estimated in this way are used later in this thesis in conjunction with a standard statistical t-test (see e.g. Mason et al. 2003) to assess the significance of parameter values.

2.7 Model trimming

A model hoping to reproduce the behaviour of a system via the existing theory surrounding all the constituent parts of the system in hand may require a large number of input variables to satisfy the model equations. However, for the purposes of producing a model which is useful, user-friendly and good at predicting the future, one may have to reduce the model to be more 'parsimonious'. It is both important and interesting to identify which aspects of the model (and thus which parts of the modelled system) are most important in affecting the model output, and which may be unnecessary components adding nothing but statistical noise to the model output. A technique termed 'model trimming' has been developed for this thesis to assess the relative importance of input variables.

Over a given time period, we may consider that every individual variable (interpolated from a dataset) at a certain time has a value composed of the mean value of the variable for the whole time period, x_μ, plus some variation for that time, $\sigma(x_i)$:

$$x_i = x_\mu + \sigma(x_i) \tag{2.18}$$

The importance of the term $\sigma(x_i)$ can be assessed by introducing a parameter β to the model, and changing the input variable to $x_i^{'}$.

$$x_i^{'} = \beta x_i + (1 - \beta)x_\mu \tag{2.19}$$

where β is a parameter with a value between 0 and 1. The model is then executed and goodness of fit calculated for various values of β. If the best fit is found as β tends towards 1, the variability in x_i is clearly important in producing the model output. However if the better fit is found as β tends to zero, x_i may be adding noise to the model output. An alternative interpretation may be that the equations involving x_i are wrongly formulated or unnecessary for the description of the system as a whole, having an adverse effect on the goodness of fit. Varying

β may have little or no effect on the goodness of fit. In this case, the model may be 'indifferent' to x_i because the size of the variation in x_i is insignificant compared to other variables, or has been scaled down in the model equations.

This technique is intended for investigating a model based on background scientific theory and equations, with parameters that have been optimised to values within realistic ranges, producing a reasonably good fit to the model data. Variables should be tested one by one, and reset to their original state ($\beta = 1$) before testing the next variable. The purpose is to inform the development of simpler, less computationally intensive models of a system which may in practice be more useful for predicting the future of a system. However the technique should not be taken as justification for definitively discarding certain variables or equations, as it considers only one variable at a time. In complex models with many variables and parameters, the effects of different variables on the model output may be closely interlinked, so it may be more definitive to assign parameters $\beta_1 ... \beta_{n_x}$ to each variable $x_1 ... x_{n_x}$ and optimise them all. However, without prior knowledge of realistic starting values of the β parameters, this may run the risk of falling into local minima, at the same time as being computationally very intensive. It seems more viable to use model trimming to develop simpler models, which can be compared to the original model, using techniques such as the model selection criteria described in the next section.

2.8 Model selection

A number of model selection criteria are used throughout this thesis to measure the relative merits of different modelling approaches. Each of these relies on some measure of the complexity of the model and some measure of the goodness of fit, providing a number which will be minimised for the model judged better by the criteria. Each was calculated on the basis of their descriptions in Myung (2000), shown in Table 2.2. The code for each calculation was added to the Levenberg-Marquardt optimisation procedure in MatLab described above.

Each criterion is only valid when calculated for a model in which some acceptable 'optimum' parameter values have already been chosen. The first three criteria in Table 2.2 (AIC, BIC and RMSD) depend only on the number of parameters in the model in their measure of the model's complexity. The more advanced MDL technique takes into account the functional form of the model via the Hessian matrix of the minus log-likelihood, which is defined as $H(\bar{p}) = -\nabla^2_{\bar{p}} \ln(ML)$. On

Criteria	Formulation
Akaike Information Criterion	$AIC = -2\ln(ML) + 2n_p$
Bayesian Information Criterion	$BIC = -2\ln(ML) + n_p \ln n_d$
Root Mean Squared Deviation	$RMSD = \sqrt{\frac{\chi^2}{n_d - n_p}}$
Minimum Description Length	$MDL = -\ln(ML) + \frac{1}{2}\ln\lvert H(\bar{p})\rvert$
Information-theoretic measure of complexity	$ICOMP = -\ln(ML) + \frac{n_p}{2}\ln\left(\frac{trace(\Omega(\bar{p}))}{n_p}\right) - \frac{1}{2}\ln\lvert\Omega(\bar{p})\rvert$

Table 2.2: Model selection criteria, as described in Myung (2000). $\ln(ML)$ is the maximised log-likelihood of the model, n_p the number of adjustable parameters, n_d the number of datapoints used in fitting the model, χ^2 the residual sum of squared errors, $H(\bar{p})$ the Hessian matrix of the minus log-likelihood, and $\Omega(\bar{p})$ the covariance matrix of parameter estimates.

returning to Equation 2.8, it can be seen that the log-likelihood is linear in $-\chi^2$, and so $-\nabla^2_{\bar{p}} \ln(ML)$ is proportional to $\nabla^2_{\bar{p}}\chi^2$. This is equivalent to the matrix α defined in Equation 2.13. Therefore, for the purposes of providing a number 'MDL' for comparison with other models, it is sufficient to replace the matrix $H(\bar{p})$ with $\alpha(\bar{p})$. For the calculation of the final criteria ICOMP, the covariance matrix $\Omega(\bar{p})$ is often approximated by the inverse of the Hessian, but by the same arguments as above it is sufficient to define $\Omega(\bar{p}) = \alpha^{-1}(\bar{p})$.

The numbers provided by each criteria are intended to help with the choice of a so-called 'true' model for a given system. However such a choice remains subjective; no mechanical data analytic procedure for evaluating model fit should ever replace or override human judgement (Browne 2000); it should merely assist such judgements. Therefore knowledge of the theoretical background to each model selection technique is essential. In fact one outcome of this thesis is a discussion of the relative merits of different model selection criteria, and their suitability for the particular case of ice modelling.

2.9 Cross-validation

Cross-validation (CV) is a method of evaluating the predictive validity of a model. The idea is that a model should be selected on the basis of its ability to capture the behaviour of unseen or future observations from the same underlying process (Myung 2000). Data are divided into two non-overlapping samples for model calibration and validation. Parameters values are estimated using the calibration sample, and the model then run again for the validation sample. In its simplest form, the cross validation index CV is calculated as the goodness of fit to the validation sample when using the calibration sample parameters, for example:

$$CV = \chi^2_{validation}\left(\bar{p}_{calibration}\right) \tag{2.20}$$

The two-sample form of cross-validation can be wasteful because only about half of the available observations are used to calculate parameters, leading to less accurate calibrations (Browne 2000), so often large calibration samples and small validation samples are used. However the results may be erroneous and misleading in the presence of correlations in the data (Hart and Lee 2005). Autocorrelation is especially likely in data spread over time, as for many variables the value one day is to some extent dependent on the previous day; CV results may therefore be deceptively good. In this thesis it is argued that for real-time models of an environmental system, a truly accurate cross-validation requires large calibration and validation samples spread across separate blocks of time designated by the turnover time of the system, i.e. the length of the longest scale repetitive cycle which may be expected to affect the system. In most cases this is the annual cycle of the seasons, so datasets must come from separate years.

Chapter 3

A physics-based model of lake ice - Development

3.1 Overview

This chapter gives a full description of the algorithms, parameterisations and input data involved in the development of a detailed physics-based model of the ice layer on Crooked Lake, Antarctica. This includes descriptions of some related experimental fieldwork, a number of short modelling investigations, and careful discussion of the literature to determine which equations from the literature are most suitable for the Antarctic climate in general and Crooked Lake in particular.

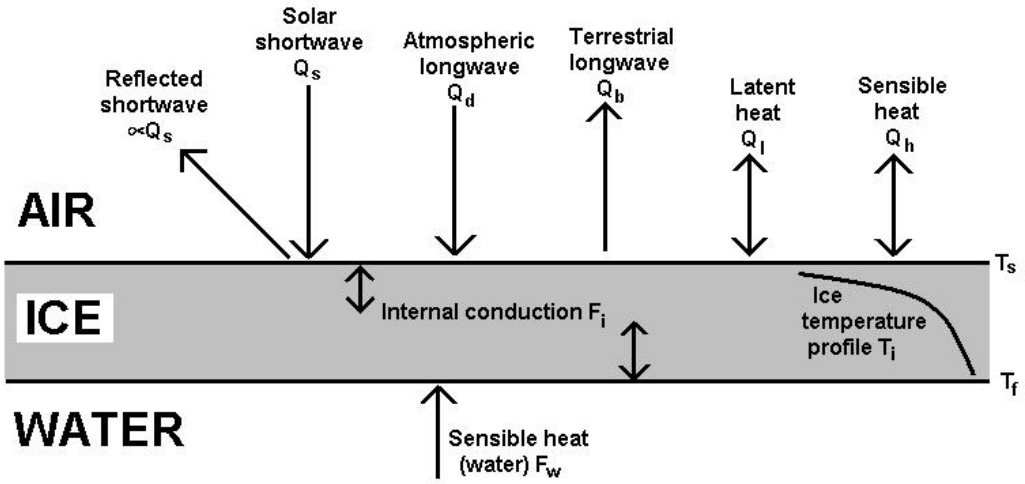

Figure 3.1: Schematic of the physics-based model, showing the heat and radiation fluxes affecting the ice layer.

The fundamental structure is based on the model described in Launiainen and Cheng (1998), Cheng and Launiainen (1998) and Cheng (2002), although many parameterisations have been tailored to suit a freshwater Antarctic system (as opposed to saline Arctic systems in their study). The key processes are the balance of heat at the ice surface and the ice bottom, and the conduction of heat through the ice layer (Figure 3.1). According to the definitions of model quantities given in the Methods chapter, the input variables to the model are a number of quantities that were measured throughout the year at Crooked Lake and at Davis station. The heat fluxes are intermediate variables, providing boundary conditions for heat conservation in the ice layer. The main model output is the ice thickness. The model also predicts the temperature at the top and bottom ice surfaces, and at intervals throughout the ice layer.

3.2 Input variables

A number of meteorological data were available to provide the necessary input variables and driving forces for a thermodynamic model of the ice on Crooked Lake (Table 3.1). The automatic probe on Crooked Lake measured physical parameters in the atmosphere, the ice layer and the water column. A number of data recorded by Australian Bureau of Meteorology staff at Davis station were also found to be useful.

Details on the automatic probe and methods employed in measuring each of the variables are in Palethorpe et al. (2004). Data were recorded at five-minute intervals. Deployment of the probe on Crooked Lake was limited to times of sufficient ice thickness on the lake: 22:15 on 17 January 2003 until 15:00 on 31 January 2003, and 15:40 on 12 May 2003 until 11:00 on 13 January 2004. However as some of the equipment developed faults due to the cold or severe weather, and some sensors were added at later dates, not all of the variables in Table 3.1 were recorded for the entire period of probe deployment. In particular, the sensors to measure relative humidity at 1 m and 2 m, wind speed at 1 m and temperature at 2 m were added by the author and Malcom Foster on 7 December 2003, so those variables were only measured for around 6 weeks.

All of the variables from Davis station were measured every three hours over the study period, giving eight datapoints per day at 00:00, 03:00, 06:00, 09:00, 12:00, 15:00, 18:00 and 21:00, with the exception of cloud cover which was not recorded at 00:00 and 03:00. Unlike the 'one-off' data from the Crooked Lake probe, these

Variable	Units	Details (CL=Crooked Lake, D=Davis)
Air Temperature	K	CL - 1 m and 2 m above the ice surface D - 10 m above MSL
Water Temperature	K	CL - 3 m and 5 m below the ice surface
IceThickness	m	CL
Wind Speed	m s^{-1}	CL - 1 m and 2 m above the ice surface D - 10 m above MSL
Wind Direction	^{o}	CL - 2 m above the ice surface
Relative Humidity	%	CL - 1 m and 2 m above the ice surface D - 10 m above MSL
UVB Radiation	W m^{-2}	CL - 1 m above and 3 m below the ice surface
Ice Temperature	K	CL - at 5 cm intervals throughout the ice layer
PAR	W m^{-2}	CL - 1 m above the ice surface (upwelling and downwelling), and 3 m, 5 m, 10 m, 20 m below
Air Pressure	Pa	D - 10 m above sea level
Cloud Cover	fraction	D

Table 3.1: Data used in formulating the physics-based model of Crooked Lake, and details on where each was recorded. All were converted to S.I. units. PAR stands for Photosynthetically Active Radiation, MSL stands for Mean Sea Level.

data are available for the whole year of study, are recorded on a routine basis, and will continue to be recorded as long as Davis station is manned. A model formulated on the basis of these data as inputs may therefore be more useful in the future. However as Davis is 16 km away from the site at Crooked Lake, correlations were calculated between the two datasets (Table 3.2).

The correlations are good. Given the especially good air temperature correlation, which is the most important variable governing ice growth and melt, the benefits of parameterising the model with Davis data inputs were deemed to outweigh any intuitive reasons against it. Therefore the Davis data is used throughout this thesis except where otherwise stated.

Variable	Correlation Coefficient	Number of datapoints
Air temperature	0.981	2041
Relative humidity	0.798	387
Wind speed	0.799	1938

Table 3.2: Correlations between the three variables that were measured at both Davis station and Crooked Lake, with the number of 3-hour datapoints used in calculating them.

3.3 Initial calculations

Several intermediate variables relating to the atmosphere, ice and water were calculated during the model execution. Equations were carefully selected on the basis of their suitability for application in the Antarctic, and this section gives a thorough discussion of this process.

3.3.1 Humidity

The available data for Crooked Lake included relative humidity (RH), the ratio of the amount of water vapour in the air to the amount of water vapour the air can hold at saturation point. However this quantity is not particularly useful in physical calculations, and a number of other quantities related to moisture were calculated.

Saturation vapour pressure e_s is the pressure that water vapour molecules would exert if air were saturated at a given temperature (Ahrens 1994). It was calculated in units of Pa from air temperature T_a in K using a form of the empirical Tetens (1930) equation:

$$e_s = 610.8 \exp\left(\frac{17.27(T_a - 273.15)}{237.3 + (T_a - 273.15)}\right) \tag{3.1}$$

Actual vapour pressure, which is the actual pressure in Pa exerted by water vapour molecules, was found using the relative humidity data:

$$e_a = e_s \frac{RH}{100} \tag{3.2}$$

Specific humidity in kg kg^{-1}, which is the ratio of the mass of water vapour in an air parcel to the total mass of the parcel, was calculated using an empirical

formula incorporating the air pressure p_a in Pa (see e.g. Gill 1982):

$$q_a = \frac{0.622 e_a}{p_a - 0.378 e_a} \tag{3.3}$$

3.3.2 Air density

Air density ρ_a is related to both temperature T_a and pressure p_a. The ideal gas law relates these quantities as follows:

$$p_a V_a = n_a R_g T_a \tag{3.4}$$

where V_a is the volume of an air parcel, n_a is the number of moles in the parcel and R_g is the universal gas constant (8.31 J mol^{-1} K^{-1}). This can be rewritten for density ρ_a as:

$$\rho_a = \frac{p_a M_a}{R_g T_a} \tag{3.5}$$

since $\rho_a = \frac{M_a n_a}{V_a}$, where M_a is the average molar mass of air (0.029 kg mol^{-1}). The assumption of an ideal gas is commonly used in meteorology as being an accurate parameterisation for the atmosphere. However in the Antarctic, where the world's most extreme temperatures occur, the error in taking this approach may be higher, and so a comparison of the ideal and non-ideal gas approaches was made. For a non-ideal gas corrections must be made to the pressure and volume quantities to account for intermolecular interactions. The most common parameterisation used for this is the Van der Waal's equation of state:

$$\left(p_a + a\left(\frac{n_a}{V_a}\right)^2\right)(V_a - n_a b) = n_a R_g T_a \tag{3.6}$$

where a and b are constants particular to a given gas. For air $a = 0.1358$ J m^3 mol^{-2} and $b = 3.64 \times 10^{-5}$ m^3 mol^{-1}. Equation 3.6 was rewritten and solved for density ρ_a using an iterative solving command in MatLab.

The extremes of pressure and temperature measured for Crooked Lake in 2003 were 95630 Pa and 101480 Pa, 232 K and 283 K respectively. ρ_a was calculated for an ideal and a non-ideal gas at these extremes (Table 3.3).

Pressure Pa	**Temperature** K	**Density (ideal gas)** kg m^{-3}	**Density (non-ideal gas)** kg m^{-3}
95500	232	1.437	1.439
95500	283	1.178	1.179
101500	232	1.527	1.530
101500	283	1.252	1.253

Table 3.3: Air density calculated using the ideal gas law and the non-ideal Van der Waal's equation of state, for every combination of the extreme values of pressure and temperature at Crooked Lake, 2003.

At each combination of the extreme values shown in Table 3.3, the air density calculated under the ideal gas assumption gives a change of less than 0.2 % with respect to the more accurate value calculated by the Van der Waal's equation. Therefore for the ease of calculation, Equation 3.5 was deemed sufficient for the calculation of air density throughout this thesis.

3.3.3 Atmospheric stability

For modelling the interactions of a surface with the atmosphere, it is useful to have a measure of atmospheric stability close to the surface. Stability refers to the balance between laminar flow (straight) and turbulent flow (where air swirls in small loops called eddies). A parameter used in fluid dynamics to assess flow stability close to a surface is the Bulk Richardson number R_z, which is calculated using:

$$R_z = \frac{z_a g(T_a - T_s)}{\frac{1}{2}(T_a + T_s)V^2} \tag{3.7}$$

where z_a is the height of measurement of air temperature (1 m), g is the acceleration due to gravity (9.8 m s^{-2}), V is wind speed, T_a is air temperature and T_s is surface temperature. This is an approximation of the gradient Richardson number, a dimensionless ratio related to the buoyant production or consumption of turbulence divided by the shear production of turbulence. When the Richardson number is above a critical value R_c the surface layer will tend to be stable, with laminar air flow, while a Richardson number below R_c means the layer is dynamically unstable and likely to become or remain turbulent. This value is usually taken as $R_c = 0.25$, although values may vary depending on the environment in question. Some ice layers such as those at sea have sizeable bumps and ridges that increase surface roughness, however the isolated freshwater ice

on Crooked Lake is very smooth and glass-like for the majority of the year, so will not readily induce turbulence, and thus the atmospheric surface layer may remain stable down to relatively very low values of R_z. Launiainen and Cheng (1998) adopt $R_c = 0$ for ice, which was used for initial model runs. The effects of varying R_c are investigated in Chapter 4.

3.3.4 Ice albedo

Ice reflectivity, or albedo, is one of the key factors governing the behaviour of an ice system, as well as being a key optical parameter for climatological studies (Perovich 2003). Many ice models use constant values of albedo for short-term simulations, but over the course of a year it may be useful to allow some temporal variability. Albedo depends on both surface properties and the sun's altitude, and a wide range of values have therefore been reported for snow and ice. Models exist to predict albedo from air temperature, solar radiation and snowfall data (e.g. Henneman and Stefan 1999). For this study, an attempt was made to implement albedo as a dynamic input variable, informed by measured values of upwelling and downwelling radiation.

A downward-facing PAR sensor was added to the Crooked Lake probe on 13 May 2003 (by Malcom Foster, at the author's request). It was hoped that ice albedo could then be calculated from the ratio of upward to downward PAR. However the results of taking this approach were highly variable. The sensor was supported on an arm protruding sideways from the probe, and the bulk of the probe occasionally cast a shadow over the area of ice directly below it. Also, snowdrifts and blizzard-tails built up against the sides of the probe on several occasions, such that the ice around the probe had a disproportionate amount of snow cover in comparison to the rest of the lake. In winter, the low light levels made albedo more difficult to quantify, especially on cloudy or hazy days of diffuse light, where the upwelling PAR was measured to be greater than downwelling. However despite these uncertainties some estimates were made of daily albedo values by considering only a 3-hour period straddling midday (10:30 to 13:30), when the sun was at it's highest point. This provided 37 5-minute datapoints of upwelling and downwelling PAR for each day. The average of these was used to calculate the albedo for that day. For the period 13 May 2003 to 12 January 2004, albedo was calculated for 220 days in total, shown in Figure 3.2.

The mean albedo was 0.43, with a standard deviation of 0.17. This value is similar to that found by Henneman and Stefan (1999) who measured (and predicted via

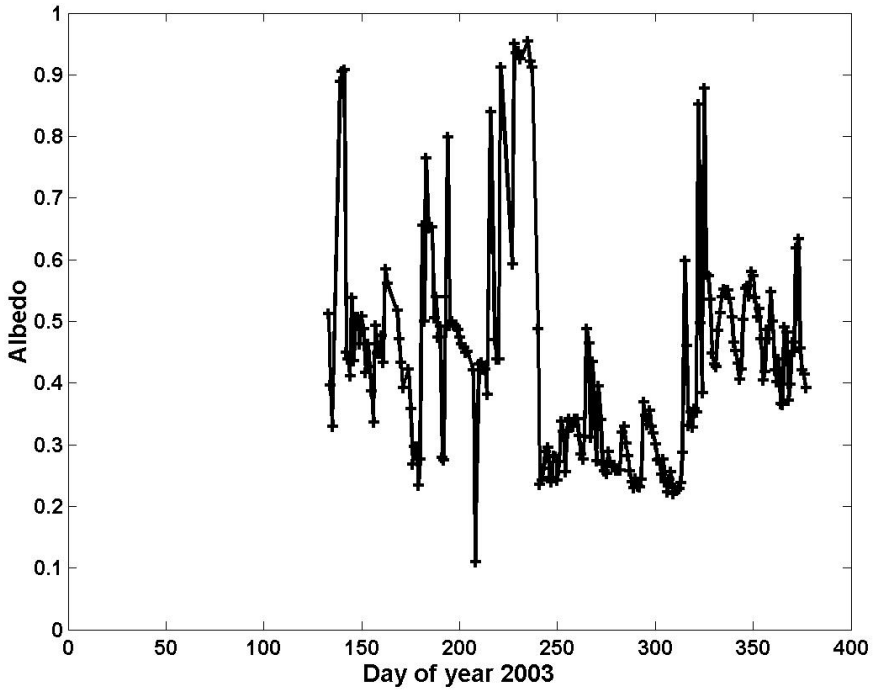

Figure 3.2: Daily values of albedo of Crooked Lake calculated from measurements of upwelling and downwelling PAR. The mean of 37 5-minute measurements between 10:30 and 13:30 were used.

models) albedos of 0.3 to 0.55 for freshwater ice on a lake in Minnesota, USA. There is large variability in measured values, and the method of measurement is simplistic (true albedo should represent a higher wavelength band than the PAR band, 400-700 nm). However there is sufficient spread of data across the year to provide an albedo input variable for the model.

3.3.5 Attenuation of radiation

According to Beer's Law for the transmission of radiation through a medium, the fraction of light absorbed by each equal-sized layer of the medium is the same. This gives an exponential dependence on depth z below the surface of the medium:

$$Q(z) = (1 - \alpha)Q_0 \exp(-\kappa z) \tag{3.8}$$

where $Q(z)$ is the flux density of radiation at depth z, Q_0 is the power of downwelling radiation at the surface of the medium, α is the albedo of the surface

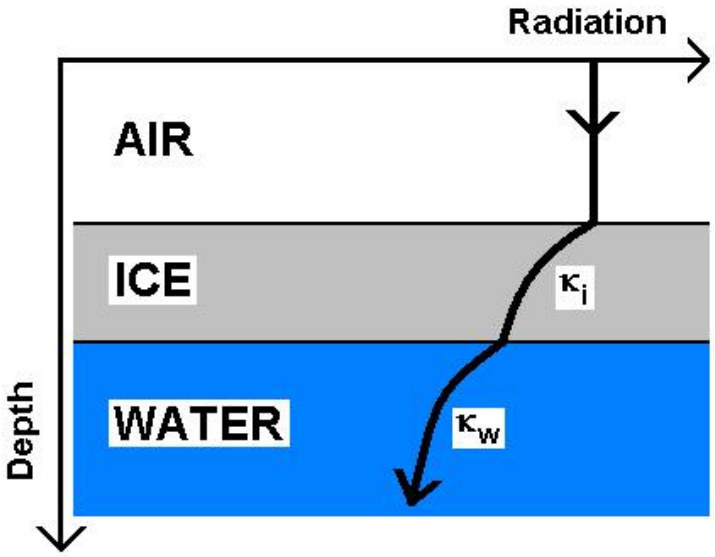

Figure 3.3: Exponential attenuation of radiation in ice with extinction coefficient κ_i and water with extinction coefficient κ_w.

and κ is the extinction coefficient of the medium in m^{-1}. In a lake system, ice and liquid water have different values of extinction coefficients, κ_i and κ_w (Figure 3.3).

The PAR measurements on Crooked Lake were used as an approximation for total radiation flux density $Q(z)$. As with the albedo calculations, only measurements in the 3-hour period 10:30 to 13:30 were used. To estimate values of κ_i for use in a model, Equation 3.8 was first rewritten for the lake water as:

$$\ln PAR(z) = -\kappa_w z + c \tag{3.9}$$

where c is a constant. This implies that a plot of $\ln PAR(z)$ against z will give a straight line of gradient $-\kappa_w$. The four measured underwater values of PAR could therefore provide an estimate of κ_w.

The PAR sensor at the surface measured only cosine-corrected downwelling radiation from the upper hemisphere of view, while the underwater sensors were of a bulb type which measured total scalar PAR (PAR from all directions around the sensor). This is important for biologists who need to consider all directions because of the random orientation of phytoplankton cells. The ratio of scalar irradiance to downwelling irradiance in a water column ($\frac{E_0}{E_d}$) increases with the ratio of scattering to absorption coefficients (i.e. the more scattering that occurs, the higher the upwelling irradiance component). Kirk (1986) reports values of

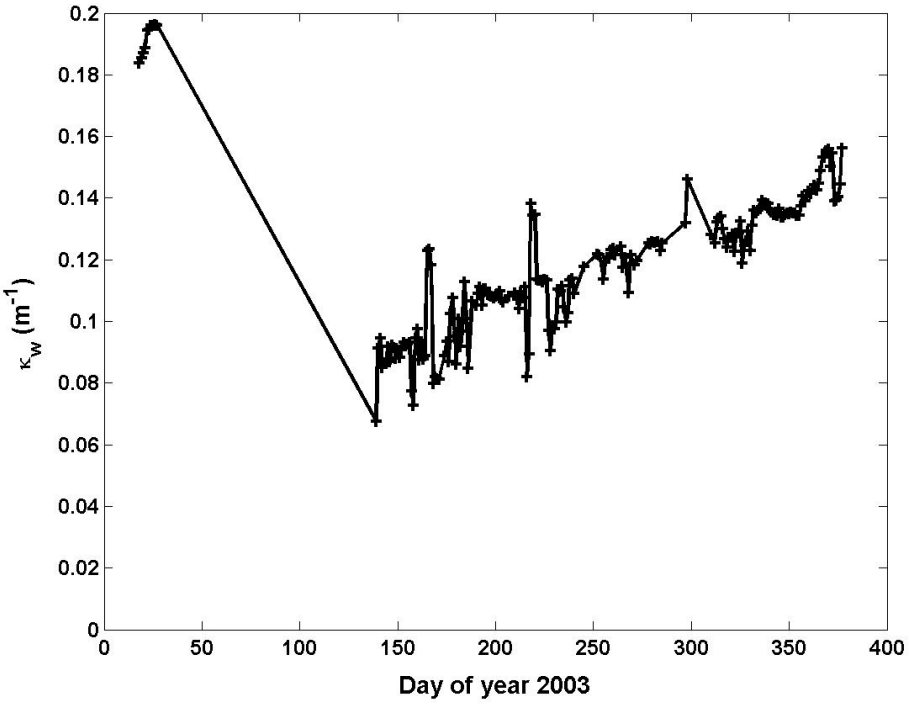

Figure 3.4: Calculated extinction coefficient κ_w of water in Crooked Lake.

$\frac{E_0}{E_d}$ of up to 1.2 for clear oceanic waters, increasing to 1.4-1.8 for some inland or coastal waters and 2.0-2.5 for very turbid waters. In Crooked Lake, the absence of fish or marine mammals results in very clear, clean water; in addition the ice layer inhibits extensive turbulent mixing by the wind, preventing the dispersion of sediment from the lake bed. Considering also the absence of salt, the lake can be deemed to have less scattering than even the clearest oceanic waters, and hence a value of $\frac{E_0}{E_d} = 1.1$ was adopted.

Calculated values of κ_w across the year are shown in Figure 3.4. The highest values of almost 0.2 m^{-1} were calculated for the first probe deployment in January 2003. This was a time when there was open water 'moating' around the lake edges, which may have allowed some wind-induced mixing of sediment, causing higher κ_w. When the probe was redeployed in May 2003, κ_w was around 0.1, and the general trend thereafter was approximately a linear increase with time, reaching 0.16 m^{-1} in January 2004. A possible explanation for this is in terms of the spectral properties of the ice. In clear ice the attenuation of red light is greater than that of blue (hence the ice appeared blue in winter). Therefore the light reaching the water column would have a higher proportion of blue light than the light at the surface (Wharton Jr. et al. 1992). Clear water also attenuates blue light slightly less than red, so the measurements of radiation in the water column indicate less attenuation than if the light had a more uniform spectrum.

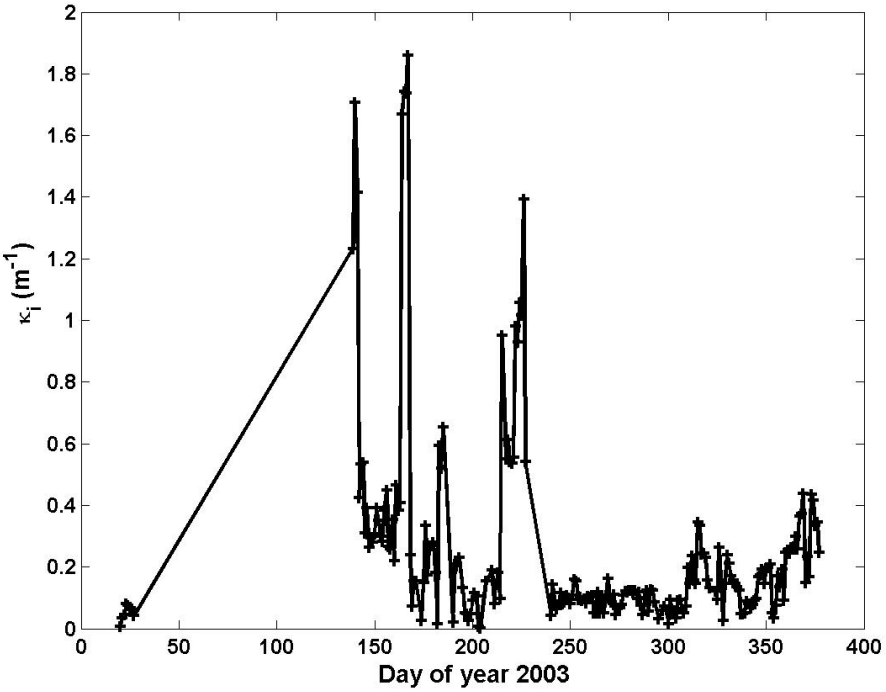

Figure 3.5: Calculated extinction coefficient κ_i of ice on Crooked Lake.

As ice ages, and particularly as it begins to melt, it whitens and opacifies, so the transmitted light spectrum is more uniform. With more red light in the spectrum the measured attenuation coefficient is higher.

The straight line represented by Equation 3.9 was extended to find the downwelling radiation at the bottom of the ice layer, which is at a depth determined by the ice thickness H_i:

$$PAR(H_i) = \exp(-\kappa_w H_i + c) \tag{3.10}$$

The extinction coefficient for ice κ_i was found using $PAR(H_i)$ and the surface measurements $PAR(0)$:

$$\kappa_i = \frac{\ln((1-\alpha)PAR(0)) - \ln PAR(H_i)}{H_i} \tag{3.11}$$

where α is the ice albedo. With the values of albedo calculated in the previous section, the average value of the extinction coefficient over the year was found to be $\kappa_i = 0.27$ m^{-1} (Figure 3.5). Apart from some high peaks (which may correspond to periods of snow) κ_i was around 0.1 m^{-1}, but showed a slight increase

to around 0.4 m^{-1} in the summer period, December 2003 to January 2004. This was the period over which the ice had begun to rot, and became more opaque. As with albedo, there is sufficient spread of data across the year to provide an input variable for the model.

Some measurements find that the extinction coefficient for thermal radiation is in fact large near the ice surface and decreases by more than an order of magnitude below the top 0.1 m of ice, where only visible light remains (Grenfell and Maykut 1977). This is accounted for in the model of Launiainen and Cheng (1998), and is an important consideration for accurate calculations of in-ice temperatures. However the model development in this thesis is mostly concerned with accurate predictions of ice thickness. Making the assumption that the extinction coefficient is constant with depth (or effectively a mean value of the top 0.1 m and the rest of the layer) will not significantly affect the ice thickness prediction. Therefore the model investigations in this thesis were undertaken with an extinction coefficient which was constant with depth.

Note: As can be seen in Figures 3.2 and 3.5, the input variables α and κ_i have no measured values in the periods when ice was too thin to support the sensing probe (31 January to 12 May 2003). However this is also the case for the ice thickness data which is used to fit the model, so the effects of using linearly interpolated values for α and κ_i (also water temperature T_w) in these periods are assumed to be negligible (i.e. those days on which the model output is fitted to data have 'real' values of all input variables).

3.3.6 Micrometeorological parameters

Sensors were added to the Crooked Lake probe by the author on 7 December 2003 to provide measurements of wind speed, relative humidity and temperature at two heights, and logged data until 13 January 2004. Having such profiles allows estimations of the roughness lengths for momentum, heat and water vapour on the Crooked Lake ice. These are important micrometeorological quantities involved in the transfer of latent and sensible heat to and from the ice layer.

In addition, a wind profile mast (Figure 3.6) was deployed on the ice on Crooked Lake on 7, 9 and 12 December 2004, to provide some more accurate calculations of the aerodynamic roughness length. This consisted of six cup anemometers mounted at heights of 0.26, 0.43, 0.67, 0.98, 1.42 and 1.87 m, with a counting box built by the University of Nottingham. On each occasion the equipment was

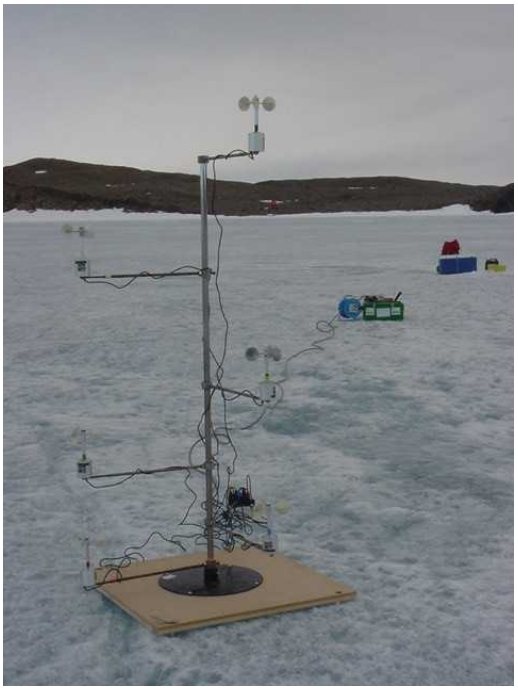

Figure 3.6: Wind profile mast on Crooked Lake. Anemometers were arranged pointing in the prevailing wind direction, with datalogging equipment and the supporting mast downwind.

deployed for two periods of 40 minutes either side of midday, and the number of revolutions of the anemometer vanes were converted to the average wind speeds over the period for each height. The mast was deployed in a position close to the Crooked Lake probe site, with over 500 m upwind 'pitch' of flat ice to the edge of the lake. It was therefore representative of the main internal area of lake ice cover, away from hills and the lake edge which may induce localised roughness variation.

The aerodynamic roughness length, z_0, is the characteristic length scale defined for a surface as the height at which wind speed becomes zero. For an area with large obstacles such as trees, vegetation or buildings, z_0 may be up to the order of tens of meters, whereas for a flat smooth surface like ice it may be expected to be less than 1 millimetre. Assuming near-neutral stability in Monin-Obukhov similarity theory (see e.g. Denby and Snellen 2001, Handorf et al. 1998, Andreas 2002), z_0 is related to the average wind speed $V(z)$ at height z and the friction velocity u_*, (a fundamental velocity scale in the atmospheric surface layer which remains constant with height) by:

$$V(z) = \frac{u_*}{k} \ln\left(\frac{z}{z_0}\right) \tag{3.12}$$

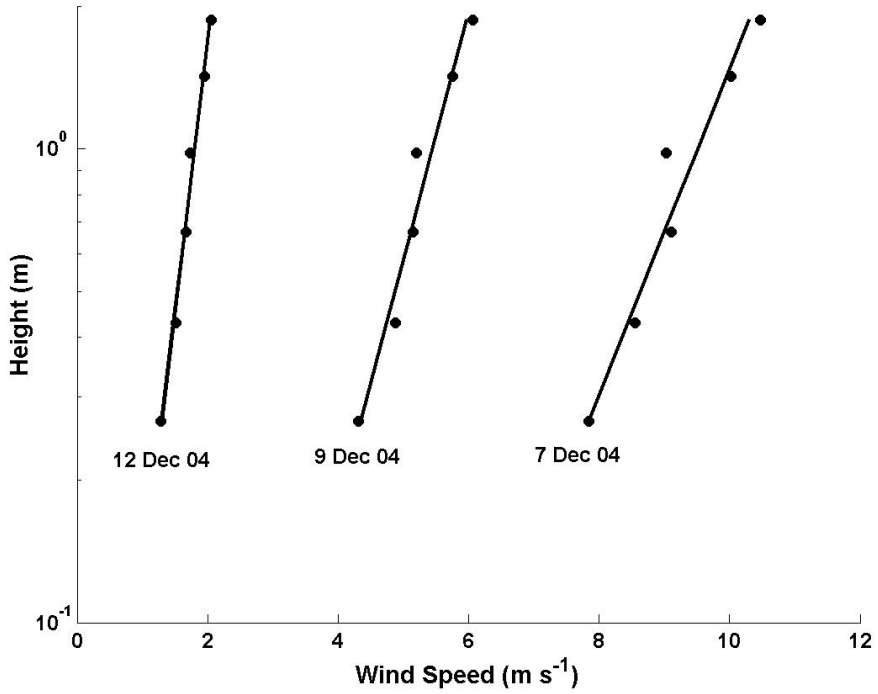

Figure 3.7: Logarithmic profiles of wind speed in the atmospheric surface layer above Crooked Lake, measured over two 40-minute periods either side of midday on 7, 9 and 12 December 2003.

Date	z_0 **(m)**	u_* **(m s^{-1})**
07/12/2003	0.000535	0.505
09/12/2003	0.001386	0.331
12/12/2003	0.008819	0.152

Table 3.4: Calculated values of aerodynamic roughness length z_0 and friction velocity u_* for Crooked Lake.

where k is the von Karman constant. Therefore with measurements of V at several heights plotted in a co-ordinate system which is logarithmic in z, the data should lie on a straight line with a gradient of $\frac{u_*}{k}$, which intersects the $V = 0$ axis at $\ln z_0$ (Andreas 1996). This was done for the three measurement days (Figure 3.7), and z_0 and u_* were calculated (Table 3.4).

With the assumption of near-neutral stability, the wind profiles all fitted a straight line with r^2 values of 0.94, 0.96 and 0.99 for the three respective days. This is plausible for a surface such as Crooked Lake, as the absence of nearby obstacles and smoothness of the surface would not be expected to cause instability in air flow. In addition, the Antarctic summer environment of 24-hour daylight means that the diurnal variations in solar radiation and temperature are relatively insignificant. As a result of this and the high surface albedo of ice, there may

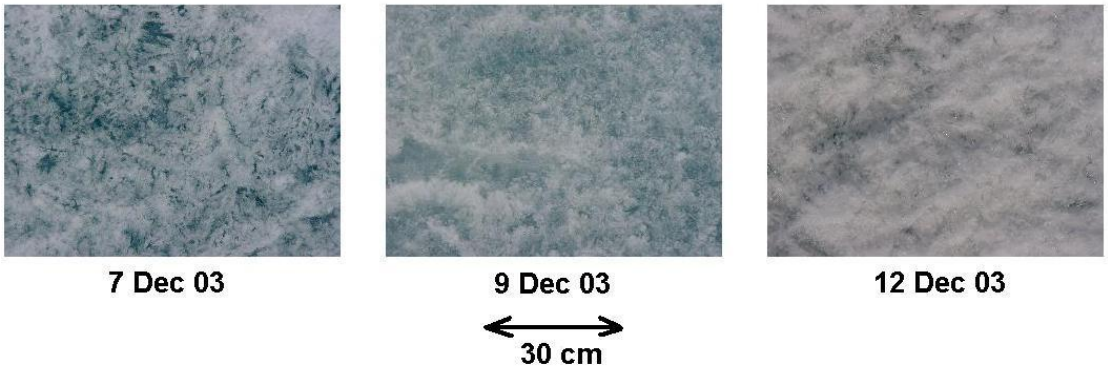

Figure 3.8: Photographs of Crooked Lake ice cover, December 2004.

be very little variation in surface heating, thermals and buoyancy with time, the usual factors which could cause large differences in turbulence between different times of day.

The calculated values of z_0 increase by an order of magnitude over the week in which the three measurements were taken. This was a period in which average daily air temperature rose from around -2 ^{o}C to 7 ^{o}C, and the ice thickness dropped by 12 cm. The surface became visibly rougher, whiter and more opaque during this time, as shown in Figure 3.8.

In addition to the aerodynamic roughness length, two length scales must be defined for transfer of heat and water vapour - the roughness lengths for temperature (z_T) and humidity (z_Q). In neutral stability conditions they are related to their respective vertical profiles as follows:

$$T(z) = T_s + \frac{t_*}{k} \ln\left(\frac{z}{z_T}\right) \tag{3.13}$$

$$q(z) = q_s + \frac{q_*}{k} \ln\left(\frac{z}{z_q}\right) \tag{3.14}$$

where t_* and q_* are fundamental temperature and velocity scales analogous to the friction velocity u_*, and T_s and q_s are the surface values of temperature and specific humidity.

The measurements of wind speed, temperature and humidity at two heights (Figure 3.9) were less successful in predicting these roughness lengths, as the differences between values at the two heights were negligible (in the case of temperature) or were alternately positive and negative, undermining the assumptions.

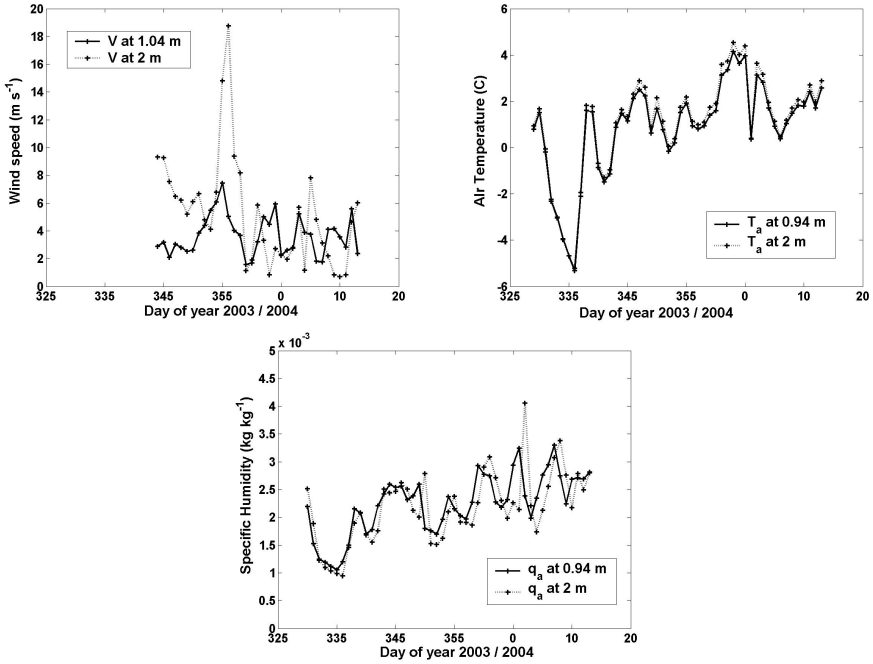

Figure 3.9: Measurements of wind speed, air temperature and specific humidity at two heights above Crooked Lake (24-hour means).

It was therefore not possible to calculate roughness lengths directly from the data for individual days, apart from the three days of accurate estimates of z_0 using the wind profile mast. However taking mean values for wind speeds in Figure 3.9 allowed a calculation of the average aerodynamic roughness length as $z_0 = 0.006$ m, which is within the range of values measured in Table 3.4. In the model, each roughness length was set to a constant value based on measurements or calculated from empirical formulae from the literature.

3.3.7 Other ice characteristics

A number of other physical values relating to the ice layer are necessary for the model, and may vary over time along with the albedo, extinction coefficient and roughness lengths. Ice density ρ_i, specific heat capacity c_i and thermal conductivity k_i are strictly speaking dependent on ice structure and the physical environment, and this is usually approximated with functions of temperature and salinity of the ice (e.g. Maykut and Untersteiner 1971). However as this dependence tends to be linear in the salinity s, which in the case of Crooked Lake is negligible, constant values can be used to a high degree of accuracy (see List of Symbols for values).

The enthalpy of vaporization of water R_l is required for calculations involving

phase changes at the ice surface. When the ice surface temperature T_s is at or above freezing point T_f, the surface must hold an infinitesimal layer of liquid water, and thus R_l represents the latent heat of vaporization, i.e. the heat lost or gained by the air when liquid water changes into vapor or vice versa. However when T_s is below T_f, R_l represents the latent heat of sublimation, i.e. the heat lost or gained by air when ice changes directly to water vapor or vice versa (i.e. the sum of the heat quantities required to melt water then turn it to vapour). The two quantities differ by around 335000 J kg^{-1}, and are expressed as:

$$R_l = 2500000 - 2375(T_s - T_f) \quad \text{for} \quad T_s \geq T_f \tag{3.15}$$

$$R_l = 2500000 - 2375(T_s - T_f) + 335000 \quad \text{for} \quad T_s < T_f \tag{3.16}$$

3.4 Heat and radiation fluxes

This section describes the model parameterisations of heat and radiation fluxes between the atmosphere, water and ice on Crooked Lake. These are important intermediate variables for use in predicting the ice thickness and ice temperature. As in the previous section, equations were carefully selected on the basis of their suitability for application to the Antarctic.

3.4.1 Solar shortwave radiation

Shortwave (SW) radiation is usually defined as the band of wavelengths at 400-4000 nm. It leaves the sun and enters the Earth's atmosphere where it is absorbed, scattered and transmitted by ozone, oxygen, carbon dioxide, water vapour, aerosols and clouds in the troposphere. Clouds reflect some incident shortwave back to space but may also contribute a substantial amount to the downward flux at surfaces with high albedos, due to multiple reflections between the surface and the cloud base (Key et al. 1996) (Figure 3.10).

A number of methods were available for estimating this important flux. The Crooked Lake probe provided measurements of PAR (400-700 nm). The SW radiation can be calculated from PAR by integrating Planck's equation for photon energy ($E = \frac{h_p c}{\lambda}$) across the wavelength bands:

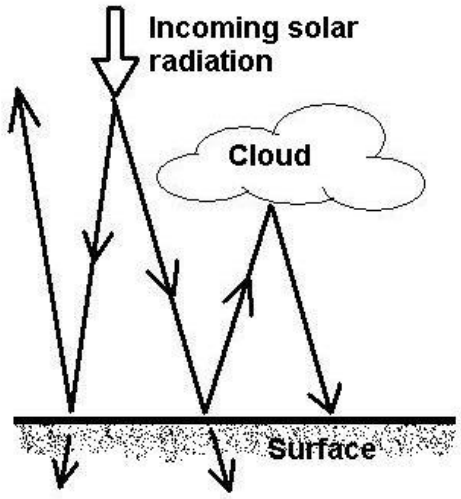

Figure 3.10: Multiple reflections of solar radiation between surface and cloud base.

$$Q_s = \frac{\int_{400nm}^{4000nm} \frac{h_p c}{\lambda} d\lambda}{\int_{400nm}^{700nm} \frac{h_p c}{\lambda} d\lambda} \times PAR \approx 1.475 \times PAR \tag{3.17}$$

where λ is wavelength, c is the speed of light and h_p is the Planck constant. However as PAR data was not collected for the entire year, and for the benefit of future predictions, it is useful to find an accurate, generalisable parameterisation of the atmospheric shortwave radiation at this particular Antarctic site. The amount of radiation striking the top of the atmosphere can be expressed as a fraction of the solar constant S, which is not strictly a constant but represents the average flux of solar radiation striking a plane normal to the earth-sun line, and has a value of approximately 1367 W m^{-2}. The downwelling shortwave at the top of the atmosphere normal to the Earth's surface is:

$$Q_t = S \cos Z \tag{3.18}$$

where the zenith angle Z is calculated from the latitude ϕ, solar declination δ and hour angle HA by: $\cos Z = \sin\phi \sin\delta + \cos\phi \cos\delta \cos HA$. The hour angle depends on solar time h_t, $HA = 15^o \times (12 - h_t)$ and declination depends on the Julian day J, $\delta = 23.45^o \times \sin\left(\frac{2\pi(J+284)}{365.24}\right)$. 15^o is the angle of rotation of the Earth in 1 hour and 23.45^o is the inclination angle between the Earth's rotational axis and it's orbital plane (Figure 3.11). For these formulae, latitudes for the Southern Hemisphere must be expressed as negative, giving -68.6^o for Crooked Lake. In addition, when the sun is over the horizon the cosine will be negative -

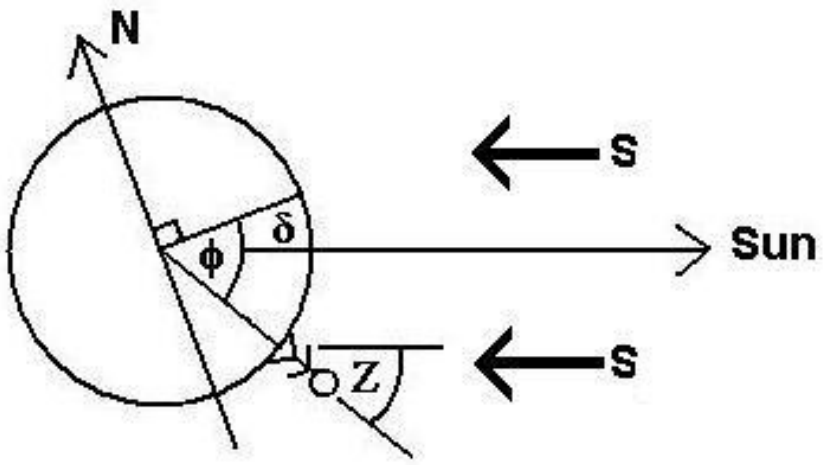

Figure 3.11: The zenith angle for a Southern Hemisphere observer at noon (hour angle HA = 0).

the equation does not account for the fact that the Earth is not transparent, and hence any values calculated for Q_s which are less than zero are set to zero.

The reduction of this 'top of atmosphere' radiation on reaching the surface is somewhat more difficult to parameterise, due to the high variability of atmospheric phenomena that may affect scattering, absorption and transmission. The surface fluxes are therefore a highly complex function of many variables in the entire air column, and would require a radiative transfer model and extensive vertical distributions of temperature and moisture to calculate. Instead a number of equations have been developed to approximate the atmospheric attenuation for general use, calculating the flux from a number of common meteorological surface measurements. Simpler forms for the solar radiation from a clear sky include that of Lumb (1964), who used data from the mid-Atlantic, and Bennett (1982). Zillman (1972) developed a slightly more complex formula using data from the Indian Ocean, which was modified for high-latitude (Arctic) use by Shine (1984). It includes the saturation vapour pressure e_a and is used in the Baltic Sea ice model of Launiainen and Cheng (1998). However it must be noted that all the equations (Table 3.5) are calibrated for the specific sites at which their authors worked, for example the constants of 0.61 and 0.2 for the mid-Atlantic used in the Lumb (1964) equation were re-calculated by Moritz (1978) to be 0.47 and 0.47, respectively, for a site in Canada.

Cloud cover considerably affects the surface shortwave and corrections have to be made to the above parameterisations to derive the true downwelling SW at the surface, Q_s. Some studies include a cloud cover factor C which takes values

Reference	Equation
Lumb (1964)	$SW_{clear} = S\cos Z(0.61 + 0.2\cos Z)$
Bennett (1982)	$SW_{clear} = 0.72S\cos Z$
Shine (1984)	$SW_{clear} = \frac{S\cos^2 Z}{(\cos Z+1)e_a\times 10^{-5}+1.2\cos Z+0.0455}$

Table 3.5: Parameterisations of 'clear sky' shortwave radiation fluxes from the literature.

References	Calibrated form	r^2 fit
Lumb (1964), Moritz (1978)	$Q_s = (1 - 0.48C)S\cos Z(0.33 + 0.43\cos Z)$	0.862
Bennett (1982)	$Q_s = (1 - 0.49C)0.57S\cos Z$	0.847
Zillman (1972), Shine (1984)	$Q_s = (1 - 0.48C)\frac{S\cos^2 Z}{(\cos Z+7.05)e_a\times 10^{-5}+1.69\cos Z+0.02}$	0.853

Table 3.6: Shortwave radiation models calibrated for Crooked Lake data.

between 0 and 1, and for the Crooked Lake case the cloud cover data from Davis can be used as an approximation for the cloud cover at the site. The most common method is to include the cloud fraction and a coefficient, as used by Bennett (1982) and Launiainen and Cheng (1998):

$$Q_s = SW_{clear}(1 - 0.52C) \tag{3.19}$$

where the coefficient value of 0.52 can be adjusted for each site. A polynomial form in C can also be used, for example $Q_s = SW_{clear}(1 - xC - yC^2 - zC^3)$ to account for the fact that as surface-measured cloud cover increases, the amount of low cloud, which reduces radiation the most, is increased disproportionately, such that the reduction of radiation increases slowly at first, then more rapidly with increasing cloud cover. A more complicated method was used by Shine (1984), involving the surface albedo, solar zenith angle and cloud optical depth to account for multiple reflections between the surface and the cloud base (as in Figure 3.10). They consider two terms for the SW, from the clear and cloudy portions of the sky: $Q_s = (1 - C)SW_{clear} + (C)SW_{cloudy}$.

Key et al. (1996) tested some of the above methods, using data from field sites in

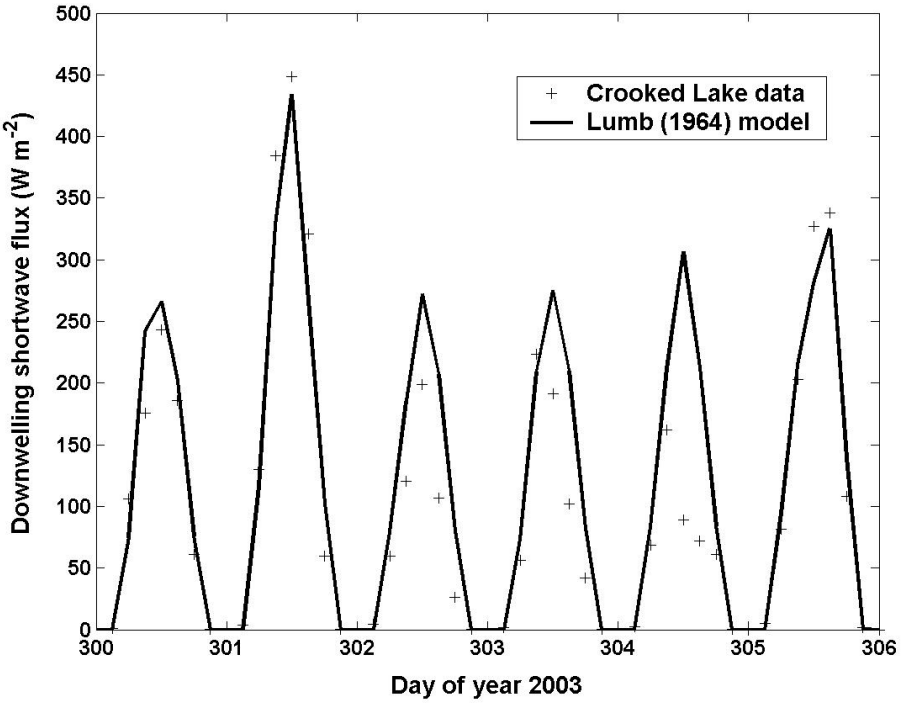

Figure 3.12: Calculated and observed surface shortwave radiation striking Crooked Lake for 6 days of 2003, using an equation of the form suggested by Lumb (1964). Goodness of fit for the whole year's data was $r^2 = 0.862$.

Canada and Alaska, and found the Shine (1984) equations to be best at estimating the shortwave flux. Given the extensive SW data available from the Crooked Lake PAR measurements, a similar test was possible. The forms of Shine (1984), Lumb (1964) and Bennett (1982) were generalised by replacing site-specific constants with adjustable parameters. For cloud cover a simple polynomial in the cloud fraction C was used, adding higher order terms to give a number of different equations. Each equation was calculated in ModelMaker using meteorological data as inputs. The parameters were adjusted using the Levenberg-Marquardt procedure to fit the Crooked Lake SW data (Table 3.6).

It was found that the addition of higher order terms in the cloud cover term gave a negligible increase in the goodness of fit of the models. The Zillman/Shine form tended to produce large discontinuities at certain values of the vapour pressure e_a, and the form of Lumb (1964) was found to provide the best fit to the Crooked Lake data (Figure 3.12). It is therefore used in models in this thesis.

3.4.2 Longwave radiation

Upwelling longwave (LW) radiation from a surface (Q_b) is well approximated by the Stefan-Boltzmann Law:

$$Q_b = \epsilon_i \sigma_s T_s^4 \tag{3.20}$$

where T_s is the temperature of the ice-air interface surface, σ_s is the Stefan-Boltzmann constant (5.67×10^{-8} W m^{-2} K^{-4}) and ϵ_i is the dimensionless surface emissivity which for ice takes values throughout the literature of 0.96-0.99 (Andreas and Makshtas 1985, Cheng 2002, Peres and DaCamara 2004).

The downwelling LW radiation from the atmosphere (Q_d) takes the same form as Equation 3.20, but emissivity ϵ takes a complex form due to atmospheric variations of clouds, temperature, particles, water vapour and contaminants. An accurate calculation of atmospheric LW can be determined from an appropriate radiative transfer model, however this requires data on temperature and humidity up to around 30km height. Since the work of Brunt (1932), a number of different empirical functional forms have been used throughout the literature, with ϵ replaced by an 'effective emissivity' ϵ_* calculated from atmospheric variables:

$$Q_d = \epsilon_*(C, T_a, e_a)\sigma_s T_a^4 \tag{3.21}$$

As with the shortwave radiation equations described in the previous section, several methods have been proposed for parameterising the effective longwave emissivity of the atmosphere. The intrinsically strong correlations between cloud cover C, air temperature T_a and vapour pressure e_a result in a three-way feedback, and therefore many of the formulae in the literature consider only one or two of these variables. Studies have looked in detail at the benefits of the various functional forms that have emerged over the years, comparing them to data from high-latitude sites (e.g. Makshtas et al. 1999, Key et al. 1996). This involves in many cases the use of complex radiative transfer models, and would require extensive measurements of longwave radiation, both of which are unavailable for Crooked Lake. It is therefore not possible to conduct a site-specific calibration of equation coefficients as was done for the shortwave equations. Instead a number of functional forms (Table 3.7) were compared on the basis of the praise they have received in the literature regarding their suitability for high-latitude (especially Antarctic) applications.

References	Equation
Guest (1998), Jacobs (1978)	$Q_d = (1 + 0.26C)(\sigma_s T_a^4 - 85.6)$
Efimova (1961), Jacobs (1978)	$Q_d = (1 + 0.26C)\sigma_s T_a^4(0.746 + 0.0066e_a)$
Prata (1996), Jacobs (1978)	$Q_d = (1 + 0.26C)\sigma_s T_a^4(1 - (1 + \frac{46.5e_a}{T_a})\exp(-\sqrt{1.2 + \frac{139.5e_a}{T_a}}))$
Zillman (1972)	$Q_d = \sigma_s T_a^4(9.2 \times 10^{-6} T_a^2) + 0.96\sigma_s T_a^4(1 - 9.2 \times 10^{-6} T_a^2)C$
König-Langlo and Augstein (1994)	$\sigma_s T_a^4(0.765 + 0.22C^3)$
Maykut and Church (1973)	$Q_d = \sigma_s T_a^4(0.7855(1 + 0.2232C^2.75))$

Table 3.7: Parameterisations of longwave radiation from the literature.

The first three entries in Table 3.7 are described as 'clear sky' equations by the authors, with a correction for cloud $Q_d = Q_d(clear) \times (1 + 0.26C)$ as suggested by Jacobs (1978). These combinations were chosen by Launianen and Cheng (1998) for their model of ice cover in the Baltic Sea. Unlike the case of solar shortwave radiation, the presence of cloud increases the atmospheric longwave. The lower three lines of Table 3.7 are 'all-sky' equations which account for cloud cover intrinsically in their functional form. Where one of the three atmospheric variables (T_a, e_a, C) is not present in the equations, the authors have indirectly accounted for that variability in their choice of coefficients and the correlations between variables.

To examine the relative merits of each equation in Table 3.7, each was applied to every 3-hour step over the entire year of 2003, using meteorological data from Davis as inputs for the calculations. The standard deviation across the estimates was highest in winter, when it reached as high as 13.3 % of the mean, and lowest in the summer (Figure 3.13).

Given the reasonable agreement between the six equations, and the lack of other information on which to base a decision, the selection of a method was subjective. In an attempt to introduce some objectivity, the following quantity was calculated for each equation, to assess which gave the best trade-off across the six options:

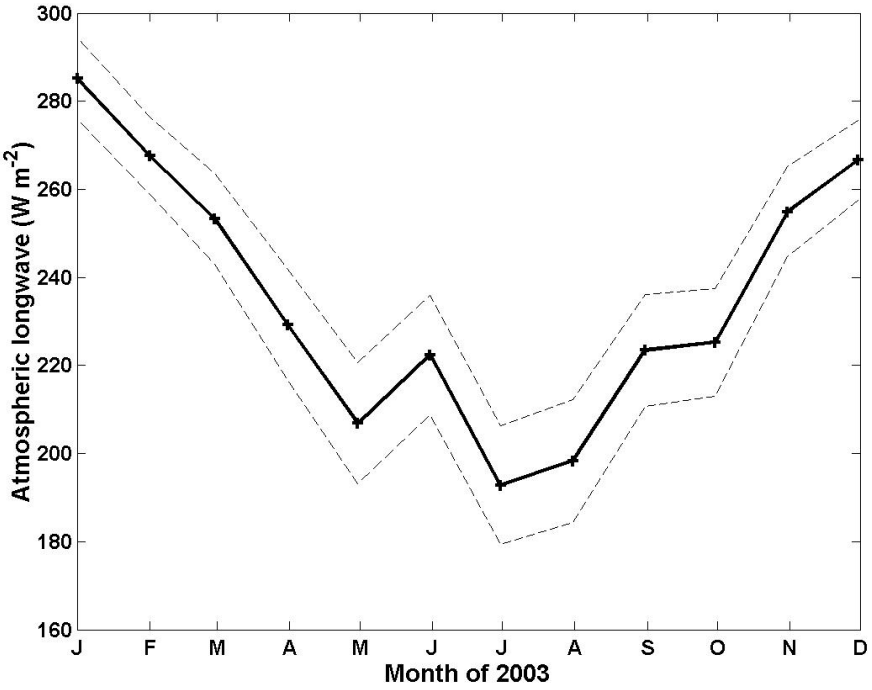

Figure 3.13: Monthly averages of longwave radiation as calculated from the mean of all six equations in Table 3.7. The dotted lines represent the standard deviation of monthly averages across all six methods.

$$D = \frac{|Q_d(2003) - \mu(Q_d)|}{\mu(Q_d)} \times 100\% \tag{3.22}$$

where $Q_d(2003)$ is the mean longwave radiation for 2003 as calculated by the relevant equation and $\mu(Q_d)$ is the mean value of $Q_d(2003)$ across all six equations. D therefore represents the difference between the equation result and the mean for all six equations, as a percentage. Table 3.8 gives the value of D for each of the equations in Table 3.7.

A discussion of the relative merits of the equations as tested by other researchers is also necessary for an informed choice. Makshtas et al. (1999), using data from both the Russian North Pole and Ice Station Weddell in the Antarctic, found that the König-Langlo method was best out of a number of equations at handling the total cloud amount and longwave flux, and at reproducing the seasonal variability of sea-ice thickness in a 1D thermodynamic model. Meanwhile the combined parameterisations of Efimova (1961) and Jacobs (1978) were preferred by Key et al. (1996) for data from two Arctic sites in the Northwest Territories, Canada and Barrow, Alaska. They found that the Zillman (1972) form performed poorly, but they did not test the König-Langlo method. Both Makstas et al. and Key

References	Site of testing	D (%)
Guest (1998), Jacobs (1978)	Weddell Sea, Antarctica	5.67
Efimova (1961), Jacobs (1978)	Various Russian stations, Arctic	4.15
Prata (1996), Jacobs (1978)	13 sites across world	4.20
Zillman (1972)	Southern Ocean	2.01
König-Langlo and Augstein (1994)	Georg von Neumayer, Antarctic and Ny Alesund, Arctic	1.81
Maykut and Church (1973)	Barrow, Alaska	1.89

Table 3.8: Known information on the longwave parameterisations from Table 3.7, for informing the choice between them. D is the difference between the equation result for all of 2003 and the mean for all six equations, as a percentage of the mean.

et al. found that the Maykut and Church (1973) method gave only 'moderately accurate' results.

Guest (1998) suggests that different forms are required between the Antarctic and the Arctic because of the greater amount of anthropogenic and natural particulate and aerosol contamination in the Northern Hemisphere. He suggests his equation as a simple method for the Antarctic, since it provided a better fit to his Weddell Sea data than a number of more complex forms from other authors. However Launiainen and Cheng (1998) suggest that the formula by Prata (1996) is based on the best arguments, taking into account an integration of the precipitable water in the air column to include the possibility of an atmospheric inversion. Prata tested his equation using measurements from a wide range of sites across the Arctic, North America, West Africa, the Middle East, Australia and Antarctica, so his form may be one of the most generalisable for applications across the world.

However the König-Langlo method gives the best trade-off between the six equations according to Table 3.8. Therefore given that it is also of a relatively simple form for numerical computation, and has been specifically developed and validated for Antarctic applications, it is chosen as the method for calculation of longwave radiation fluxes throughout this thesis, except where otherwise stated.

3.4.3 Sensible and latent heat

The fluxes of sensible and latent heat can be discussed together as they rely on the same basic theory and atmospheric conditions. Both are dependent on scalar transfer coefficients which in turn are derived from the parameterisation of a number of surface-atmosphere interactions. The calculations used are mostly the same as those chosen by Launianen and Cheng (1998). The approach is rooted in Monin-Obukhov Similarity Theory, a full discussion of which is beyond the scope of this thesis, but a summary is given here.

The transfer of sensible heat Q_h between the air and the ice layer is dominated by the temperature difference between the air (measured at height z_a) and the ice layer, $(T_a - T_s)$, according to:

$$Q_h = \rho_a c_a C_H (T_a - T_s) V \tag{3.23}$$

where V is the wind speed, ρ_a and c_a are the density and specific heat capacity of air, and C_H is the bulk transfer coefficient for sensible heat.

Analagously, the transfer of latent heat between the air and the ice layer is dominated by the difference in specific humidity between the air and the ice layer, $(q_a - q_s)$.

$$Q_l = \rho_a R_l C_E (q_a - q_s) V \tag{3.24}$$

where C_E is the bulk transfer coefficient for latent heat and R_l is the enthalpy of vaporization of water. At the ice surface, where water can be assumed to exist near triple point conditions, the air is assumed to be saturated, and hence q_s is calculated from Equation 3.3 with saturation vapour pressure e_s in place of actual vapour pressure e_a.

Parkinson and Washington (1979) approximate the heat transfer coefficients as constant values, with $C_H = C_E = 1.75 \times 10^{-3}$ for their models of sea ice. However the coefficients are strictly dependent on both the roughness of the surface in question and the stability of the atmospheric surface layer.

A drag coefficient C_D is also necessary due to the inclusion of wind speed in Equations 3.23 and 3.24. The three coefficients are calculated from:

$$C_D = \frac{k^2}{\left(\ln\left(\frac{z_a}{z_0}\right) - \Psi_M(\zeta)\right)^2} \tag{3.25}$$

$$C_H = \frac{k^2}{\left(\ln\left(\frac{z_a}{z_0}\right) - \Psi_M(\zeta)\right)\left(\ln\left(\frac{z_a}{z_T}\right) - \Psi_H(\zeta)\right)} \tag{3.26}$$

$$C_E = \frac{k^2}{\left(\ln\left(\frac{z_a}{z_0}\right) - \Psi_M(\zeta)\right)\left(\ln\left(\frac{z_a}{z_q}\right) - \Psi_E(\zeta)\right)} \tag{3.27}$$

where k is the von Karman constant, z_a is the height of measurements and z_0, z_T and z_q are the roughness lengths for momentum, temperature and humidity respectively. Ψ_M, Ψ_H and Ψ_E are stability corrections which are expressed as functions of ζ, the non-dimensional Monin-Obukhov parameter which quantifies stability effects.

Under neutral stratification, the drag coefficient C_D takes a value C_{DN}. This can be related to the geometrical surface roughness ξ by an empirical function found by Banke et al. (1980) for sea ice in the Arctic. ξ is defined as the r.m.s surface roughness, and was acquired by measuring surface elevation at 1m intervals upwind of their instruments. Their result was:

$$C_{DN} = 1.1 \times 10^{-3} + 7.2\xi \tag{3.28}$$

where ξ is in metres. This may not be completely accurate for a freshwater lake in the Antarctic, however the related theory gives a chance to replace the three inaccurately known roughness lengths z_0, z_T and z_q with one adjustable parameter ξ, which may not strictly give the true geometric roughness, but given the linear form of Equation 3.28, works well as a 'fitting parameter' for the model. ξ was given an initial value of 0.1 m on advice from Cheng (2004).

z_0 can be calculated from C_{DN} by setting $\Psi_M(\zeta) = 0$ in Equation 3.25 to represent neutral stability, and rewriting:

$$\ln z_0 = \ln z_a - kC_{DN}^{-\frac{1}{2}} \tag{3.29}$$

z_T and z_q depend on the roughness Reynolds number R_e, a quantity proportional to the ratio of inertial to viscous forces in a fluid, which is used in momentum, heat, and mass transfer calculations to account for dynamic similarity. It can be

calculated using:

$$R_e = \frac{z_0 C_{DN}^{\frac{1}{2}} V}{\gamma} \tag{3.30}$$

where γ is the kinematic viscosity of the fluid, taken as a function of air temperature:

$$\gamma = 0.9065 \times 10^{-7} T_a - 112.7 \times 10^{-7} \tag{3.31}$$

Andreas (1986) performed a second-order polynomial modelling exercise in which he found the following relationships between z_T, z_q and R_e, z_0 for ice and snow:

$$\ln z_T = \ln z_0 + a_0 + a_1 \ln R_e + a_2 (\ln R_e)^2 \tag{3.32}$$

$$\ln z_q = \ln z_0 + b_0 + b_1 \ln R_e + b_2 (\ln R_e)^2 \tag{3.33}$$

where the a and b coefficients take values that depend on R_e, covering three ranges which Andreas defined to cover the 'smooth', 'transition' and 'rough' dynamic regimes. His values are adopted in this thesis (Table 3.9).

Coefficient	$R_e \leq 0.135$	$0.135 < R_e < 2.5$	$2.5 \leq R_e \leq 1000$
a_0	1.250	0.149	0.317
a_1	0	-0.550	-0.565
a_2	0	0	-0.183
b_0	1.610	0.351	0.396
b_1	0	-0.628	-0.512
b_2	0	0	-0.180

Table 3.9: Values of the coefficients for Equations 3.32 and 3.33 as applied to snow and ice, from Andreas (1986). The three ranges of R_e represent 'smooth', 'transition' and 'rough' dynamic regimes in the surface layer.

The Ψ and ζ functions in Equations 3.25, 3.26 and 3.27 are empirical and must be found by experiment. An assessment of the relative merit of different functional forms is beyond the scope of this thesis, and so the forms chosen by Launiainen and Cheng (1998) for Arctic sea ice are deemed to be a good approximation for Crooked Lake. For unstable stratification (when $R_z < R_c$, see Section 3.2), these are:

$$
\begin{aligned}
\zeta &= \left(\frac{\left(\ln\left(\frac{z_a}{z_0}\right)\right)^2}{\ln\left(\frac{z_a}{z_T}\right)} - 0.55 \right) R_z \\
\Psi_M &= 2\ln\left(\frac{1+(1-19.3\zeta)^{\frac{1}{4}}}{2}\right) + \ln\left(\frac{1+(1-19.3\zeta)^{\frac{1}{2}}}{2}\right) - 2\arctan(1-19.3\zeta)^{\frac{1}{4}} + \frac{\pi}{2} \\
\Psi_H &= \Psi_E = 2\ln\left(\frac{1+(1-12\zeta)^{\frac{1}{2}}}{2}\right)
\end{aligned} \tag{3.34}
$$

and for stable stratification ($R_z \geq R_c$),

$$
\begin{aligned}
\zeta &= \left(1.89\ln\left(\frac{z_a}{z_0}\right) + 44.2\right) R_z^2 + \left(1.18\ln\left(\frac{z_a}{z_0}\right) R_z - 1.5\ln\left(\frac{z_0}{z_T}\right) - 1.37\right) R_z \\
\Psi_M &= \Psi_H = \Psi_E = -10.7 - 0.7\zeta - 0.75(\zeta - 14.3)\exp(-0.35\zeta)
\end{aligned} \tag{3.35}
$$

This provides all the necessary equations for calculating sensible and latent heat fluxes from Equations 3.23 and 3.24.

3.4.4 Conductive heat fluxes

Internal conductive heat fluxes in the ice layer are incorporated in the main numerical solution of the heat conservation equation (Section 3.5). However when considering the surface heat balances at the top and bottom of the ice it is important to include the limiting value of the conductive flux at the boundary. This depends on the limiting gradient of ice temperature at the surface and the thermal conductivity of ice k_i according to:

$$
F_i = -k_i \left(\frac{\partial T_i}{\partial z}\right)_{sfc} \tag{3.36}
$$

$$
F_b = k_i \left(\frac{\partial T_i}{\partial z}\right)_{bot} \tag{3.37}
$$

for the top and bottom of the ice layer respectively. The signs are different because of the convention used throughout this thesis whereby direction of positive heat flux is towards the ice layer.

The derivatives in Equations 3.37 and 3.37 were calculated numerically by an approximation considering the top and bottom of N defined layers of ice. This requires the internal ice temperatures next to the surfaces:

$$F_i = -k_i \frac{T_i(1) - T_s}{h} \tag{3.38}$$

$$F_b = k_i \frac{T_f - T_i(N-1)}{h} \tag{3.39}$$

3.4.5 Sensible heat from water

The water in Crooked Lake, provides a heat sink for the ice, and changes in water temperature T_w as a result of changes in the ice layer can be ignored as negligible. However the temperature difference between water and ice will contribute a sensible heat flux F_w to the ice layer. This may be approximated by a formula analogous to the transfer of sensible heat at the top of the ice (Equation 3.23):

$$F_w = \rho_w c_w C_{HW} (T_w - T_f) W \tag{3.40}$$

where ρ_w and c_w are the density and specific heat capacity of water, W is the current velocity and C_{HW} is the dimensionless heat exchange coefficient (analogous to C_H for the atmosphere). Launianen and Cheng (1998) argue that a proper determination of F_w may require coupling to a larger scale mixed-layer oceanic model. However underneath ice, which inhibits mixing of water by the wind, the stratification of water is very stable. In an isolated system like Crooked Lake this is particularly true, with most movement resulting from convection in the water column, so the value of current flow W will be very small indeed.

Launiainen and Cheng claim that a small constant value of $F_w \approx 5$ W m^{-2} is sufficient for the Baltic Sea. However given that the Crooked Lake probe provided extensive data on water temperature, this thesis investigates the benefit of introducing an adjustable parameter k_w to approximate the heat transfer as:

$$F_w = k_w (T_w - T_f) \tag{3.41}$$

An initial estimate of k_w is required. Holland and Jenkins (1999) use a value

of $C_{HW} = 1.5 \times 10^{-3}$ for sea ice which is sufficient as an estimate for fresh ice. An estimate for the current velocity would be of the order of 10^{-3} m s^{-1}. Hence the product $k_w \approx \rho_w c_w C_{HW} W \approx 1000 \times 4190 \times 1.5 \times 10^{-3} \times O(10^{-3})$ gives an estimate on the order of $k_w \approx 10$ W m^{-2} K^{-1}.

3.5 Modelling of the ice layer

This section describes the main body of calculation involved in the physics-based model, which predicts the ice temperature and ice thickness on Crooked Lake.

3.5.1 Heat conservation in the ice layer

The one-dimensional heat conservation equation used for the ice layer is an approximation of that used by Launiainen and Cheng (1998). It utilises the partial derivatives of the ice temperature T_i with respect to time t and depth z:

$$\rho_i c_i \frac{\partial T_i(z,t)}{\partial t} = -\frac{\partial}{\partial z}\left(-k_i \frac{\partial T_i(z,t)}{\partial z} + I(z,t)\right) \tag{3.42}$$

where the downwards direction is positive, the product $\rho_i c_i$ represents the volumetric heat capacity of ice, and $I(z,t)$ is an internal heat source term, equivalent to the fraction of the downwelling radiation flux that has penetrated to depth z. The only flux that penetrates substantially to any depth is the solar shortwave Q_s (the other fluxes are defined only at boundaries), and hence it can be considered the only flux that contributes to this term. Q_s is reduced to I by reflection off the ice surface according to the albedo, α, and by an exponential decay with depth according to the extinction coefficient, κ_i (as described in Equation 3.8).

$$I(z,t) = (1-\alpha) Q_s \exp(-\kappa_i z) \tag{3.43}$$

Equation 3.42 must be solved by an iterative numerical interpolation scheme. On evaluating the derivative of Equation 3.43 with respect to depth, Equation 3.42 can be rewritten:

$$\rho_i c_i \frac{\partial T_i(z,t)}{\partial t} = \frac{\partial}{\partial z}\left(k_i \frac{\partial T_i(z,t)}{\partial z}\right) + \kappa_i (1-\alpha) Q_s \exp(-\kappa_i z) \tag{3.44}$$

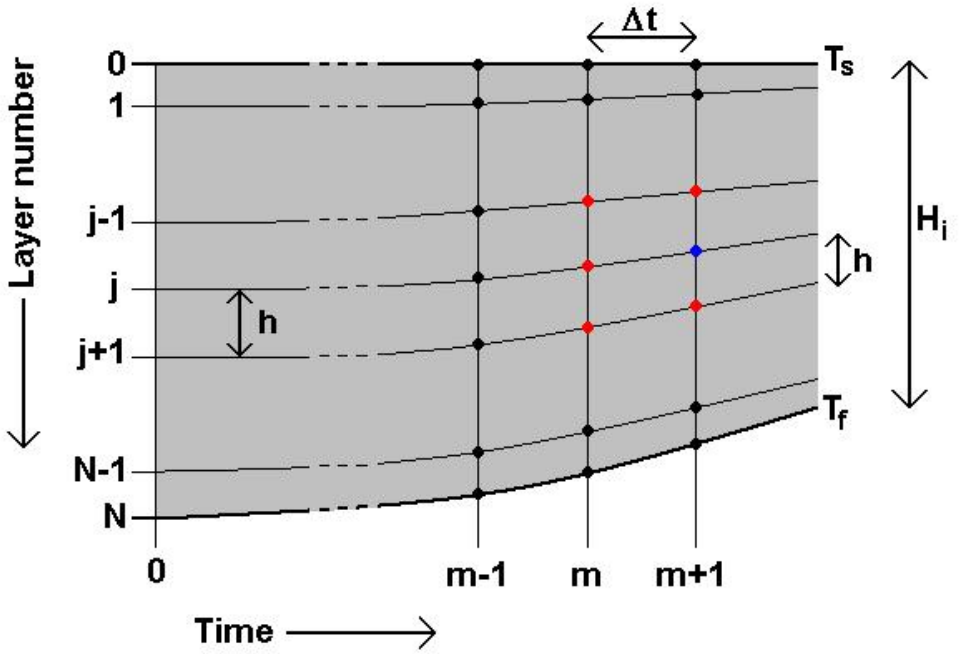

Figure 3.14: The numerical interpolation scheme for heat conservation in the ice layer. The temperature T_j^{m+1} at the point marked in blue depends on the temperatures at all the points marked in red. The scheme is solved using the Crank-Nicholson form with boundaries defined by the known surface temperature T_s and ice bottom temperature T_f. The vertical grid size $h = \frac{H_i}{N}$ changes with ice thickness H_i.

The ice layer of thickness H_i must be divided into N equal-sized layers, where each layer has thickness $h = \frac{H_i}{N}$. So the jth layer is at depth $z_j = jh$, $(j = 0, 1, 2...N)$. The maximum number of layers used was $N = 100$. Similarly, for the model timestep Δt, the mth timestep is at time $t_m = m\Delta t$, $(m = 0, 1, 2...)$. As a result of this approach the thickness of the internal layers changes on each timestep in proportion with the ice thickness (Figure 3.14).

Equation 3.44 can then be solved for an arbitrary ice layer by integrating it over the intervals $[z_{j-\frac{1}{2}}, z_{j+\frac{1}{2}}]$ and $[t_m, t_{m+1}]$. For simplicity, the subscript i for ice is dropped in the following calculations and the notation T_j^m, for the ice temperature at timestep m in layer j, is adopted.

The first term of Equation 3.44 becomes:

$$\int_{z_{j-\frac{1}{2}}}^{z_{j+\frac{1}{2}}} \int_{t_m}^{t_{m+1}} \rho c \frac{\partial T}{\partial t} dz dt \approx h\rho c(T_j^{m+1} - T_j^m) \tag{3.45}$$

The second term of Equation 3.44 must be rewritten by defining a function $X(z,t) = \frac{\partial T}{\partial z}$. The value of this derivative at a depth of (e.g.) $z_{j+\frac{1}{2}}$ can be

approximated by the central difference method as:

$$X^m_{j+\frac{1}{2}} \approx \frac{T^m_{j+1} - T^m_j}{h} \tag{3.46}$$

so the integral of the second term of Equation 3.44 is:

$$\begin{aligned} &\int_{z_{j-\frac{1}{2}}}^{z_{j+\frac{1}{2}}} \int_{t_m}^{t_{m+1}} k\frac{\partial X}{\partial z} dz dt = k \int_{t_m}^{t_{m+1}} (X^m_{j+\frac{1}{2}} - X^m_{j-\frac{1}{2}}) dt \\ &\approx \left(\frac{k\Delta t}{2}(X^{m+1}_{j+\frac{1}{2}} + X^m_{j+\frac{1}{2}}) - \frac{k\Delta t}{2}(X^{m+1}_{j-\frac{1}{2}} + X^m_{j-\frac{1}{2}}) \right) \end{aligned} \tag{3.47}$$

where the time integration is an approximation which is sufficient provided the timestep is short. Expanding all the X terms according to Equation 3.46 and rearranging gives:

$$\frac{k\Delta t}{2h}(T^{m+1}_{j+1} - 2T^{m+1}_j + T^m_{j+1} - 2T^m_j + T^{m+1}_{j-1} + T^m_{j-1}) \tag{3.48}$$

The integral of the third term of Equation 3.44 is approximated by:

$$\int_{z_{j-\frac{1}{2}}}^{z_{j+\frac{1}{2}}} \int_{t_m}^{t_{m+1}} \kappa(1-\alpha)Q_s \exp(-\kappa z) dz dt \approx h\Delta t \kappa (1-\alpha) Q_s \exp(-\kappa z_j) \tag{3.49}$$

Rearranging all the terms, the iterative scheme representing Equation 3.44 can be rewritten for an arbitrary layer j at time t_{m+1} and time t_m:

$$\begin{aligned} T^{m+1}_j - T^m_j &= \frac{k\Delta t}{2\rho c h^2}\left(T^{m+1}_{j+1} - 2T^{m+1}_j + T^m_{j+1} - 2T^m_j + T^{m+1}_{j-1} + T^m_{j-1}\right) \\ &\quad + \frac{k\Delta t}{2\rho c h^2}\left(\frac{2h^2}{k}\kappa(1-\alpha)Q_s \exp(-\kappa j h)\right) \end{aligned} \tag{3.50}$$

Equation 3.50 includes terms depending on both the known temperatures at the previous time t_m and the unknown values at time t_{m+1}. It also depends on the temperatures of the neigbouring ice layers at depths z_{j-1} and z_{j+1}. It must therefore be written in the Crank-Nicholson form and solved by Gaussian elimination,

as described in Smith (1985). This requires known boundary conditions at the top and bottom of the ice layer.

The top boundary condition is the surface temperature $T_s(t)$, which is calculated at every timestep by considering the balance of heat fluxes (see later). The bottom boundary condition occurs where the ice is in contact with the lake water, so can be assumed to stay constant at the freezing point of water, $T_f = 273.15$ K. Putting everything known on the right hand side, and everything unknown on the left, the Crank-Nicholson form is:

$$\begin{aligned}
T_0^{m+1} &= T_s(t_{m+1}) \\
+b_1 T_1^{m+1} - c_1 T_2^{m+1} &= d_1 \\
-a_2 T_1^{m+1} + b_2 T_2^{m+1} - c_2 T_3^{m+1} &= d_2 \\
... &= ... \\
-a_j T_{j-1}^{m+1} + b_j T_j^{m+1} - c_j T_{j+1}^{m+1} &= d_j \\
... &= ... \\
-a_{N-1} T_{N-2}^{m+1} + b_{N-1} T_{N-1}^{m+1} &= d_{N-1} \\
T_N^{m+1} &= T_f
\end{aligned} \tag{3.51}$$

where the a's, b's, c's and d's are all known quantities. Defining a constant $C = \frac{k\Delta t}{2\rho c h^2}$, Equation 3.50 can be written with known quantities on the right and unknowns on the left:

$$\begin{aligned}
&-CT_{j-1}^{m+1} + (2C+1)T_j^{m+1} - CT_{j+1}^{m+1} \\
&= CT_{j-1}^m + (1-2C)T_j^m + CT_{j+1}^m + \tfrac{2Ch^2}{k}\kappa(1-\alpha)Q_s \exp(-\kappa j h)
\end{aligned} \tag{3.52}$$

On comparing Equations 3.51 and 3.52, the required constants are:

$$\begin{aligned}
a_j &= C \\
b_j &= 2C+1 \\
c_j &= C
\end{aligned} \tag{3.53}$$

for all j where $j = 1...N-1$. The values of d_j are:

$$\begin{aligned} d_1 &= CT_s(t_{m+1}) + CT_s(t_m) + (1-2C)T_1^m \\ &\quad + CT_2^m + \frac{2Ch^2}{k}\kappa(1-\alpha)Q_s\exp(-\kappa h) \\ d_j &= CT_{j-1}^m + (1-2C)T_j^m + CT_{j+1}^m \\ &\quad + \frac{2Ch^2}{k}\kappa(1-\alpha)Q_s\exp(-\kappa jh) \\ d_{N-1} &= 2CT_f + CT_{N-2}^m + (1-2C)T_{N-1}^m \\ &\quad + \frac{2Ch^2}{k}\kappa(1-\alpha)Q_s\exp(-\kappa h(N-1)) \end{aligned} \tag{3.54}$$

where the second equation applies to $j = 2...N-2$. Continuing to follow the notation of Smith (1985), we define two variables A and S:

$$\begin{aligned} A_1 &= b_1 \\ A_i &= b_i - \frac{a_i}{A_{i-1}}c_{i-1} \end{aligned} \tag{3.55}$$

$$\begin{aligned} S_1 &= d_1 \\ S_i &= d_i + \frac{a_i}{A_{i-1}}S_{i-1} \end{aligned} \tag{3.56}$$

where $i = 2, 3...N-1$. The ice temperature at each internal layer in the ice for the new time t_{m+1} can be calculated using:

$$\begin{aligned} T_{N-1}^{m+1} &= \frac{S_{N-1}}{A_{N-1}} \\ T_j^{m+1} &= \frac{1}{A_j}(S_j + c_j T_{j+1}) \end{aligned} \tag{3.57}$$

where the calculations for the second equation must be done in reverse order, $j = N-2, N-1...2, 1$. For a full proof of the Gaussian elimination technique see Smith (1985).

3.5.2 Calculation of ice surface temperature

The air-ice interface temperature T_s is important for the calculation of the surface heat balance, the physical phase transitions and as a boundary condition in the solution of the heat conservation equation. To calculate, it is considered to be the temperature which will cause the sum of fluxes at the ice surface to be zero. Some of the parameterised fluxes depend on T_s while some do not, but it is possible to write the equation to be solved as:

$$F(T_s) = 0 \tag{3.58}$$

where $F(T_s)$ represents the sum of all the surface fluxes, as a function of T_s. An iterative Newton-Raphson method is used for the solution of Equation 3.58. An initial guess of $T_s(n = 0)$ must be made, in each case it is set equal to the air temperature T_a at the current timestep. Thereon the succeeding step $n + 1$ is calculated according to:

$$T_s(n+1) = T_s(n) - \frac{F(T_s(n))}{F'(T_s(n))} \tag{3.59}$$

where $F'(T_s)$, the derivative term with respect to T_s, was calculated numerically. Equation 3.59 was calculated repeatedly until the point where $|T_s(n+1) - T_s(n)| < 0.001$. This condition was deemed to give sufficient accuracy (to the third decimal point in T_s).

3.5.3 Calculation of ice thickness change

The change in ice thickness H_i is proportional to the balance of fluxes at the top and bottom of the ice layer. In each case the positive direction is taken as downwards at the top of the ice and upwards at the bottom of the ice:

$$\frac{dH_i(sfc)}{dt} = -\frac{1}{\rho_i L_f} \sum (\text{Surface Fluxes}) \tag{3.60}$$

$$\frac{dH_i(bot)}{dt} = -\frac{1}{\rho_i L_f} \sum (\text{Bottom Fluxes}) \tag{3.61}$$

where ρ_i is ice density and L_f is the latent heat of freezing for water. The total change in ice thickness is found by adding together Equations 3.60 and 3.61.

3.5.4 Periods of ice break-up

A number of complex factors come into play in the period of summer ice break-up, such as the effects of wind-induced mixing when open areas of water appear. Such factors are somewhat stochastic and difficult to model, and were found to be unnecessary for modelling the 2003 ice thickness, which did not go to zero. Therefore they are not considered in this chapter; instead they are indirectly assumed to cancel one another out. The model contained code which ensured that if the calculated ice thickness went to zero or below it was reset to a minimum value of 0.001 m.

The implications of such an approach with regard to model predictions are discussed further in Chapter 6.

3.6 Running the model

3.6.1 Initial conditions

The model was started at a given time with known values of the input variables from the data, but it was necessary to choose initial values for the 'unknowns' in the model, in order to calculate the first values of the heat and radiation fluxes. The values assigned for time $t = 0$ were:

- **Ice surface temperature** - $T_s(0)$ was set equal to the initial air temperature $T_a(0)$.
- **Ice internal temperature** - $T_i(0, j)$ for the internal layers $j = 1, 2...N-1$ was set as linear between the top (T_s) and bottom (T_f) temperatures of the ice layer.
- **Ice thickness** - $H_i(0)$ was set to the first measured ice thickness value from the data.

With iterative calculations of ice temperatures, initial values do not significantly affect the model output, and after the first timestep they reach accurate values,

so do not require a 'spin-up' period. However for the main model output, only the *changes* in ice thickness are calculated iteratively. Setting $H_i(0)$ equal to the data assumes that the first datapoint is completely accurate, with no component of noise. This is unlikely, so such an approach may cause a consistent error to propagate through the model output. This approach was used in model development, but on fitting the model to data, it is more accurate to allow $H_i(0)$ to be an adjustable parameter.

3.6.2 Model integration

The main differential equation to be solved is the heat conservation equation (Equation 3.42). Its solution has been explained, but the choice of timestep Δt requires some consideration with regard to integration over time.

The Crooked Lake probe data was measured at intervals of 5 minutes, but the Davis meteorological data was only taken every 3 hours. Some initial model runs were undertaken using the 5-minute data, but as explained in Section 3.2 it was deemed preferrable to parameterise the model with the Davis data, so the benefit or dangers of using a 3-hour timestep were considered. During the deployment of the Crooked Lake probe, the mean change in ice thickness over each 3-hour period was less than 10^{-3} m. This is less than 0.1 % of the mean ice thickness over the year, and at the minimum scale of accuracy of the measurements (3 decimal points), so evaluating the model directly from the previous values is unlikely to propagate errors over three hours. Also on considering the timescales of changes in the atmospheric variables that affect the ice layer, such as seasonal changes (many months) or shifts in weather patterns (3 days or more), the shortest significant change is the diurnal cycle. A 3-hour timestep gives 8 steps in the space of a day so adequately illustrates any day-to-night effects.

This notion was supported when the model was evaluated using firstly the Euler method with a 3-hour timestep, then the Runge-Kutta method, where data was linearly interpolated to allow the method to choose intermediate timesteps. No difference was found between the model outputs from the two methods, so for ease and speed of calculation the Euler method was adopted.

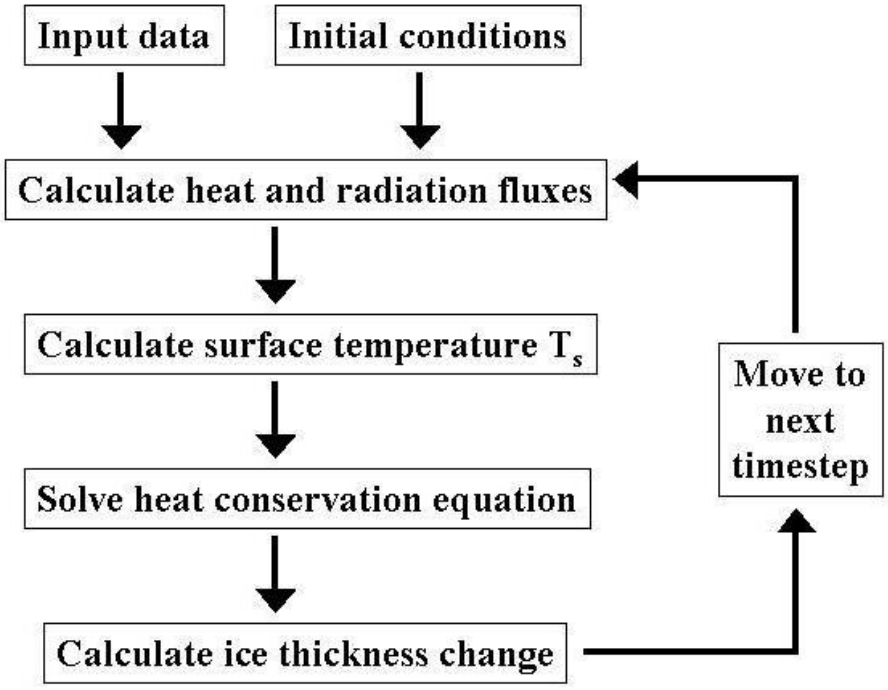

Figure 3.15: Flowchart summarising the solution method of the physics-based model of Crooked Lake.

3.7 Summary

This chapter has outlined the processes involved in developing and running a real-time thermodynamic model of the ice on Crooked Lake, Antarctica. It has included the initial calculations of important variables from field data, the approach employed when choosing between different equations from the literature, and the solution methods that were implemented. Figure 3.15 summarises the model, and Table 3.10 classifies all the quantities in the model according to the definitions in Chapter 2. All scalar quantities have been estimated in the model development based on values from the literature - those quantities known to high degree of accuracy have been named as 'constants', while those quantities known to a lesser degree of accuracy are named 'parameters' and the effects of adjusting them are investigated later. This includes the number of layers N defined in the ice temperature calculation, which does not strictly represent a real physical quantity but is treated in a similar way. It also includes the initial value given to the ice thickness ($H_i(0)$) - an unusual measure for a model of this sort.

The model has been developed using the working definition of 'hierarchical reductionism' described in Chapter 1. It may be said that the model includes as much detail as could reasonably be expected in a full description of the processes

Definition	Quantities
Input variables	$T_a\ T_w\ RH\ V\ C\ p_a\ \alpha\ \kappa$
Constants	$R_g\ M_a\ z_a\ g\ T_f\ \rho_i\ c_i\ k_i\ \epsilon_i\ L_f\ S\ \sigma\ c_a\ \pi$
Parameters	$R_c\ N\ \xi\ k_w\ H_i(0)$
Intermediate variables	$e_s\ e_a\ q_s\ q_a\ T_s\ T_i\ \rho_a\ R_l\ I\ Z\ C_H\ C_D\ C_E\ C_{DN}\ Q_s\ Q_b$ $Q_d\ Q_h\ Q_l\ F_i\ F_b\ F_w\ z_0\ z_T\ z_q\ \Psi_M\ \Psi_H\ \Psi_E\ R_e\ \gamma\ R_z\ h$
Model output	H_i
Dimensions	z t

Table 3.10: Quantities used in the physics-based model defined according to the categories outlined in Chapter 2.

affecting the ice layer on Crooked Lake. The model does not stray beyond the necessary fields of solid state thermodynamics (for the ice) or fluid dynamics (for the atmosphere and water), but includes nearly all the applicable physical theory from within those fields. Some aspects are not explicitly parameterised, for example the appearance of leads (cracks) in the ice or areas of open water, but these are later indirectly accounted for by allowing certain parameters (e.g. surface roughness) to vary over the course of the year. In other words, it is close to being as complex a model as even the most hardened reductionist could argue for without being over-pedantic. Chapters 5 and 6 examine the benefits and disadvantages of this reductionist approach when compared to more holistic or parsimonious models.

Chapter 4

A physics-based model of lake ice - Analysis

4.1 Overview

This chapter outlines the parameterisation and statistical analysis of the physics-based model described in Chapter 3. The model is close to being entirely mechanistic, as all the quantities involved have been estimated or modelled using values and equations from established literature. Excessive parameterisation has been avoided, in that no arbitrary equations have been invented for adjusting to fit data without physical meaning. The analyses in this chapter are kept within strict constraints, so that the procedures will not lead to any unrealistic parameter values. This distinguishes the model from empirical models where parameters can be adjusted without limit to improve the fit; such approaches are concerned with the 'usefulness' of a model over the physical insight gained, and are examined in the next chapter.

The accuracy of the model was assessed by varying the number of finite layers used in the numerical solution of the heat conservation equation for the ice layer, and weighing up any changes in model fit against the time taken for calculations. The sensitivity to parameters was assessed by individually varying them over realistic ranges and calculating the goodness of fit, as well as using Levenberg-Marquardt optimisation. This led to information on which parameters were most important in producing the model output, and which could be set to constant values. The importance of individual input variables was assessed using the 'model trimming' technique described in Chapter 2.

4.2 Initial model runs

Five model parameters were defined in Table 3.10, which were chosen because they were not known to a high degree of accuracy. Estimates for these were discussed in the Chapter 3, and the initial values are given in Table 4.1. Each is also given an upper and lower constraint value for optimisation, which are both physically realistic. The constraint for the initial ice thickness value $H_i(0)$ was set to be 0.01 m either side of the starting value indicated by the data, corresponding to an estimate of the measurement error on the data. The number of layers N used in the internal ice temperature calculations was constrained between 3 (giving simply an ice surface temperature T_s, internal ice temperature T_i and ice bottom temperature T_f), and 200 (giving a layer size of less than 1cm for the whole year). The other parameter constraints were chosen to represent what may be expected as the extreme physical values from numerical estimates and manual observation of the system. In Chapter 3, k_w was estimated to be on the order of 10 W m^{-2} K^{-1}, so was constrained to values between 5 and 20. ξ was constrained to values between 0.001 m (for smooth, flat ice) and 0.2m (for rough, broken ice or ice with scattered snow cover). R_c was kept between -1 and 1 to represent a range of atmospheric stability regimes that may be induced by the surface.

Parameter	Units	Initial value	Lower constraint	Upper constraint
k_w	W m^{-2} K^{-1}	10	5	20
ξ	m	0.1	0.001	0.2
R_c	(unitless)	0	-1	1
$H_i(0)$	m	$D_i(0)$	$D_i(0) - 0.01$	$D_i(0) + 0.01$
N	(unitless)	10	3	200

Table 4.1: Initial values of parameters for model analysis, and the upper and lower constraints on each. $D_i(0)$ corresponds to the first measured value of ice thickness for the time period.

With the initial parameter values, the model was successfully run to completion (Figure 4.1). The goodness of fit ($\chi^2 = 150.3$, $r^2 = 0.08$, $\nu = 2009$) was low, but the general shape of the data was reproduced, with what appeared to be a consistent offset, so it was decided that model analysis would continue using the equations in the current form.

Several model runs over much shorter timescales were undertaken during the development of this model, but will not be reported in this thesis. Instead the analysis concentrates on finding a model which covers the whole year's measured ice thickness from 17 January 2003 to 12 January 2004, as plotted in Figure 4.1. This is so that the model will not be specific to one particular time of year and

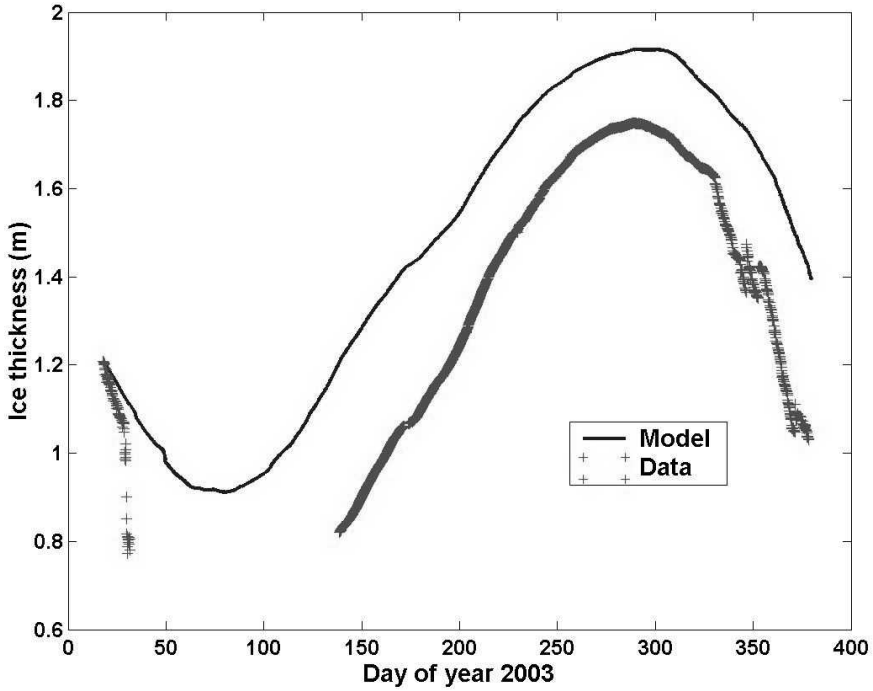

Figure 4.1: Ice thickness calculated in the first run of the physics model (solid line), plotted with the data (crosses). All parameters were estimated from the literature, not fitted to the data.

will be as generalisable as possible, to predict the future of the ecosystem as a whole.

4.3 Optimisation

The Levenberg-Marquardt optimisation procedure was used to find better-fitting parameter values (Table 4.2). The goodness of fit to the data improved ($\chi^2 = 17$, $r^2 = 0.89$, $\nu = 2005$). The calibrated values for the three parameters ξ, R_c and $H_i(0)$ were at the extreme values set by their constraint ranges.

The t-value for each parameter estimate in Table 4.2 applies to the test of whether or not the parameter value is significantly different from the initial values given in Table 4.1. For the null hypothesis $H_0 : p_i(new) = p_i(old)$ versus $H_1 : p_i(new) \neq p_i(old)$, the t-statistic is simply calculated as the ratio of the difference to the standard error: $t = \frac{p_i(new) - p_i(old)}{\sigma(P_i(new))}$. A two-tailed 5 % significance test with 'infinite' degrees of freedom requires a value for the t-variate with magnitude of at least 1.96 (the model has $\nu = N - n_p - 1 = 2009 - 4 - 1 = 2004$ degrees of freedom, which is effectively infinite for a t-test). Therefore one cannot say with 95 %

Parameter	Optimised value	Standard error	t-statistic
k_w	17.30	0.34	21.47
ξ	0.001	0.12	-0.83
R_c	1	2.31×10^4	4.33×10^{-5}
$H_i(0)$	$D_i(0) - 0.01$	0.023	-0.43

Table 4.2: Estimated values for the parameters in Table 4.1, the standard errors estimated for each from the Hessian matrix of parameter estimates, and the t-statistics which test the null hypothesis that the values are no different from the initial values in Table 4.1.

certainty that the new values of ξ, R_c or $H_i(0)$ are statistically different from the initial estimates. This is also evident from the standard errors, with R_c in particular showing a huge error, suggesting that R_c was having very little effect on the model output. This was investigated further using sensitivity analysis in the next section.

4.4 Sensitivity analysis

Each parameter was varied over the ranges defined in Table 4.1, while keeping all other parameters at the values attained in the first optimisation (Table 4.2). The calculated χ^2 values were plotted against the parameters (Figure 4.2).

Each of the graphs in Figure 4.2 were plotted on the same y-axis scale. It was immediately seen that k_w was the most important parameter in terms of the goodness of fit. Altering the initial ice thickness $H_i(0)$ gave a slightly better fit at values lower than the first data point. This may suggest the model is sensitive to initial conditions, and the ice thickness data at the start of the model run, in mid summer 2003, may be affected by phenomena that are not accounted for in the model. However the size of this change is small, and for the rest of the models in this thesis it is sufficient to take the initial value of ice thickness directly from the data.

Altering the parameters ξ and R_c also produced no significant change in χ^2. Such flat graphs demonstrate that the model fit is not affected by changes in either of these parameters. As demonstrated in section 4.3, attempts to calibrate them within the specified ranges led to high standard errors in the parameter estimates. In the case of R_c any changes in χ^2 are negligible and it is acceptable to use the value $R_c = 0$, as suggested in Launianen and Cheng (1998).

The size of the constraint range over which k_w was varied was, in absolute terms,

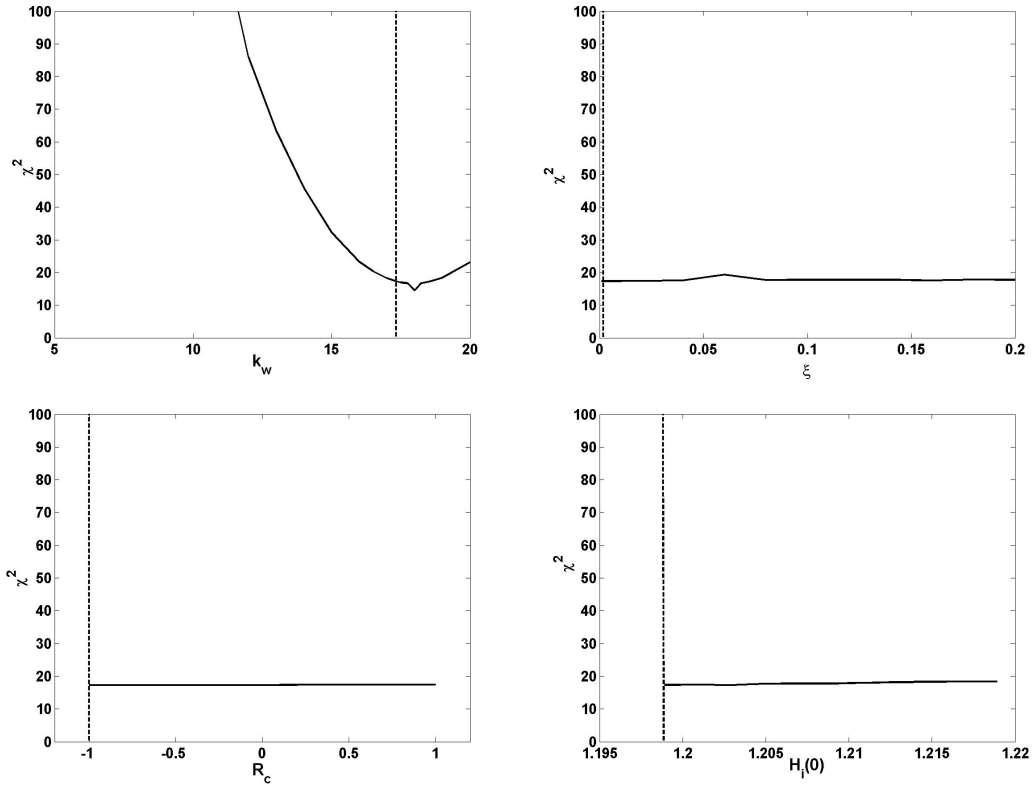

Figure 4.2: Residual sum of squares χ^2 versus parameter values across the ranges defined in Table 4.1 for, clockwise from top left: k_w, ξ, $H_i(0)$, R_c. Vertical dashed lines mark the parameter values found in optimisation.

significantly larger than the ranges of the other parameters. To give a better idea of the changes in χ^2 with respect to the numerical size of the parameter, the local gradients of χ^2 with respect to each parameter ($\frac{\partial \chi^2}{\partial p_i}$) at the optimised values were calculated. The local gradient approximation for model sensitivity ($\frac{\partial M}{\partial p_i}$) was also calculated, taking M as the mean value of ice thickness calculated for the year (Table 4.3).

In absolute terms, the rates of change of χ^2 and M with respect to ξ are greater than that for k_w. This implies that in an empirical model, where ξ is not bound by such a strict belief in the physical theory and is instead an arbitrary parameter for model-fitting, the optimisation procedure would have the freedom to find better-fitting values, and ξ may become more important (at higher or lower values than the current range allows). For example, a value of $\xi = 100$ may give a much better goodness of fit, but would no longer have any meaning in terms of surface aerodynamics (a flat surface like ice would never have a geometric roughness length as high as 100 m). In this chapter, where the model is developed using only 'textbook' equations and definitions, the parameter ranges are kept within the 'known rules'. Therefore using the information from Figure 4.2, ξ and R_c are

Parameter p_i	**Value**	$\frac{\partial \chi^2}{\partial p_i}$	$\frac{\partial M}{\partial p_i}$
k_w	18.0	0.23	-0.026
ξ	0.001	4.10	-0.075
R_c	0	0.14	-0.006

Table 4.3: Rates of change of the residual sum of squares χ^2 with parameters, and rates of change of the model output M (defined as mean ice thickness) with parameters, calculated at the optimised values.

set as constants, using the values in Table 4.3. The model has been reduced to having only one adjustable parameter, k_w.

4.5 Model accuracy

The number of layers defined during the solution of the heat conservation equation in the ice layer (N) is not strictly an adjustable parameter under some definitions, but rather an accuracy setting for the model. Also, the larger the value of N, the longer the model may take to run. A suitable value of N was required before either accepting an inaccurate model or taking a long time running a computationally intensive model.

The model was executed for a number of values of N between 3 and 200, and the goodness of fit calculated (Figure 4.3). The time taken for model execution on a Windows 2000 PC was also noted, taking care to have no other programs open which may have used computer resources.

The model execution time increased approximately linearly with N. The goodness of fit was, unexpectedly, best at low values of N (χ^2 was lower), before levelling off at higher values of N. This may be caused by 'numerical dispersion', whereby dispersion across a distance in a numerical solution to a differential equation increases with the size of finite layers used. This phenomenon is useful for modelling systems where dispersion occurs, such as trace chemicals in soil (e.g. Smith and Elder 1999), but has not been chosen for that purpose in this thesis. A solution with low N is further from the true solution to the differential equation in question (Equation 3.42), and does not provide much information on the internal temperature structure of the ice. It was decided that a value of $N = 50$, with a runtime of around 1 minute, would be used for all the forthcoming model analysis. For a typical ice layer between 1 and 2 metres thick this corresponds to a layer size between 2 and 4 cm.

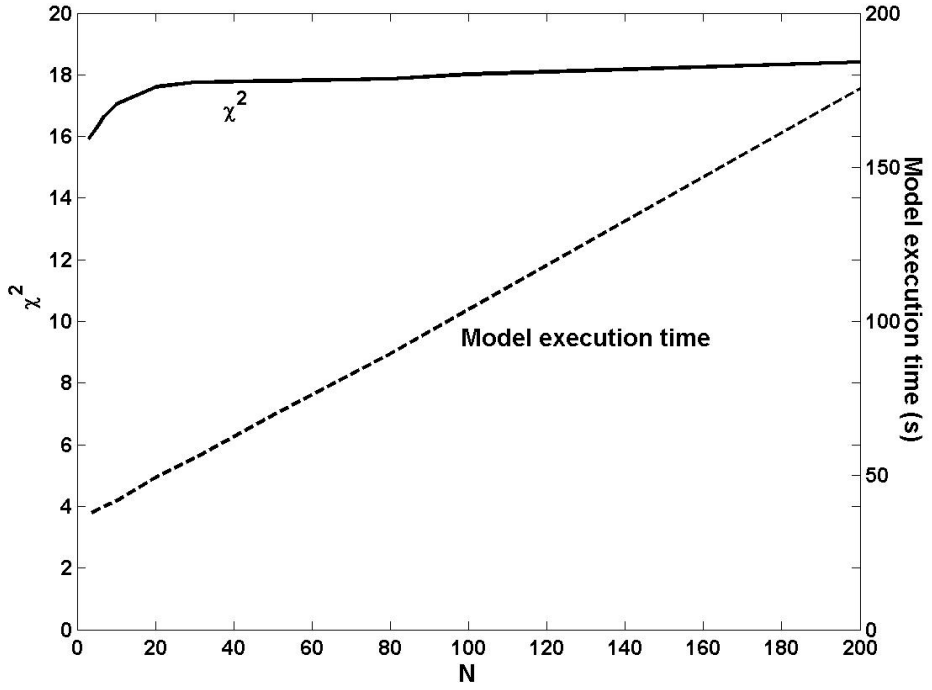

Figure 4.3: Residual sum of squares and model execution time for the physics model with the initial parameter estimates given in Table 4.1, calculated for various values of N, the number of layers defined in the ice temperature calculations.

4.6 Model results

The input variables, intermediate variables and output of the model, with the 'optimum' parameter values found above, are presented in Figures 4.4 to 4.12. Every calculated variable remained within values that may be expected from the literature.

Figure 4.4 shows all the input variables to the model plotted over the whole year of 2003. T_a, p_a, RH, V and C come from data measured at Davis station. T_w, α and κ were measured on the Crooked Lake probe and are linearly interpolated over the times when no data were recorded (1 February to 15 May 2003). Diurnal variations were apparent in the air temperature, and to a small extent in the water temperature, while all other variables showed variation over longer timescales pertaining to changes in weather. Figure 4.5 shows the specific humidity in the air (q_a) and on the ice surface (q_s), which determine the latent heat flux between the ice and the air, and were calculated from air temperature and relative humidity.

Figure 4.6 shows the daily mean values of all the calculated heat and radiation fluxes at the top of the ice layer (diurnal variation is removed for neatness of

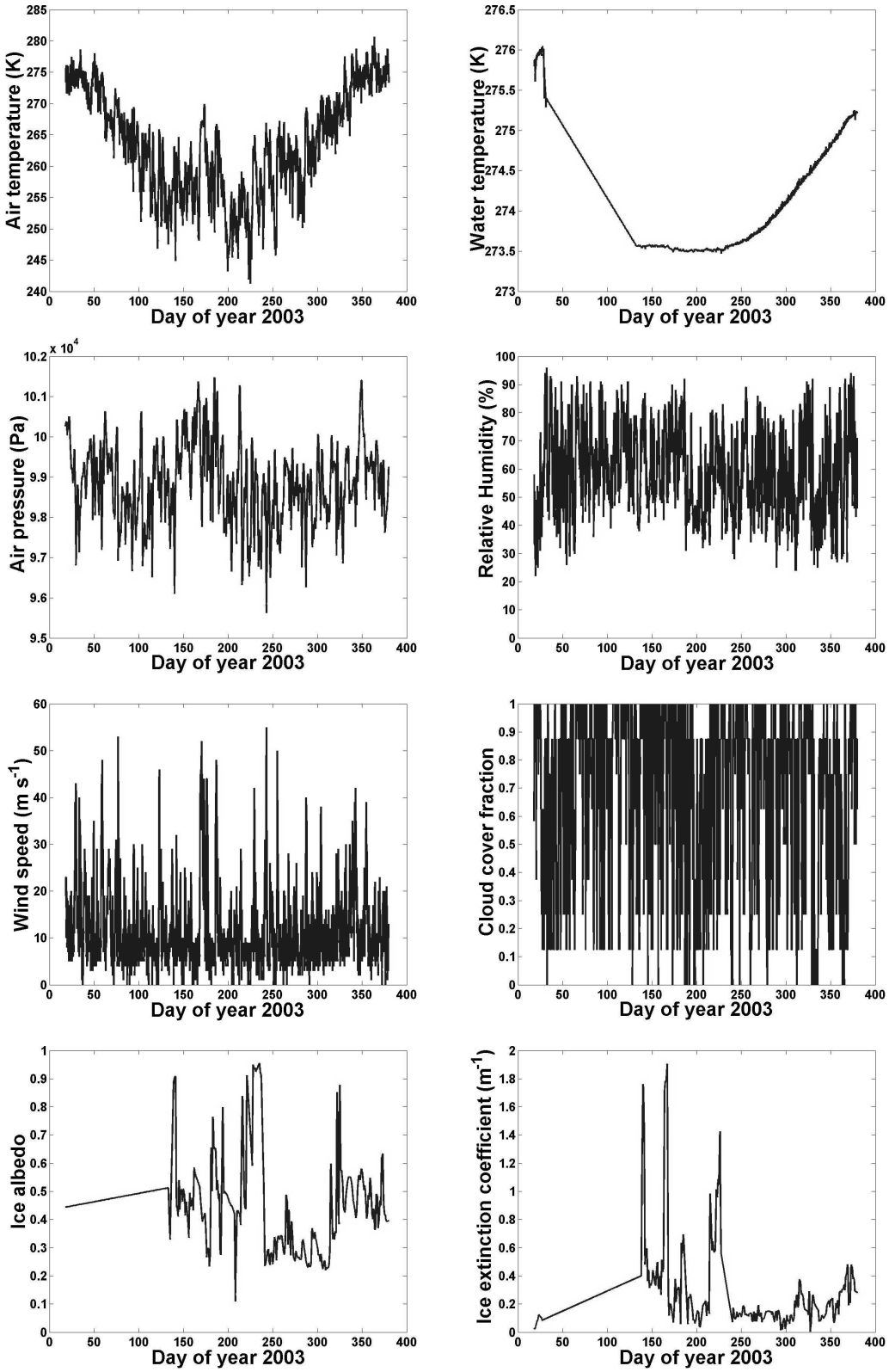

Figure 4.4: Input variables to the physics-based model: air temperature T_a, water temperature T_w, air pressure p_a, relative humidity RH, wind speed V, cloud cover fraction C, ice albedo α and ice extinction coefficient κ.

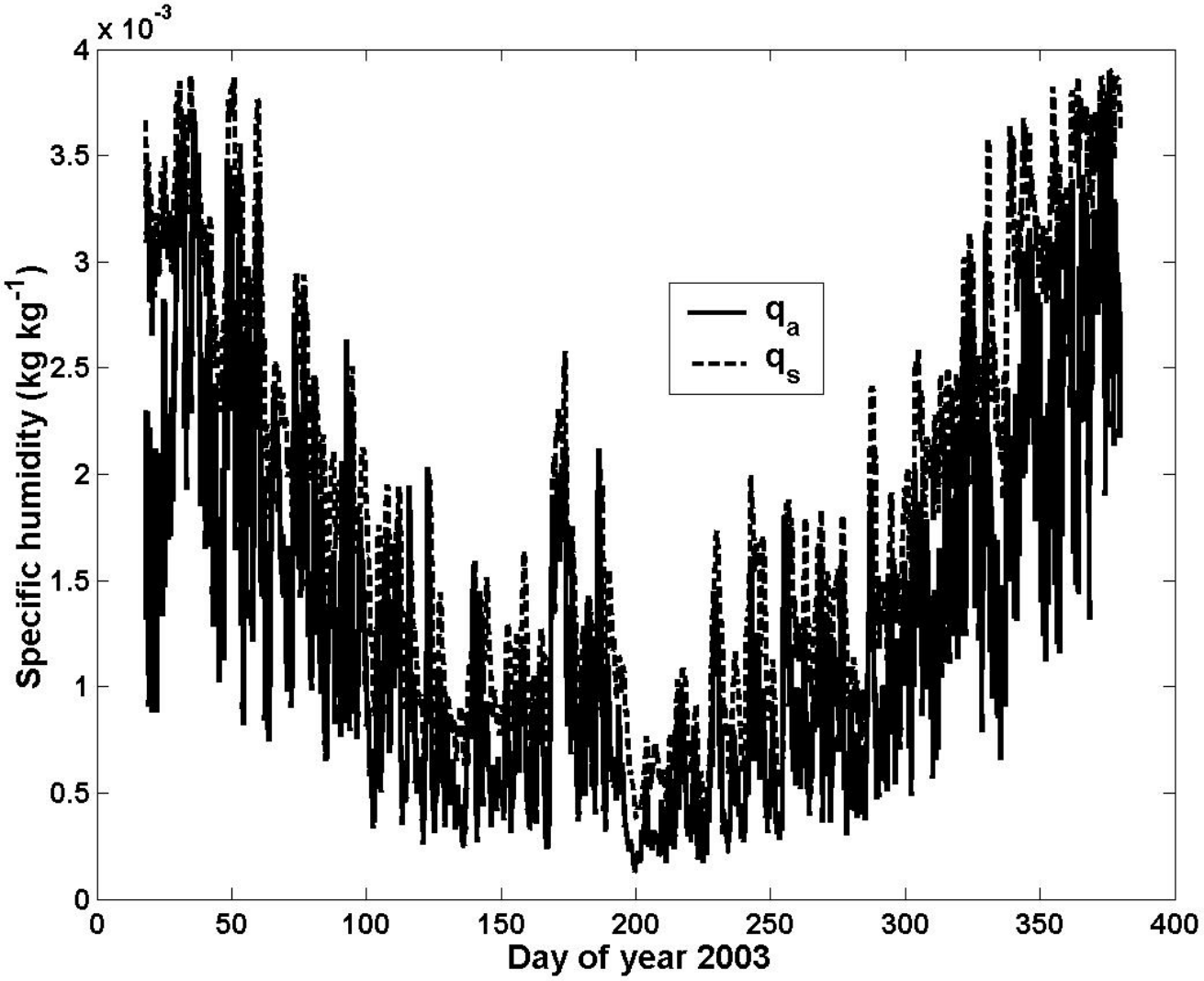

Figure 4.5: Specific humidity of air 1 m above Crooked Lake (q_a) and at the ice-air interface (q_s), as calculated in the physics-based model for 2003.

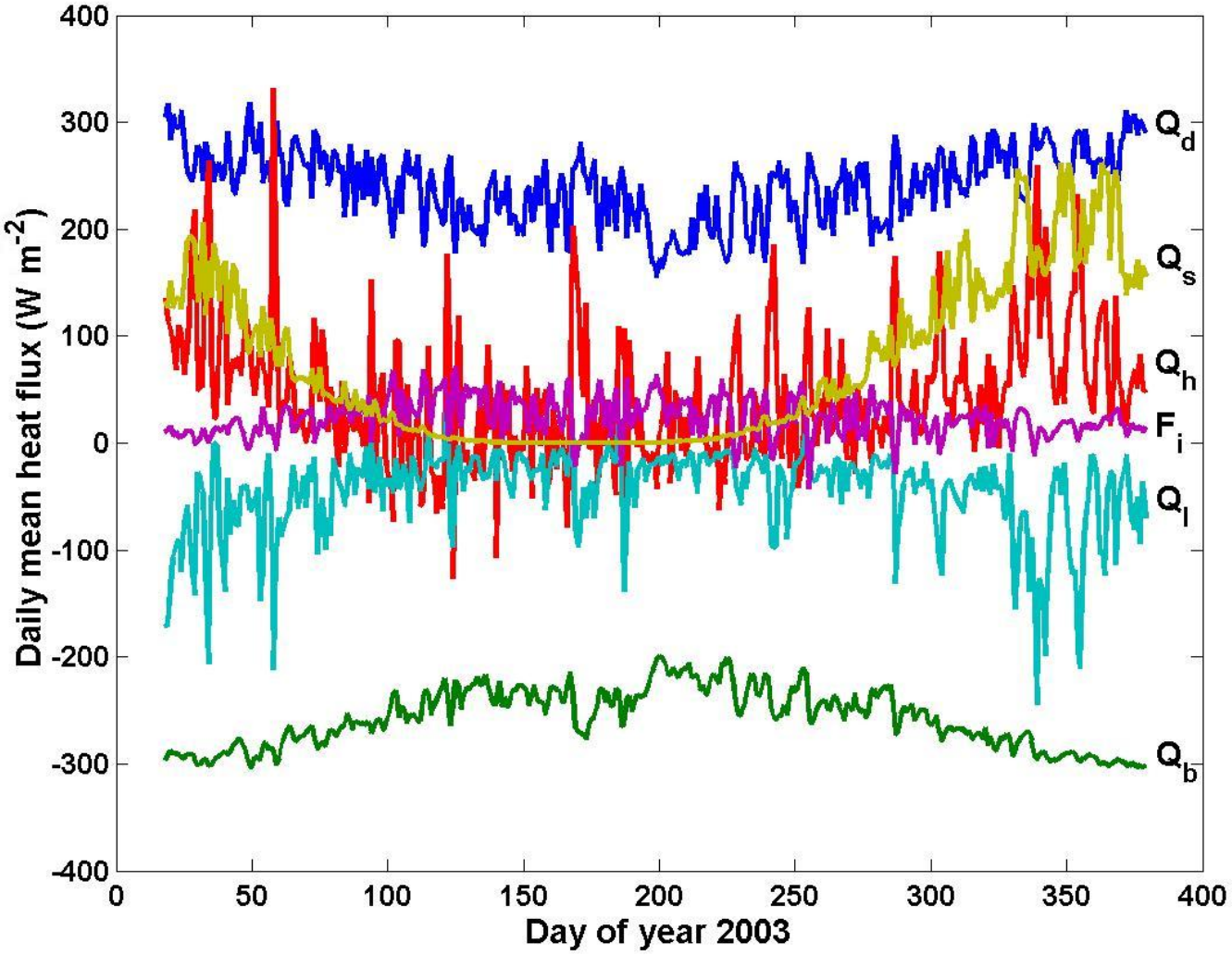

Figure 4.6: Daily means of heat and radiation fluxes at the ice-air interface on Crooked Lake as calculated in the physics-based model for 2003. These are downwelling shortwave (Q_s), downwelling longwave (Q_d), upwelling longwave (Q_b), sensible heat (Q_h), latent heat (Q_l) and conductive heat (F_i). Direction towards the ice (downwards) is positive.

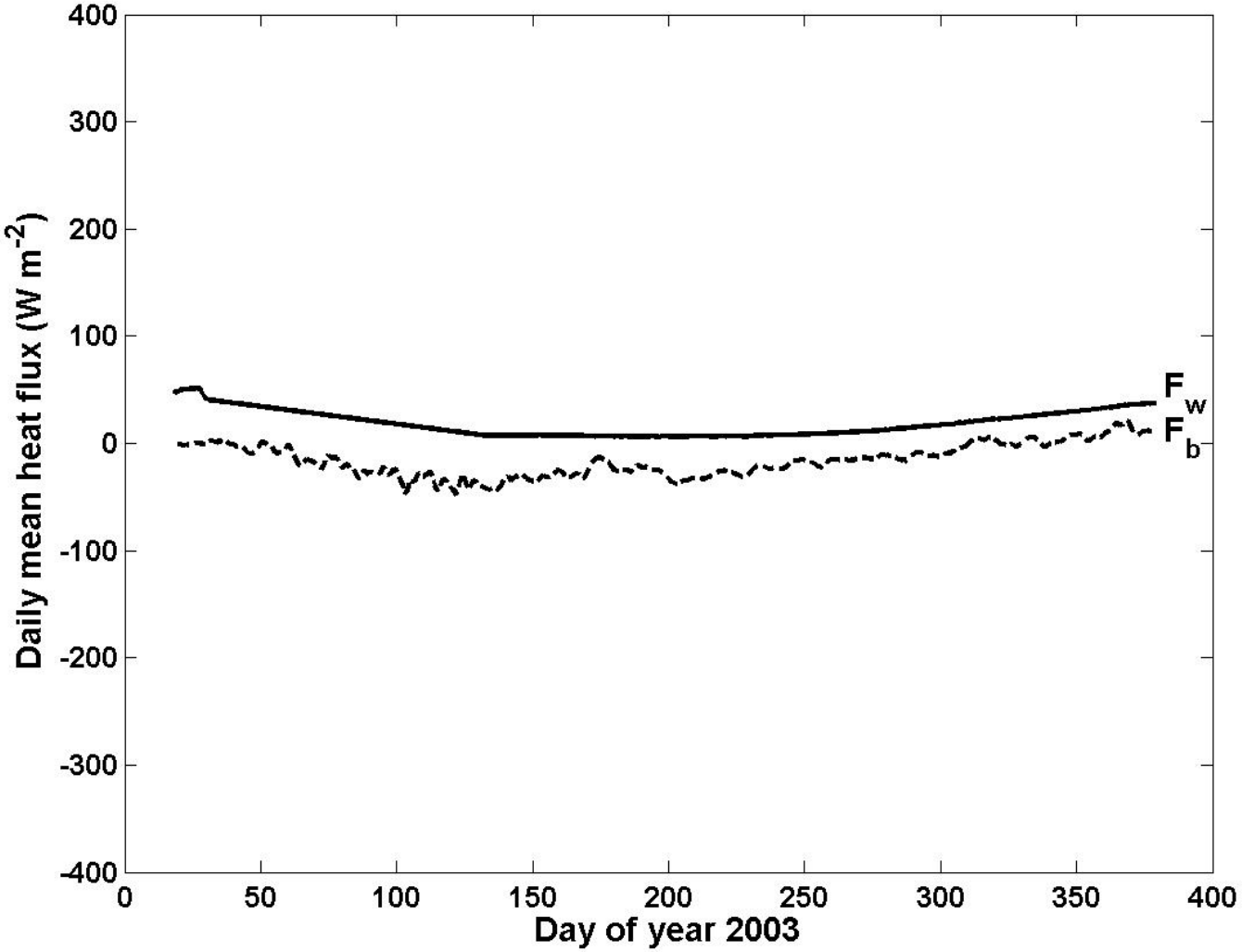

Figure 4.7: Daily means of heat and radiation fluxes at the ice-water interface on Crooked Lake as calculated in the physics-based model for 2003. These are sensible heat (F_w) and conductive heat (F_b). Direction towards the ice (upwards) is positive.

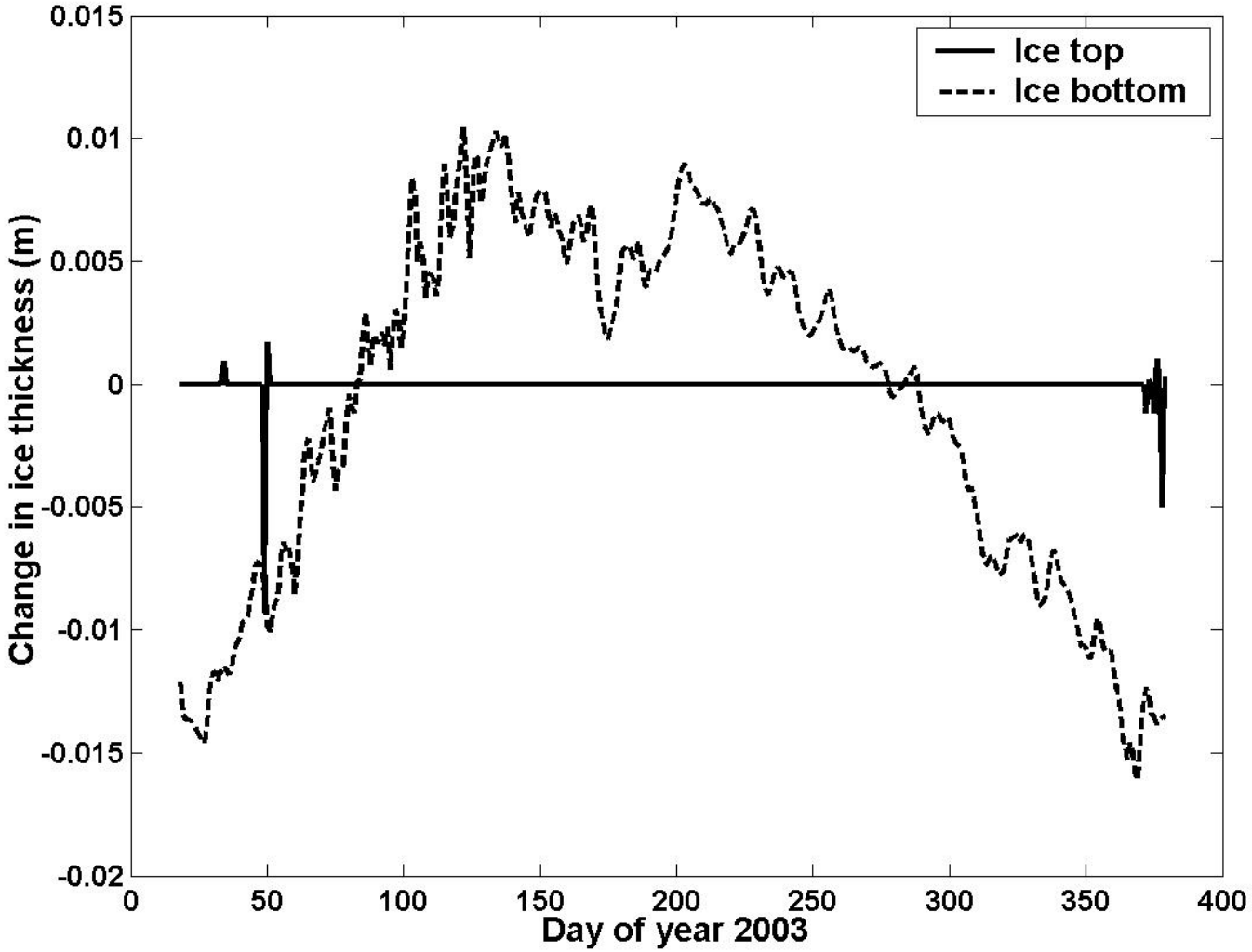

Figure 4.8: Daily changes in ice thickness at the top and bottom of the ice layer on Crooked Lake as calculated in the physics-based model for 2003.

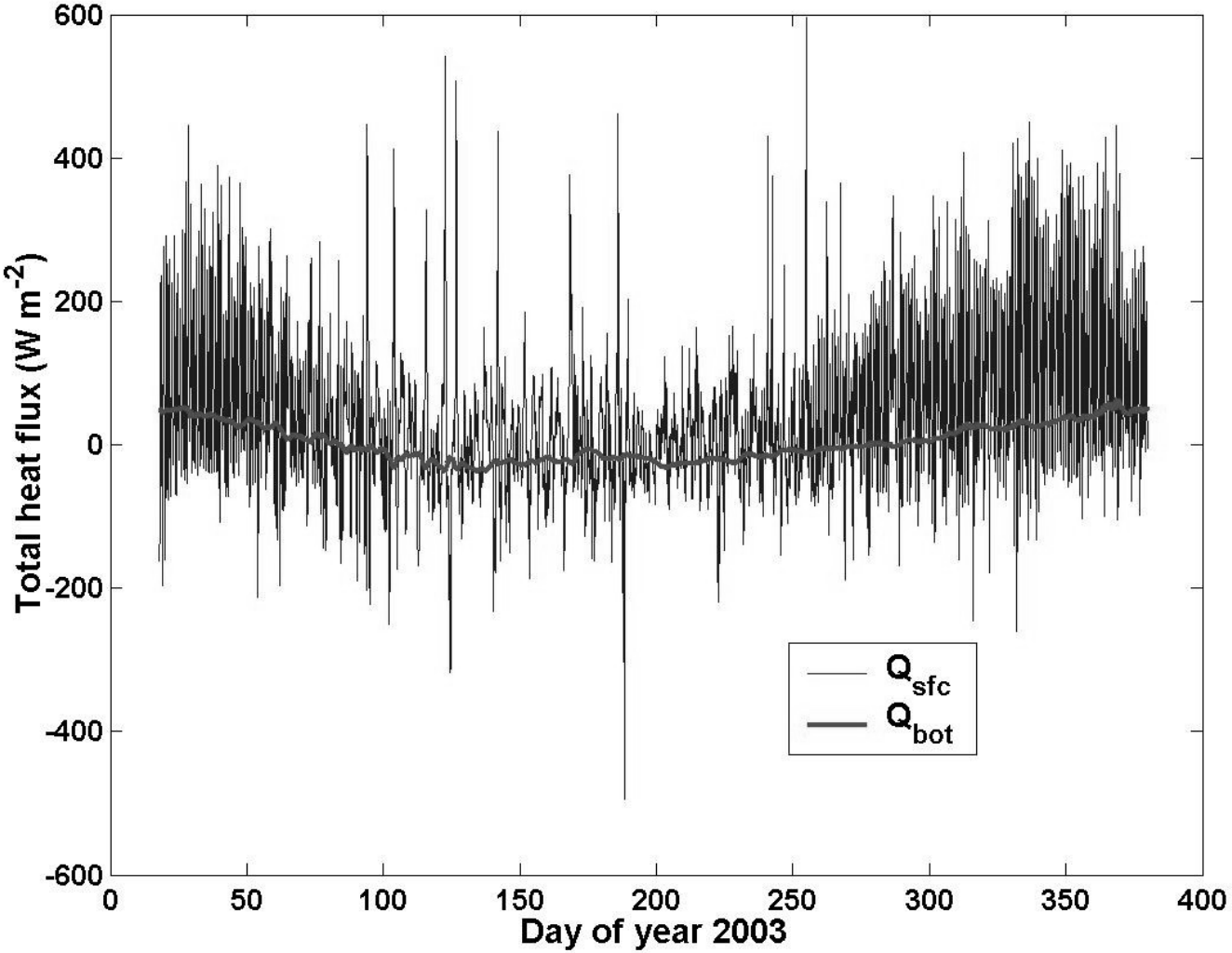

Figure 4.9: Balance of heat and radiation fluxes at the top (Q_{sfc}) and bottom (Q_{bot}) of the ice layer on Crooked Lake as calculated in the physics-based model for 2003. Direction towards the ice is positive in both cases.

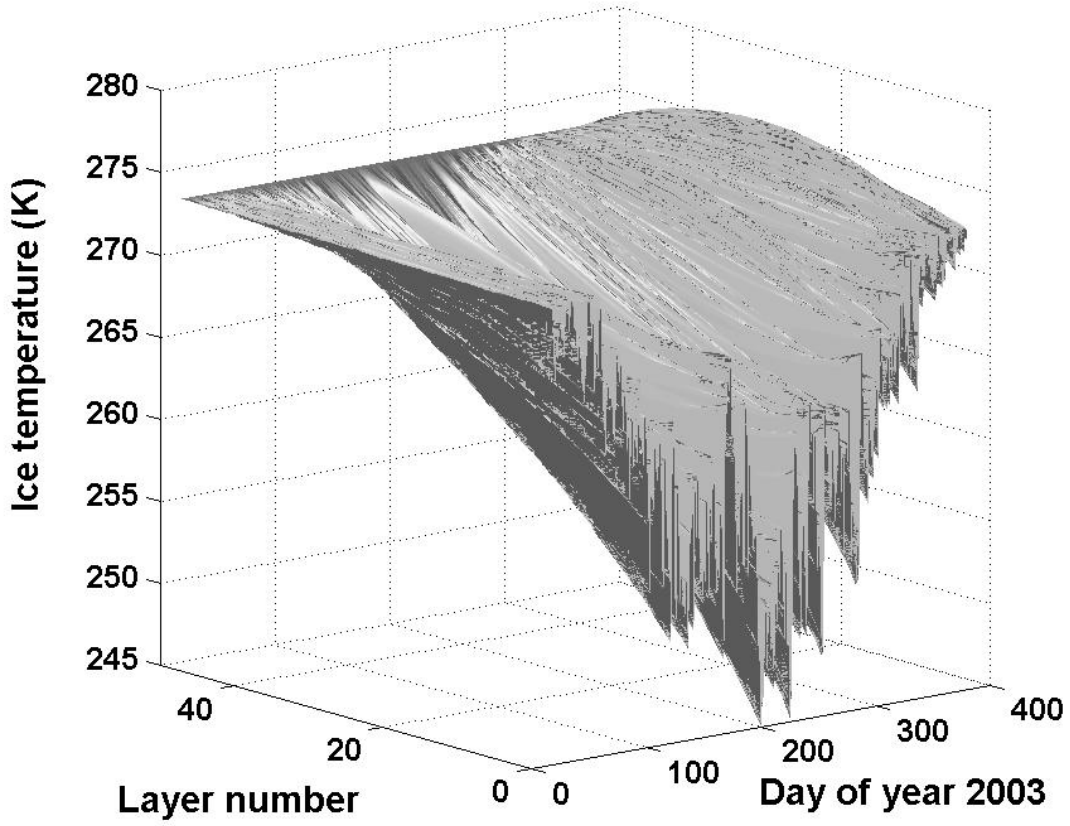

Figure 4.10: Temperature profile in the ice layer on Crooked Lake as calculated in the physics-based model for 2003. Layer 0 correponds to the surface temperature T_s while layer 50 is the ice bottom temperature, which remains at the freezing point of water, $T_f = 273.15$ K.

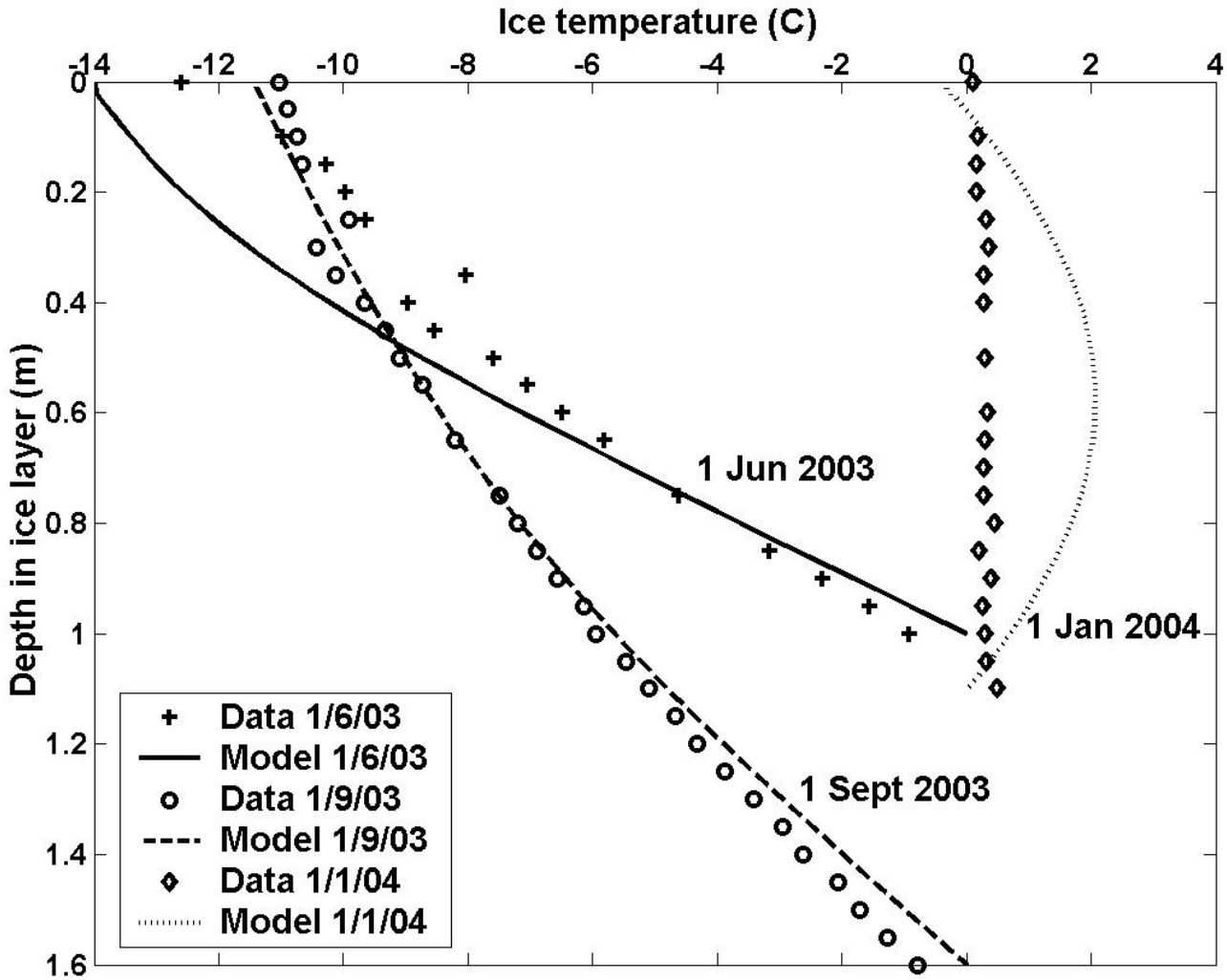

Figure 4.11: Temperature in the ice layer on Crooked Lake at noon on three separate dates across the study period, as measured by Foster (symbols), and as predicted by the physics-based model (lines): 1 June 2003 (crosses, solid line), 1 September 2003 (circles, dashed line) and 1 January 2004 (diamonds, dotted line).

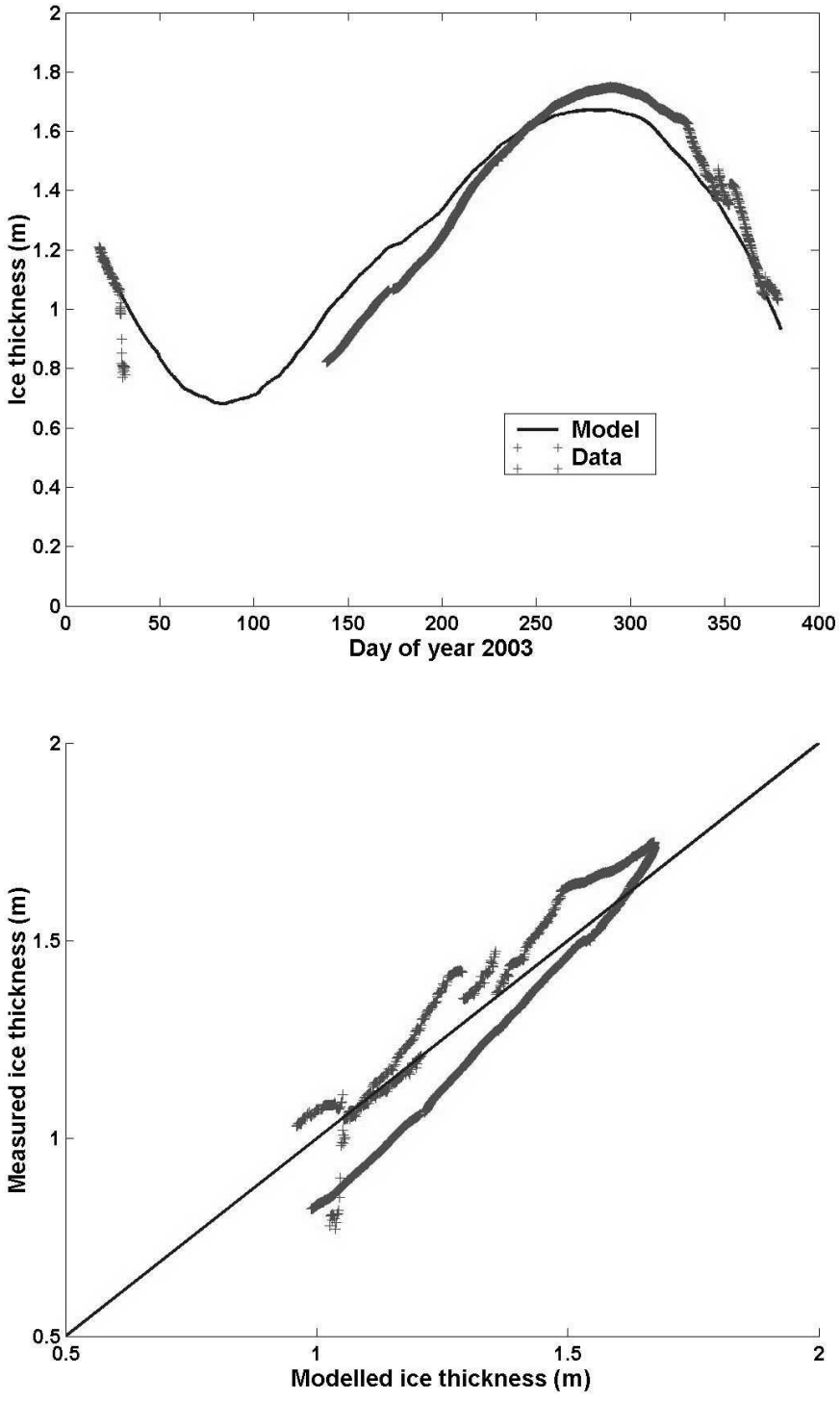

Figure 4.12: Ice thickness on Crooked Lake as calculated in the physics-based model for 2003 with optimised parameters, against time (above) and against data with a 1:1 line (below).

plotting). All the fluxes decreased in magnitude in the winter. Similarly Figure 4.7 shows the fluxes at the bottom of the ice layer. The conductive heat flux away from the ice increased in magnitude in the winter, providing the main factor for the growth of the ice layer. This is confirmed in Figure 4.8, which shows the daily change in ice thickness at the top and bottom of the ice layer for each day of 2003. The vast majority of changes in ice thickness happened at the bottom of the ice layer. Such a result is expected given that there is more water, the raw material for ice formation, below the ice than above. Also the latent heat of sublimation of ice that is required to melt (and 'remove') ice at the surface is much greater than the latent heat of fusion required below. The surface fluxes are key variables in calculating the profile of temperature in the ice layer, which in turn affects the melt and growth of ice at the bottom. Figure 4.9 shows the total balance of fluxes towards the ice layer at the top ($Q_b + Q_d + Q_h + Q_l + F_i + (1-\alpha)Q_s$) and bottom ($F_b + F_w$) surfaces of the ice. Diurnal variation was more apparent at the top surface.

Figure 4.10 shows the calculated temperature profile in the ice over the year. The temperature stayed close to freezing point T_f through the whole ice layer in the summer, when the air temperature was often above freezing; also temperatures greater than freezing point were calculated for the centre of the ice layer for January 2004. In winter, when the surface temperature fell well below freezing point, the calculated ice temperature decreased slightly with depth in the first 5cm or so before increasing towards the bottom of the ice, which remained at freezing point. A comparison with ice temperature measurements made by Foster during the study period is shown in Figure 4.11, for three dates covering the winter ice growth phase (1 June 2003), the period of maximum ice thickness (1 September 2003) and the summer ice melt phase (1 January 2004). The data was best reproduced in September 2003. The model underestimated the temperature near the top of the ice in June 2003 by just over 1 K, while in January 2004 the temperature 'inversion' in the centre of the ice layer was overestimated by around 2 K. For this reason (the model was predicting ice temperatures above freezing point), a condition was built into the model that set a maximum ice temperature of T_f, such that any excess heat would contribute to melting at the ice surfaces.

Figure 4.12 shows the ice thickness output of the physics model plotted against time and against the data. The model consistently overestimated the speed of ice thickness growth at the start of the winter (around day 150), and underestimated the ice thickness reached towards the end of winter (around day 300), suggesting that certain changes in the ice system between summer and winter were unaccounted for.

4.7 Importance of variables

The importance of the input variables in the model was assessed using the 'model trimming' technique explained in Chapter 2. The variable being examined was changed using values of β =0,0.1,...0.9,1 (Figure 4.13).

The air temperature (T_a) and water temperature (T_w) variables both showed a very steep increase in χ^2 when β was reduced towards zero, and so were clearly very influential on the model output. The ice extinction coefficient (κ) exhibited similar behaviour but with a shallower slope, suggesting that the inclusion of it's variation was worthwhile but less crucial than T_a or T_w. The relative humidity (RH), cloud cover (C) and wind speed (V) variables showed even shallower slopes. The reduction in χ^2 on adding their variability (setting β to 1 instead of 0) was less than 5 % in each case.

Removing the variation in air pressure (p_a) appeared to have no effect on the model fit, suggesting that the model output was somewhat 'indifferent' to this variable. The albedo (α) gave the best fit when it's variation was completely removed (β set to 0), giving a decrease in χ^2 of 10 %. This suggested that the variation in α was having an adverse effect on the model output, simply adding noise to the model output.

The above results show that the goodness of fit may be improved by the removal of some of the variability in the model variables. Setting each β_i to the values that provided the lowest χ^2, the model was run again. The goodness of fit was improved (χ^2 = 16, r^2 = 0.90, ν = 2009). However for the remainder of this chapter the variables are returned to their original input state ($\beta_i = 1$ for all x_i), as to use anything else would be outwith the existing physical theory which has been followed for the development of this physics model. The results are used later in this thesis to inform the development of empirical models of ice dynamics on Crooked Lake.

An analysis of the parameterised heat fluxes was also undertaken. The importance of each flux was analysed one by one in a simpler way than above. In each case the flux equation was removed altogether so the flux was zero, and the resulting goodness of fit was calculated (Table 4.4).

All the fluxes caused a decrease in the goodness of fit of the model when removed. In particular the longwave radiation (Q_d and Q_b), the conductive heat at the ice bottom (F_b) and the sensible heat from the water (F_w) were crucial to the model.

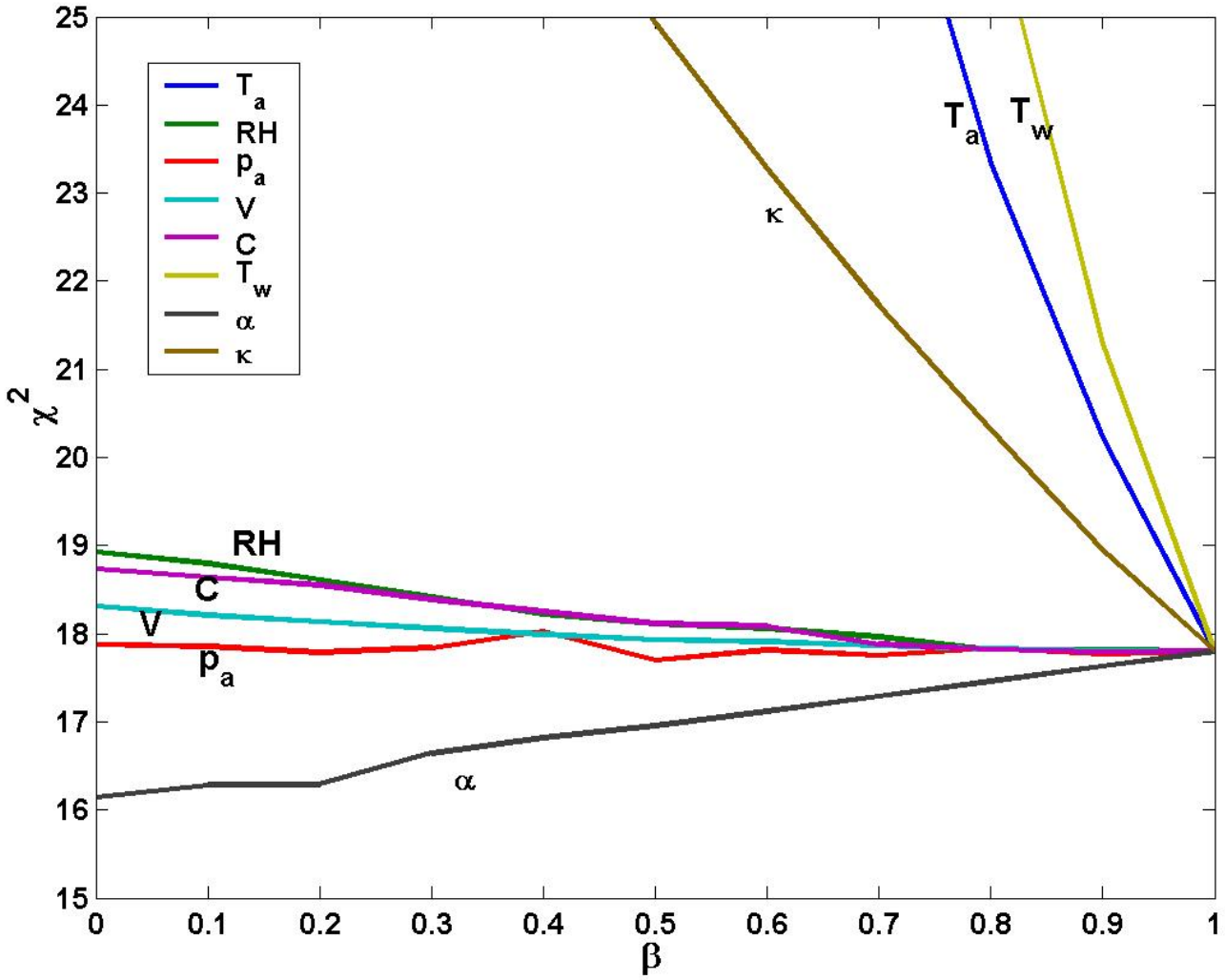

Figure 4.13: Graphs of the residual sum of squares of the physics model against the parameter β. For each individual variable x_i, β_i was set to the values 0,0.1,...,0.9,1 and x_i was set to $x_i^{'} = \beta_i x_i + (1 - \beta_i)x_\mu$. The lines all meet at $\beta = 1$, which correponds to the unaltered model with no variables changed.

Flux set to zero	χ^2	r^2
(None)	17.80	0.89
Q_s	28.08	0.83
Q_d	358.71	-1.19
Q_b	2.02×10^5	-1236.60
Q_h	30.01	0.82
Q_l	73.25	0.55
F_i	27.65	0.83
F_b	3.51×10^3	-20.47
F_w	845.77	-4.18

Table 4.4: Response of the model fit (χ^2 and r^2) when heat and radiation fluxes were individually set to zero.

4.8 Summary

This chapter has outlined the analysis and optimisation of a physics-based model of Crooked Lake ice dynamics. The procedures were kept within strict physical limits so as to avoid straying outside the existing physical and thermodynamic theory applied. The model was optimised with respect to measured ice thickness data, and a model fit of $\chi^2 = 16$, $r^2 = 0.90$, $\nu = 2008$ was achieved.

The optimisation and sensitivity analysis showed that the model was most sensitive to the parameter k_w, which is an approximation of the conductivity of water and governs the transfer of sensible heat to and from the bottom of the ice layer. With the physical constraints imposed, the model was reduced such that k_w was the only adjustable parameter, reflecting the importance of water temperature in ice dynamics. This was reconfirmed in a 'model-trimming' analysis which showed that the variability in water temperature T_w was, along with the air temperature T_a, considerably more important than the other variables in producing a good fit to the data. This suggests that there may be good correlations between these variables and the ice thickness, and it is worthwhile developing empirical models based on only these variables.

The adjustment of k_w removes much of the mechanistic nature of the model, and mirrors an empirical approach. This situation arose because k_w could only be estimated from the literature in the first place, and the optimised value of $k_w = 17.3$ for Crooked Lake may have to be readjusted for other lakes. This reflects the complex nature of such a system - it is impossible to be entirely mechanistic when processes such as the turbulent heat flux in water are so difficult to quantify. The model nonetheless captures the key processes involved in ice growth and melt, and all the calculated quantities are of realistic magnitudes.

The next chapter uses the 'clues' revealed in this chapter to develop empirical models of the Crooked Lake ice layer, with parameters that are not constrained, such that optimisation procedures may find better-fitting models. The benefits and disadvantages of such models compared with the physics-based model are discussed and analysed.

Chapter 5

Empirical models of lake ice

5.1 Overview

Chapters 3 and 4 described a model of the ice layer on Crooked Lake that is restricted by a belief in reductionism, incorporating appropriate existing physical theories. In this chapter, several simple empirical models are developed, based on correlations between datasets. These include linear regression models, continuous models consisting of linear differential equations, and 'semi-mechanistic' models incorporating some physical realism.

The empirical models are assessed using ANOVA tests to assess the significance of added complexity. A number of model selection criteria are calculated for the empirical models and the physics-based model, and the results are used to discuss the reliability of such selection formulae as a scientific tool compared to informed subjectivity on the part of the researcher.

5.2 Data correlations

The correlation coefficients between the ice thickness datapoints over 2003 (at 3-hour intervals) and the input variables for the same times were calculated (Table 5.1). The correlation coefficients are low. However, correlations are to be expected between meteorological data, given the underlying diurnal and seasonal cycles, and changing weather patterns which affect all variables. Also, with such a large amount of available data (2009 ice thickness datapoints, or 2920 per year for other variables), the degrees of freedom of a correlation are effectively infinite,

r	T_w	T_a	RH	p_a	C	V	α	κ	H_i
T_w	1	-	-	-	-	-	-	-	-
T_a	0.83	1	-	-	-	-	-	-	-
RH	-0.05	-0.01	1	-	-	-	-	-	-
p_a	0.12	0.08	-0.01	1	-	-	-	-	-
C	-0.08	0.07	0.35	-0.10	1	-	-	-	-
V	0.12	0.31	0.02	-0.10	0.12	1	-	-	-
α	-0.07	-0.14	0.19	-0.03	0.08	-0.07	1	-	-
κ	-0.31	-0.34	0.22	0.08	0.09	-0.15	0.46	1	-
H_i	-0.09	0.01	-0.16	-0.37	0.00	-0.05	-0.29	-0.39	1

Table 5.1: Correlation coefficients (r) between variables used in the physics-based model. Any correlation of magnitude 0.05 or greater is statistically significant due to the large number of datapoints involved.

and a Student's t-test can show that the correlation coefficient is significant to very low values. The following t-statistic was used to to test the null hypothesis $H_0 : r = 0$ versus $H_1 : r \neq 0$ (Mason et al. 2003):

$$t = \frac{r(n_d - 2)^{\frac{1}{2}}}{(1 - r^2)^{\frac{1}{2}}} \tag{5.1}$$

where n_d is the number of datapoints and r is the correlation coefficient. For a two-tailed 5 % significance test with infinite degrees of freedom, the critical value of the t-variate is 1.96. With $n_d = 2009$ and $t = 1.96$, a value of $r = 0.044$ is a correlation of the required significance i.e. there is only a 5 % probability that a correlation of $r = 0.044$ could arise at random. Therefore any correlation in Table 5.1 with a magnitude of 0.05 or greater is statistically significant.

The highest correlation was between air temperature and water temperature. This is a reassuring indication that the state of the atmosphere is the main driving force in determining the properties of the lake, and other sources of influence such as geothermal heat may be discounted. Also, air temperature is the main variable that is predicted by climate models in considering climate change effects, and will be measured far more frequently in future than the water temperature. Therefore empirical models based only on atmospheric conditions may be plausible when predicting the future physical environment of the ecosystem.

Other correlations that were significantly different from zero include a positive correlation between relative humidity and cloud cover and a negative correlation between wind speed and pressure, both relating to the warmer, windier nature of atmospheric depressions. Some conclusions on the nature of the ice layer could

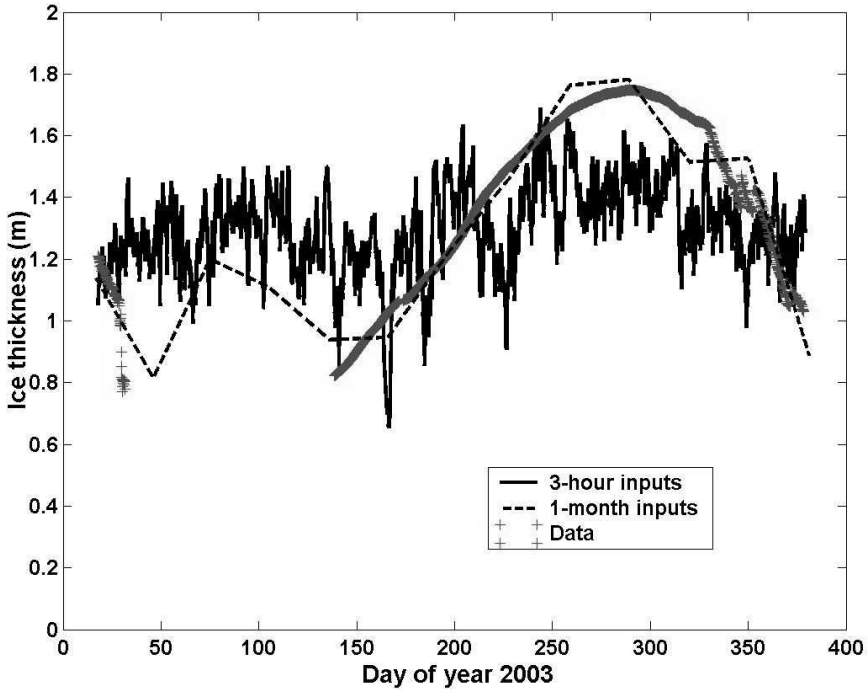

Figure 5.1: Ice thickness calculated by a linear regression model with a 3-hour timestep using 3-hour input variables (solid line) and monthly-averaged (dashed line), plotted with the data (crosses). The fit is poor because the data is not discrete on a timestep of 3 hours.

also be made - both the ice albedo α and extinction coefficient κ were negatively correlated with ice thickness. With the exception of sporadic periods of snow, both tended to be higher when the ice was thinner, as the rotting ice was rougher, whiter and more opaque.

5.3 Linear regression models

The simplest type of empirical model is a multiple linear regression model, where the model output is expressed as a linear sum of the input variables. Using the 8 input variables as in the physics model, this may be expressed as:

$$H_i = p_1 T_w + p_2 T_a + p_3 RH + p_4 p_a + p_5 C + p_6 V + p_7 \alpha + p_8 \kappa + p_9 \qquad (5.2)$$

where p_1 to p_9 are adjustable parameters. Using a 3-hour timestep with all the available input data, Equation 5.2 was optimised in ModelMaker, and parameter values were found which gave $\chi^2 = 7111$, $r^2 = 0.31$, $\nu = 2000$ (Figure 5.1).

Despite the poor fit, the F-ratio was high ($P < 0.001$). However, as Figure 5.1 shows, the model output bore little relation to the data, and the high F-ratio was simply a result of the large number of datapoints involved.

Such a poor result may be expected for a system like Crooked Lake; the ice thickness, unlike the atmospheric input variables, changes very little if at all in the space of 3 hours, and does not respond significantly to the small scale diurnal cycle (24 hours) or weather patterns (a few days) that affect the other variables. On the scale of ice thickness changes, such small-scale variations become noise. To account for this, the input data was artificially smoothed by taking monthly means and linearly interpolating. The results of optimising the model with these input variables is also plotted in Figure 5.1. The model fit was improved to $\chi^2 = 510$, $r^2 = 0.95$, $\nu = 2000$. However, such an approach is somewhat artificial, and the unexpected increase in modelled ice thickness after January (when in reality no ice thickness measurements were taken as the ice was too thin) suggests that the fit is very specific to this dataset, and nothing generic may be learned from the parameter values. Also, a true multiple linear regression should relate datasets of the same size, meaning that the monthly means of ice thickness should also be taken. On doing this the ice thickness dataset only provided 9 datapoints for the year (no data was recorded in the months February to April), meaning the model had zero degrees of freedom and hence any fit would be statistically meaningless.

Therefore it can be concluded that a linear regression model relating all or any of the input variables to the ice thickness data cannot be formulated with the data available. The ice layer is a continuous system, in that the ice thickness on any particular day is highly dependent on the ice thickness the previous day (therefore in the physics model the calculation of the *change* in ice thickness over a given timestep involves the ice thickness itself). On a larger timescale, the system may become closer to a discrete system than a continuous one. The above analysis has suggested that a month is not long enough for this to be the case, but on the scale of one datapoint per year the data may be approximately discrete. The annual cycle of seasons is (for most intents and purposes) the longest-scale variation imposed on a natural system, and over the years Crooked Lake has been observed, the ice either completely melts towards the end of summer, or becomes very thin and broken up. So the system practically starts from scratch each year (i.e. the system turnover time is approximately a year), and given long term data the yearly average ice thickness could be modelled by linear regression with atmospheric variables. Such an exercise would require large amounts of data beyond the scope of this thesis.

5.4 Continuous models

The simplest continuous model for predicting the model output with the given input variables is a linear differential equation, which is highly analagous to the linear regression model (Equation 5.2), but with the linear sum producing the *change* in ice thickness for each timestep. For this thesis, such models are termed 'linear continuous' models. Providing one adjustable parameter for each of the 8 input variables, the following model of ice thickness was formulated in Model-Maker:

$$\frac{dH_i}{dt} = p_1 T_w + p_2 T_a + p_3 RH + p_4 p_a + p_5 C + p_6 V + p_7 \alpha + p_8 \kappa + p_9 \qquad (5.3)$$

where p_1 to p_9 are adjustable parameters. The nine parameters were all given an initial value of 1, and optimised using the Levenberg-Marquardt procedure (Table 5.2). A goodness of fit of $\chi^2 = 118.33$, $r^2 = 0.99$, $\nu = 2000$ was achieved.

Parameter	**Variable**	**Value**	**Standard error**	**t-statistic**
p_1	T_w	-5.62×10^{-3}	6.89×10^{-4}	-8.15
p_2	T_a	-6.52×10^{-4}	6.10×10^{-5}	-10.67
p_3	RH	3.29×10^{-4}	4.10×10^{-5}	8.02
p_4	p_a	1.37×10^{-6}	4.87×10^{-7}	2.80
p_5	C	4.95×10^{-3}	2.79×10^{-3}	1.77
p_6	V	-2.98×10^{-4}	1.27×10^{-4}	-2.35
p_7	α	1.18×10^{-2}	3.31×10^{-3}	3.56
p_8	κ	-9.78×10^{-3}	3.03×10^{-3}	-3.23
p_9	(none)	1.55	0.17	1.33

Table 5.2: Estimated parameter values for a linear differential equation model with the same eight input variables as the physics-based model (Equation 5.3). The t-value is calculated as the ratio of the parameter value to the standard error.

The t-value for each parameter estimate in Table 5.2 relates to the test of whether or not the parameter value is significantly different from zero. For the null hypothesis $H_0 : p_i = 0$ versus $H_1 : p_i \neq 0$, the t-statistic is simply calculated as the ratio of the parameter value to the standard error. As in the previous section, a two-tailed 5 % significance test with 'infinite' degrees of freedom requires a value for the t-variate with magnitude of at least 1.96. Therefore one can say with 95 % certainty that all of the parameter values in Table 5.2 are statistically different from zero except for p_5 and p_9. This may reflect the strong correlations between variables that were found in the previous section; if variables are well correlated then they may all have similar effects on the output, and the effect of each is 'shared out', resulting in small parameter values.

However, such t-statistics based on the standard error are somewhat difficult to interpret. The standard error on parameters is calculated on the basis of the curvature matrix - the greater the curvature of the model fit with respect to the parameter ($\frac{\partial^2 \chi^2}{\partial p_i^2}$), the steeper the parabola in which the parameter value lies, and hence the lower the standard error. But such an assumption does not account for the possibility that the parameter value is in a steep parabolic well in an area of high terrain in parameter space, i.e. a local minima.

In addition, the values of some parameters may not accurately reflect the importance of their associated variable, given the relative sizes of numbers involved. For example, the air pressure p_a was measured in Pascals, so took numerical values around 100000 (corresponding to 1000 mb) with a standard deviation for the whole year of only around 1 % of the mean, while the cloud cover took values between 0 and 1, and had a standard deviation up to 50 % of it's mean. Therefore the parameter p_4 (which multiplies the air pressure in Equation 5.3) may be artificially small relative to p_5 (which multiplies the cloud cover), because of the difference in scales when each variable is expressed in S.I. units. Such a scale is not representative of the extent to which variables may interact - it is only defined by scientists for practical purposes. For example, a change of 10 mb may seem a small fraction of an air pressure of around 1000 mb (only 1 % change) but in reality it could mean the difference between settled or stormy weather. A 1 % change in cloud cover is far less significant.

For these reasons, the model was run again using normalised data for each variable, with a mean of zero and standard deviation of 1 across the whole time period. Each variable x_i was replaced with $x_i^{'}$:

$$x_i^{'} = \frac{x_i - \mu(x_i)}{\sigma(x_i)} \tag{5.4}$$

where $\mu(x_i)$ and $\sigma(x_i)$ are respectively the mean and standard deviation of all the values of x_i across the modelled time period. The parameters were calibrated (Table 5.3) and the same goodness of fit as above was acquired ($\chi^2 = 118.33$, $r^2 = 0.99$, $\nu = 2000$).

Unlike in Table 5.2 the parameter values in Table 5.3 can be compared on the basis of their magnitudes to infer the importance of the corresponding input variables. The 3 highest magnitude parameters were p_1, p_2 and p_3, which were also among the most significant parameters according to the t-statistics. A comparison of the parameter values to the t-statistics for parameters p_1 to p_8 from

Parameter	Variable	Value	Standard error	t-statistic
p_1	T_w	-3.74×10^{-3}	4.59×10^{-4}	-8.15
p_2	T_a	-5.49×10^{-3}	5.14×10^{-4}	-10.68
p_3	RH	4.91×10^{-3}	6.13×10^{-4}	8.01
p_4	p_a	1.35×10^{-3}	4.80×10^{-4}	2.81
p_5	C	1.57×10^{-3}	8.88×10^{-4}	1.77
p_6	V	-2.50×10^{-3}	1.07×10^{-3}	-2.34
p_7	α	1.70×10^{-3}	4.78×10^{-4}	3.56
p_8	κ	-2.50×10^{-3}	7.74×10^{-4}	-3.23
p_9	(none)	5.62×10^{-4}	3.04×10^{-5}	18.43

Table 5.3: Estimated parameter values for a linear differential equation model with the eight input variables as in Table 5.2, but with all input variables normalised.

Table 5.3 demonstrated a linear relationship with $r^2 = 0.96$. The results therefore give a reassuring sign that the t-statistic as calculated is a good indicator of the importance of parameters. So, given that the t-statistics were the same in the models with normalised and unnormalised variables, the rest of the empirical models in this thesis go back to using the un-normalised input variables. The normalised approach has not in this case produced any difference in the parameter significances, but in other cases may be a worthwhile exercise to investigate the possibility of local minima, given that in an optimisation procedure with normalised data some potential bias is removed.

5.5 Simplifying continuous models

The t-statistics in Tables 5.2 and 5.3 indicate that the variables T_w, T_a and RH are considerably more important than the other parameters. This suggests that a model based on these three variables alone may reproduce the data. However, the variables T_w, α and κ were measured specifically at Crooked Lake, and will not be regularly measured in the future, so a model based on changes in them may not be generally applicable. In addition, it has been shown that these variables are to a large extent determined by atmospheric variables - particularly well illustrated with the high correlation between air and water temperatures.

Therefore the continuous model of Equation 5.3 was reduced to a model using only atmospheric variables:

$$\frac{dH_i}{dt} = p_2 T_a + p_3 RH + p_4 p_a + p_5 C + p_6 V + p_9 \tag{5.5}$$

Parameter	Variable	Value	Standard error	t-statistic
p_2	T_a	-1.07×10^{-3}	1.39×10^{-5}	-76.98
p_3	RH	1.23×10^{-4}	2.86×10^{-5}	4.30
p_4	p_a	7.38×10^{-7}	2.95×10^{-7}	2.50
p_5	C	-2.59×10^{-3}	2.31×10^{-3}	-1.12
p_6	V	4.31×10^{-6}	1.10×10^{-4}	3.92×10^{-3}
p_9	(none)	0.203	0.0294	6.90

Table 5.4: Estimated parameter values for a linear continuous model using only atmospheric variables (Equation 5.5).

	n_p	df	WSS	MS	F	P
Original Model	6	5	12274	2455	40917	< 0.001
Improvement	+3	+3	86	29	483.33	< 0.001
Residual		2000	118	0.06		
Total		2008	12478			

Table 5.5: ANOVA table comparing the models from Equations 5.5 and 5.3. The 'improvement' refers to the addition of 3 parameters to Equation 5.5 to get Equation 5.3.

The above model was fitted to the data and acquired a fit of $\chi^2 = 204.17$, $r^2 = 0.98$, $\nu = 2003$ with the parameter values shown in Table 5.4.

An ANOVA test was used to assess the significance of the improvement in fit on including the 3 other variables (T_w, α and κ), and is shown in Table 5.5. This is calculated in the same way as in Table 2.1, where the original model is now that of Equation 5.5 and the improvement relates to the addition of the three other variables to give Equation 5.3.

The low P-value for the improvement in Table 5.5 indicates that the improvement is statistically significant. However, this is an illustration of the dangers of uncritically accepting such a test at high sample numbers. The F-ratio is heavily weighted by the sample size, n_d, so in the case of so many datapoints ($n_d = 2009$) models which provide only a small improvement in fit may still be deemed significant. However, the number of datapoints is artificially high in this instance for such a test, given that the ice thickness changes so slowly, especially on a timestep of 3 hours; the datapoints are not independent. Also, as Figure 5.2 shows, the error on the ice thickness means that for models which already provide a good fit (e.g. $r^2 > 0.95$), a small increase in fit simply adjusts the model closer to the *sample means* of the datapoints. The F-value for the improvement in Table 5.5 is high, but only around 1 % of the F-value for the unimproved model. So for a situation of less data, the change in fit would quickly become insignificant.

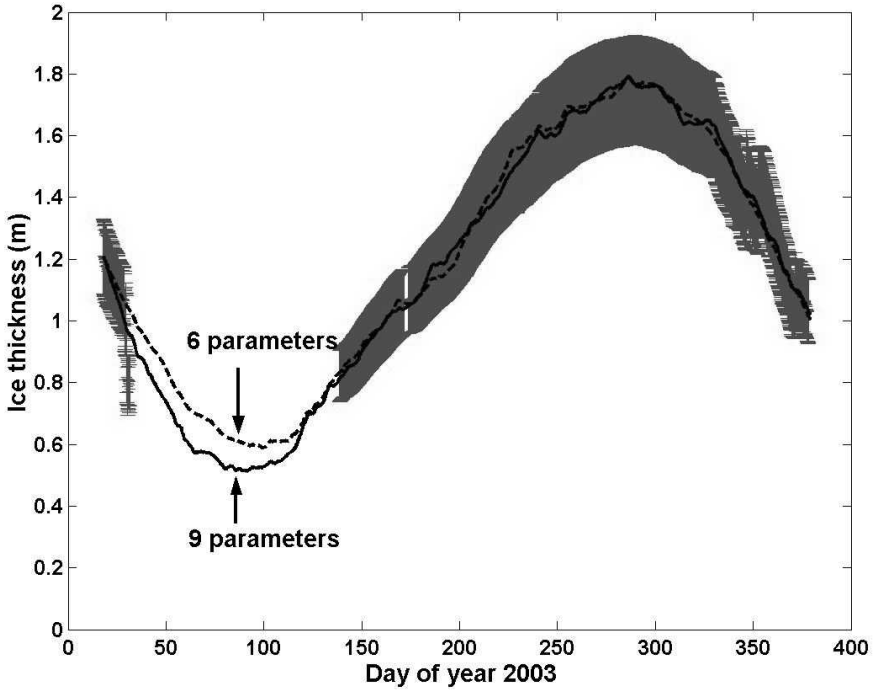

Figure 5.2: Predicted ice thickness from a linear continuous model using only 6 parameters (Equation 5.5) and using 9 parameters (Equation 5.3). The data is plotted with 10 % error bars. The large number of datapoints makes the models significantly different according to the ANOVA test, but for practical purposes the fit is no different.

For these reasons, and for the issue of practicality, models based only on atmospheric variables are sufficient for modelling Crooked Lake. The rest of this chapter presents a number of simple models based only on these variables. With hindsight, an ARIMA model approach with Box-Jenkins differencing of the data may have been a worthwhile exercise to determine the 'true' number of degrees of freedom provided by the data. However the above analysis, although somewhat 'ad-hoc', shows that with careful judgement and subjectivity specific to the job in hand, the same conclusions can be reached by simpler means.

Given the low t-statistics in Table 5.4, the variables C and V were omitted, and every combination of the variables T_a, RH and p_a was calculated. It was found that the inclusion of T_a was essential for acquiring a fit of $r^2 = 0.9$ or over, and so the models in Table 5.6 were chosen for model selection later in this chapter.

Name	Formulae
LC 1	$\frac{dH_i}{dt} = p_1 T_a + p_2$
LC 2	$\frac{dH_i}{dt} = p_1 T_a + p_2 RH + p_3$
LC 3	$\frac{dH_i}{dt} = p_1 T_a + p_2 p_a + p_3$
LC 4	$\frac{dH_i}{dt} = p_1 T_a + p_2 RH + p_3 p_a + p_4$

Table 5.6: 'Linear continuous' models of the ice layer, selected on the basis of having a fit $r^2 > 0.9$. T_a, p_a and RH are input variables and all other terms are adjustable parameters.

5.6 Simplified physics models

A number of models based around the linear models in the previous section were formulated which may be considered 'semi-mechanistic', as they mirror a number of concepts from the physics-based model, or concur with some intuitive notions on how the ice layer may behave. These were chosen in an ad-hoc fashion, with models accepted for the next stage of analysis if their goodness of fit was $r^2 > 0.9$.

The simplest such model is a linear differential equation in the air temperature T_a, written as:

$$\frac{dH_i}{dt} = c_g(T_f - T_a) \tag{5.6}$$

where c_g is an adjustable growth parameter and T_f is an adjustable 'threshold air temperature' parameter, above which the ice will melt, below which it will grow in proportion to the difference $T_f - T_a$. The equation is comparable to the parameterisation of sensible heat flux at the ice surface in the physics model (Equation 3.23), but is applied in a very different way. When optimised, the goodness of fit was $\chi^2 = 412.7$, $r^2 = 0.97$, $\nu = 2007$. The parameters took values of $T_f = 262.9$ K, $c_g = 1 \times 10^{-3}$ m K^{-1} day^{-1}. Therefore the threshold temperature for such an equation is, surprisingly, 10.2 K lower than the melting point of water. This can be explained by considering how the model is defined - the value is very close to the mean air temperature for the year (263 K), so accounts for the intuitive notion that over the whole annual cycle the ice approximately grows the same amount as it melts.

Name	Formulae
SM 1	$\frac{dH_i}{dt} = c_g(T_f - T_a)$
SM 2	$\frac{dH_i}{dt} = c_g(T_f - T_a)$ for $T_a \leq T_f$ $\frac{dH_i}{dt} = c_m(T_f - T_a)$ for $T_a > T_f$
SM 3	$\frac{dH_i}{dt} = c_g(T_f - T_a)V$
SM 4	$\frac{dH_i}{dt} = c_g(T_f - T_a)V$ for $T_a \leq T_f$ $\frac{dH_i}{dt} = c_m(T_f - T_a)V$ for $T_a > T_f$
SM 5	$\frac{dH_i}{dt} = c_{g1}(T_f - T_a) + c_{g2}(q_f - q_a)$
SM 6	$\frac{dH_i}{dt} = c_{g1}(T_f - T_a) + c_{g2}(q_f - q_a)$ where $c_{g1} \rightarrow c_{m1}$ for $T_a \geq T_f$ and $c_{g2} \rightarrow c_{m2}$ for $q_a \leq q_f$
SM 7	$\frac{dH_i}{dt} = c_{g1}(T_f - T_a)V + c_{g2}(q_f - q_a)V$
SM 8	$\frac{dH_i}{dt} = c_{g1}(T_f - T_a)V + c_{g2}(q_f - q_a)V$ where $c_{g1} \rightarrow c_{m1}$ for $T_a \geq T_f$ and $c_{g2} \rightarrow c_{m2}$ for $q_a \leq q_f$

Table 5.7: 'Semi-mechanistic' models based on intuitive physics concepts about the ice layer. T_a, q_a and V are input variables and all other terms are adjustable parameters.

More complexity can be added by assuming different rates of change of ice thickness when the ice melts and grows:

$$\begin{aligned} \frac{dH_i}{dt} &= c_g(T_f - T_a) \quad \text{for} \quad T_a \leq T_f \\ \frac{dH_i}{dt} &= c_m(T_f - T_a) \quad \text{for} \quad T_a > T_f \end{aligned} \tag{5.7}$$

where c_m is a third parameter for the rate of melting, and c_g now relates only to growth rate, such that the equation is now conditional.

Further complexity was added by considering the effect of the gradient in humidity at the ice surface, analogous to the latent heat flux in the physics model (Equation 3.24). The specific humidity of the air q_a was calculated from T_a, RH and p_a as in Equations 3.1 to 3.3. This allowed a number of similar models to be formulated,

considering a critical humidity q_f which affects whether ice will grow or melt. This approach is distinct from the linear models in that the variables are combined in a non-linear way to calculate q_a. Introducing some conditionality as above allows even more choice of model. Eight models in total were formulated which provided fits of $r^2 > 0.9$, and are summarised in Table 5.7.

5.7 Model selection results

There is no limit to the potential models that could be formulated using the inputs available. However, as has been illustrated, changes in goodness of fit on adding complexity can easily be ruled out as insignificant. For the exercise of selecting models, the analysis is limited to the 8 'semi-mechanistic' equations in Table 5.7, the 4 'linear continuous' models from Table 5.6, and the physics model from Chapters 3 and 4. This gives a spread of levels of complexity.

Model selection criteria (MSCs) were calculated for each of the models (Table 5.8). For simplicity of calculation the data was given a default error of 1, so that the models were essentially fitted in a least squares fashion, and the magnitude of numbers involved was kept lower.

A difficulty arose when assessing what constituted an adjustable parameter in the physics model. As discussed in Chapter 4, most quantities were chosen to within strict ranges consistent with theory. Figure 4.2 shows that, with the ranges imposed, the only parameter which significantly affected the goodness of fit was k_w. The other parameters can feasibly be set to any value in the range and treated as 'constants'. Therefore for the purposes of MSCs the physics model is deemed a one-parameter model with 8 inputs.

5.8 Model selection discussion

The results in Table 5.8 illustrate a number of interesting points about the models, and the application of MSCs in general.

The model LC 4 provided the best fit to data. It was also selected by the RMSD criteria. However it can be seen that the values for RMSD directly follow the goodness of fit values. This reflects a problem with the criteria for large datasets: the term $n_d - n_p$ accounts for complexity in the equation ($RMSD = \sqrt{\frac{\chi^2}{n_d - n_p}}$),

Model	n_p	n_x	χ^2	r^2	$ln(ML)$	AIC	BIC	$RMSD$	MDL	$ICOMP$
SM 1	2	1	4.19	0.97	-1848.24	**3700.5**	**3711.7**	0.0457	1859.9	1855.1
SM 2	3	1	4.18	0.97	-1848.23	3702.5	3719.3	0.0457	1867.2	1868.2
SM 3	2	2	6.80	0.96	-1849.55	3703.1	3714.3	0.0582	1863.1	1858.0
SM 4	3	2	6.39	0.96	-1849.34	3704.7	3721.5	0.0564	1871.9	1872.6
SM 5	4	3	2.96	0.98	-1847.60	3703.3	3725.7	0.0384	**1852.5**	1905.1
SM 6	6	3	2.61	0.98	-1847.45	3706.9	3740.5	0.0361	1862.8	1899.2
SM 7	4	4	3.03	0.98	-1847.66	3703.3	3725.7	0.0389	1856.6	1909.2
SM 8	6	4	2.19	0.99	-1847.24	3706.5	3740.1	0.0331	1872.3	1895.6
LC 1	2	1	4.19	0.97	-1848.24	**3700.5**	**3711.7**	0.0457	1866.9	1858.7
LC 2	3	2	2.33	0.99	-1847.31	3700.6	3717.4	0.0341	1875.2	1862.3
LC 3	3	2	2.40	0.99	-1847.35	3700.7	3717.5	0.0346	1879.5	1871.6
LC 4	4	3	**2.10**	**0.99**	**-1847.21**	3702.4	3724.8	**0.0324**	1888.2	1878.6
Physics	1	8	17.80	0.89	-1855.05	3712.1	3717.7	0.0941	1855.2	**1855.0**

Table 5.8: Model selection criteria calculated for the eight 'semi-mechanistic' models from Table 5.7, the four 'linear continuous' models from Table 5.6, and the physics-based model. The 'winning' model for each criteria is higlighted in bold.

and if n_d is much greater than n_p, any change in n_p becomes negligible. The goodness of fit (χ^2) value in the numerator becomes the crucial factor, so RMSD is of little theoretical use.

The models SM 1 and LC 1 gave equally the lowest values of all models for the AIC and BIC criteria. These are essentially the same model expressed in a different form, and the selection reflects their remarkably good fit despite having only two parameters and one input variable. However on comparing the two models it is interesting to note that the numbers for MDL and ICOMP are different: both select SM 1 over LC 1. Given that these are the only criteria that take into account not only the number of parameters but also the functional form of the models, such a result suggests that SM 1 has more stable parameter values, and therefore is more generalisable. This is a small victory for the semi-mechanistic approach: applying a little bit of realism by considering a threshold temperature for ice melt/growth appears to suit the situation more accurately than simply using a linear sum of the input variables, even if the fit to data is unchanged.

The lowest MDL value was calculated for SM 5. This is the simplest of models SM 5 to SM 8, which all have terms approximating both temperature and water vapour gradients at the ice surface. SM 5 does not use the variable V, so the wind speed data may have been adding undesirable noise to the model - in fact SM 5 also has a better fit than SM 7 despite having one less input variable. SM 8, which uses both V and separate growth/melt conditions, has the best fit of all the semi-mechanistic models. However the selection of SM 5 by MDL indicates that this may be a case of over-fitting, and the simpler model is more reliable.

The physics model provided the lowest goodness of fit of all the models. This was due to the restrictions that were imposed on it to keep all parameters within realistic theoretical limits; it was not fitted to the data as freely as the simpler models. However the ICOMP criteria selected the physics model, and it was the 'second choice' of the MDL criteria.

The idea behind MDL is that any regularity in data can be used to compress the data, thus describing it with fewer symbols than are required to describe the data literally (Grünwald 2000). In selection this amounts to minimising the stochastic complexity of the dataset with respect to the model, which in algorithmic coding theory is defined as the shortest code length of the dataset obtainable when the encoding is done with the help of that model (Rissanen 1996). ICOMP, meanwhile, is defined as an entropic measure of statistical dependence between parameter estimates (Myung, 2000). Selection by this criteria may therefore

suggest that the physics model provides stable parameter values, such that the rate of change of the output with respect to each parameter is very small. This means that on fitting the model to other datasets the standard deviation of parameter values across the datasets will be small.

Therefore the inclusion of several input datasets in the physics model appears to be useful for identifying any regularities in the ice thickness data that would be important in predicting future behaviour - the output of the physically-based model is a much smoother curve than SM 1 (Figure 5.3) - i.e. the physics model captures the general long-term sinusoidal behaviour of the ice layer without being affected by short-term variability, which on the scale of a year is essentially noise. A more simple explanation for this is that using more input variables leads to noise from their datasets cancelling out, whereas in SM 1 the noise on the air temperature carries through to the output.

However, there are serious flaws in making conclusions for the physics model from the MSC values. The key factors considered in the MSCs, such as the Hessian matrix, are related to parameters and how stable they are. So to draw conclusions the parameters must be crucial quantities in the model as a whole. The only parameter adjusted in the physics model is k_w, which although influential on model fit is only used in the calculation of one of the eight heat fluxes affecting the ice layer in the model. For an MSC assessment of the performance of the model as whole, more quantities may have to be treated as adjustable parameters, for example all eight of the heat fluxes. Nonetheless the physics model was selected by ICOMP, despite having the lowest goodness of fit. ICOMP is the most extensive of the criteria in terms of the model aspects it considers, and the most successful criteria tested by Myung (2000). This is a reassuring sign that for at least one parameter, the inclusion of all the known physics is worthwhile.

All the other models have a number of parameters n_p equal to or greater than the number of input variables n_x, and are represented by one short differential equation, so the parameters are hugely influential on the model output, and the MSC values can be trusted more directly. Choosing the best model is still somewhat subjective, but a number of arguments point to SM 1 as the most useful. It was selected by AIC and BIC, and was the 'second choice' of ICOMP after the physics model. It also relies on air temperature T_a alone, which is, as argued above, the most important variable in the linear continuous models. Any terms in the other variables are statistically far less significant (as shown by the t-statistics in Table 5.4), so models LC 2 to LC 4 can be ruled out. For the semi-mechanistic models, the fit was improved by adding terms in the specific humidity

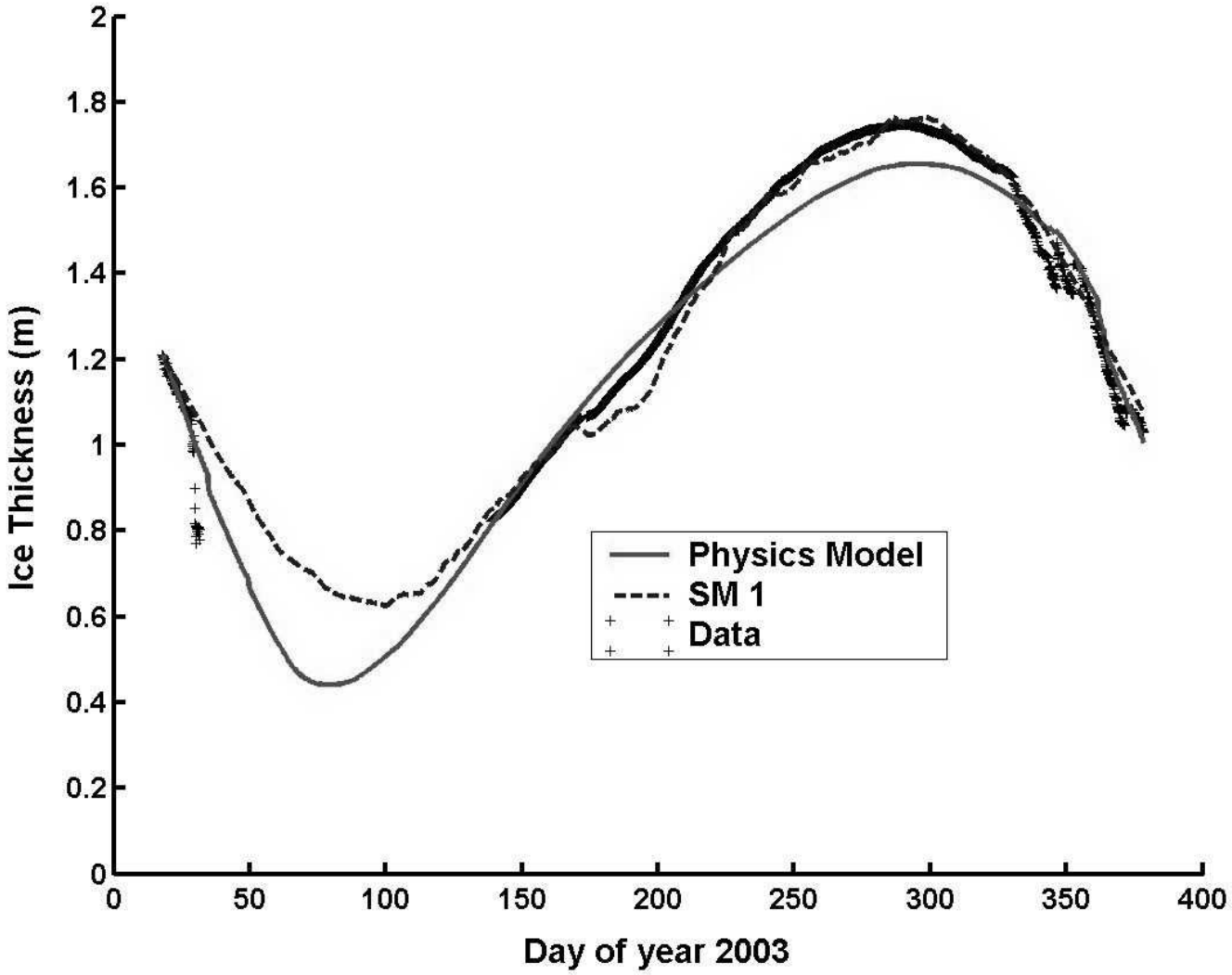

Figure 5.3: Ice thickness calculated by the physics-based model (solid line) and by model SM 1 (dashed line), with the data (crosses). The physics-based model has lower goodness of fit due to the 'realistic' constraints on all quantities, but a smoother line because the noise from 8 input variables cancels out.

q_a, and MDL selected model SM 5. However, q_a is partly calculated from T_a, and the two variables have a correlation of $r = 0.86$. The small improvement in fit thus stems from a more complex function in T_a, and may cause the over-fitting.

5.9 Summary

In this chapter a number of empirical models of lake ice were developed and analysed using data from Crooked Lake. Some were discarded on the basis of ANOVA tests, and others were tested using model selection criteria. A discussion referring to these results indicated an informed preference for a simple 'semi-mechanistic' model and the physics-based model from Chapters 3 and 4 as the best two candidates for further analysis.

Several methods exist for selecting models, and this section has looked at only a few of the most simple ones. However it has highlighted a number of complicating factors that arise: when using a large dataset some of the criteria become less useful, and when testing a highly mechanistic model based on physical theories it is difficult to attain a concrete definition of what is and isn't an adjustable parameter. It has illustrated that subjectivity is still required for selecting a model of such a system.

Chapter 6

Climate change responses

6.1 Overview

Antarctic lakes may be sensitive indicators of climate change (Vincent et al. 1998, Wharton Jr. et al. 1992). In this chapter it is argued that a modelling investigation of climate change effects on an ice layer amounts to an assessment of long-term model responses to changes in air temperature. The physics-based model from Chapter 3 is adapted to run with air temperature as the only input variable. Climate averages from 1957-2003 data are used as a 'baseline' for long-term model runs with imposed perturbations on air temperature. The predicted ice responses in both the physics-based model and a simple empirical model are contrasted.

6.2 Models based on temperature alone

Excess concentrations of greenhouse gases in the atmosphere lead to an increased amount of infrared radiation at the surface, and 'climate change' is defined as a change in all the long-term weather phenomena as a whole at the surface. Air temperature T_a is just one of the variables involved in such a change, but is influential on all other variables. Therefore in climate change scenarios, the air temperature is the most commonly considered variable, relating to the ubiquitous term 'global warming'.

As was illustrated in Chapter 4, T_a is the most important variable in the physics-based model of lake ice (Figure 4.13). The other variables deemed important by

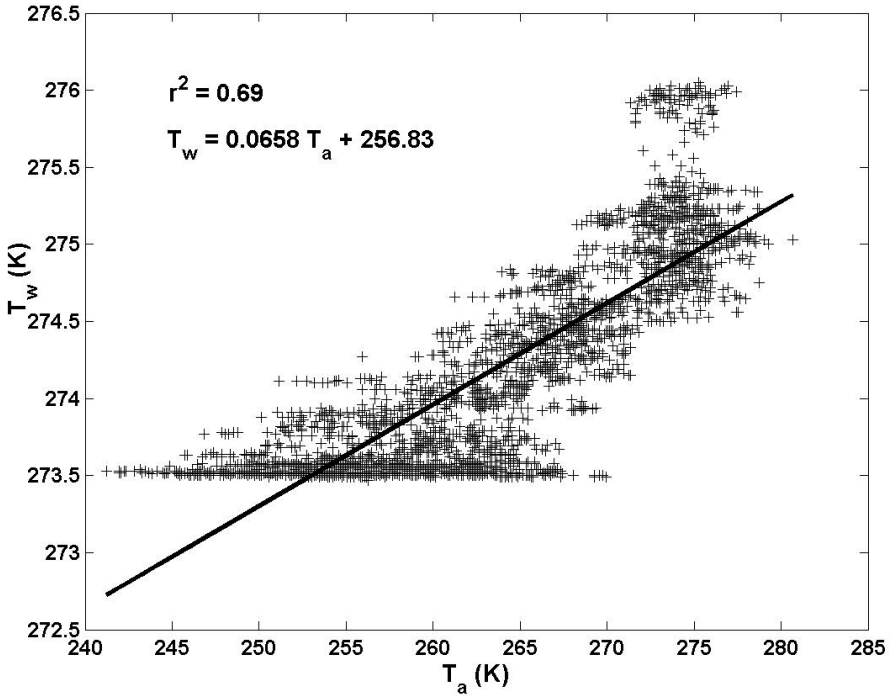

Figure 6.1: Linear regression of 2003 water temperature and air temperature.

the 'model trimming' technique were water temperature T_w and the ice extinction coefficient κ, and these had the highest correlation to T_a (Table 5.1). Chapter 5 highlighted a similar dominance of air temperature in simple empirical models. Climate change scenarios for other variables are less common, and more uncertain, than temperature scenarios.

Therefore for the purposes of predicting climate change effects on the Crooked Lake system, models based on temperature alone were selected. The simple 'semi-mechanistic' empirical model SM 1 was chosen because of it's performance as measured by model selection criteria (Table 5.8). In addition, the physics-based model was adapted to run with only air temperature as an input. Each of the input variables was expressed as a linear function of T_a, fitting a straight line in a linear regression:

$$x_i = mT_a + c \tag{6.1}$$

where m and c are the gradient and offset of the straight line, respectively, which were fitted for each variable (Table 6.1). It was found that using higher order terms in T_a gave a negligible improvement in fit.

Variable	m	c	r^2
RH	-0.0140	61.9486	0.0027
p_a	9.3936	96308.6029	0.0149
V	0.1576	-35.4256	0.0904
C	0.0025	0.0241	0.0044
T_w	0.0658	256.8331	0.6987
α	-0.0023	1.0762	0.0199
κ	-0.0103	2.9697	0.1426

Table 6.1: Gradients m and offsets c for straight line regression between air temperature T_a and other variables used in the physics model for 2003, and the associated r^2 values.

The r^2 values in Table 6.1 are small, reflecting the low correlations in Table 5.1. However the second most 'important' variable T_w gave the strongest fit (Figure 6.1), and the goodness of fit of the resulting 'T_a only' model to the 2003 ice thickness data was $\chi^2 = 42.98$, $r^2 = 0.74$, $\nu = 2008$ (compared to $\chi^2 = 16$, $r^2 = 0.90$, $\nu = 2008$ with all variables present).

6.3 Historic data

Climate history data collected by the Australian Bureau of Meteorology at Davis station from 1957 to 2003 allows a comparison of the year 2003 to the previous 45 years (Figure 6.2). The variables all show clear variation with the annual cycle, which is more apparent because a large amount of noise is removed when monthly means are taken. They therefore provide more accurate linear regressions for expressing the variables RH and V in terms of T_a (Table 6.2). The 2003 data follows the historic data fairly closely, particularly air temperature and the daily hours of sunshine, suggesting that 2003 was quite typical of the past 45 years. Exceptions were a slightly lower then average relative humidity from August to November, and considerable noise on the wind speed data. On the whole one could tentatively make the conclusion that 2003 was a typical year for the area. However we cannot necessarily assume that the state of ice on Crooked Lake was also close to the average, as it is to some extent dependent on previous years, for which there is no substantial data.

The historic air temperature data was examined for any sign of long-term temperature change at Davis. A full 12 months of data were available for 40 of the 46 years from 1957 to 2003. These were used to calculate 40 annual mean temperatures over the period. A straight line was fitted to the data (Figure 6.3). This

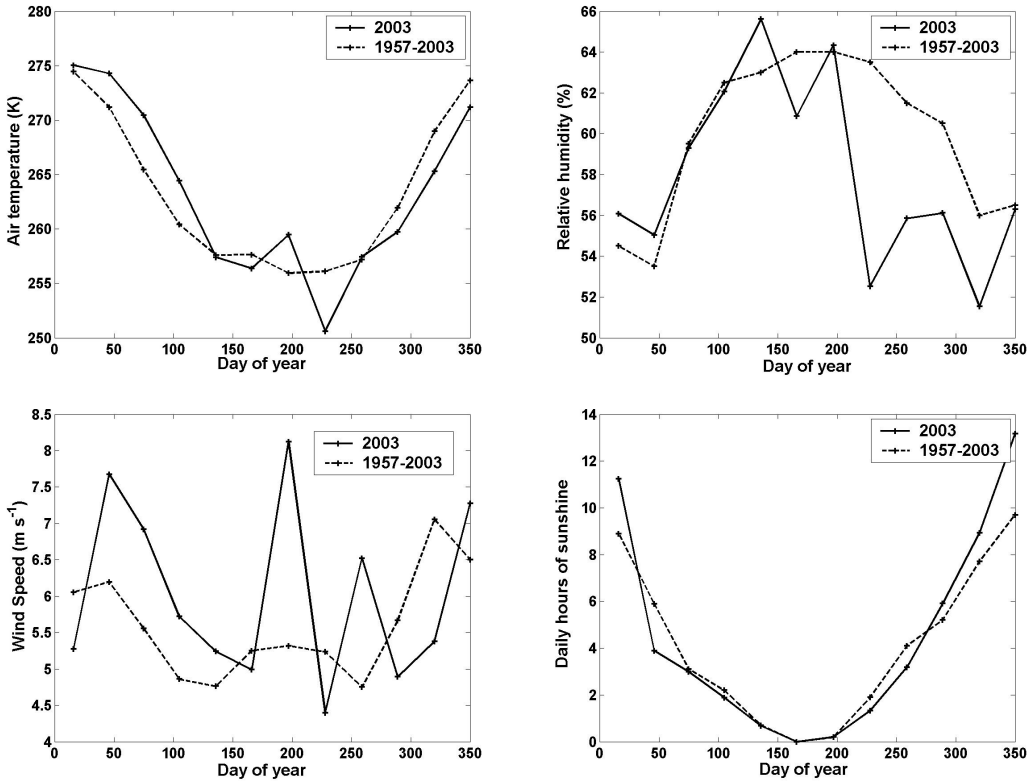

Figure 6.2: Monthly means for 2003 (solid lines), and averaged over the period 1957-2003 (dotted lines) for, clockwise from top left: air temperature, relative humidity, daily sunshine hours and wind speed.

Variable	m	c	r^2
RH	-0.518	196.34	0.903
V	0.301	-59.22	0.663

Table 6.2: Gradients m, offsets c and the associated r^2 values for straight line regressions of relative humidity RH and wind speed V with air temperature T_a, based on monthly means for 1957-2003.

revealed a small average annual warming of 0.0083 K per year, but the correlation was of low statistical significance ($P = 0.22$).

Previous ice thickness data for Crooked Lake is sporadic. The most extensive limnological studies of Crooked Lake were undertaken in 1993 (Laybourn-Parry and Bayliss 1996) and in 1999 (Henshaw 2001). In both studies, visits were made to the lake on average once every two weeks, and ice thickness data was measured manually using ruled poles. The available monthly means of these datasets are plotted with the 2003 data in Figure 6.4. The 2003 ice thickness was generally lower than in the two earlier years. Across all three years the mean ice thickness was 1.49 m.

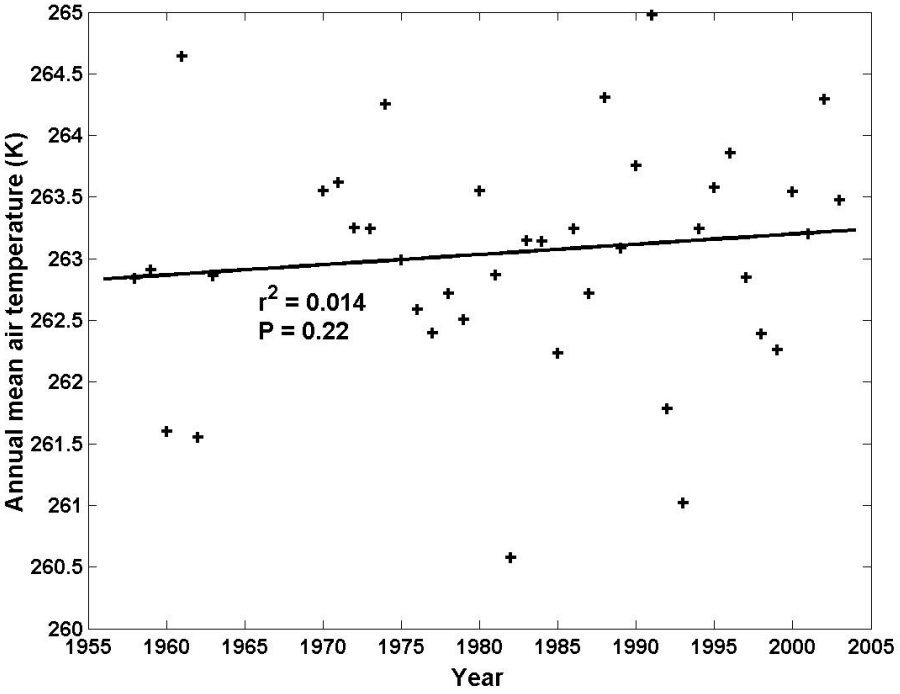

Figure 6.3: Annual mean air temperatures at Davis station, 1957 to 2003.

6.4 Cross-validation

In chapters 3 to 5, both the physics model and SM 1 were fitted to high-resolution data from the 2003 probe deployment and performed well under model selection criteria. However the most directly informative test of parameter estimates is a cross-validation with other datasets - i.e. if the parameter values fit several known past datasets, then model predictions may be expected to be a reasonable representation of future datasets. This was attempted with the high-resolution data, by fitting each model to data from the first half of the year, then running them for the second half of the year. However the results are not reported as this led to parameter values specific to ice growth, which did not fit the second half of the year when ice was melting, so were not as useful as 'compromising' parameters calculated for the whole year. Also, removing a one-datapoint validation sample from the series, (as described in Browne, 2000) was not worthwhile given the autocorrelation in the data (ice thickness is highly dependent on previous ice thickness, especially on a timestep of 3 hours).

Therefore it seems that for a system such as Crooked Lake with a one-year 'turnover time', a cross-validation requires more than one dataset, each of which provides good coverage of a year or more. This was made possible by the ice

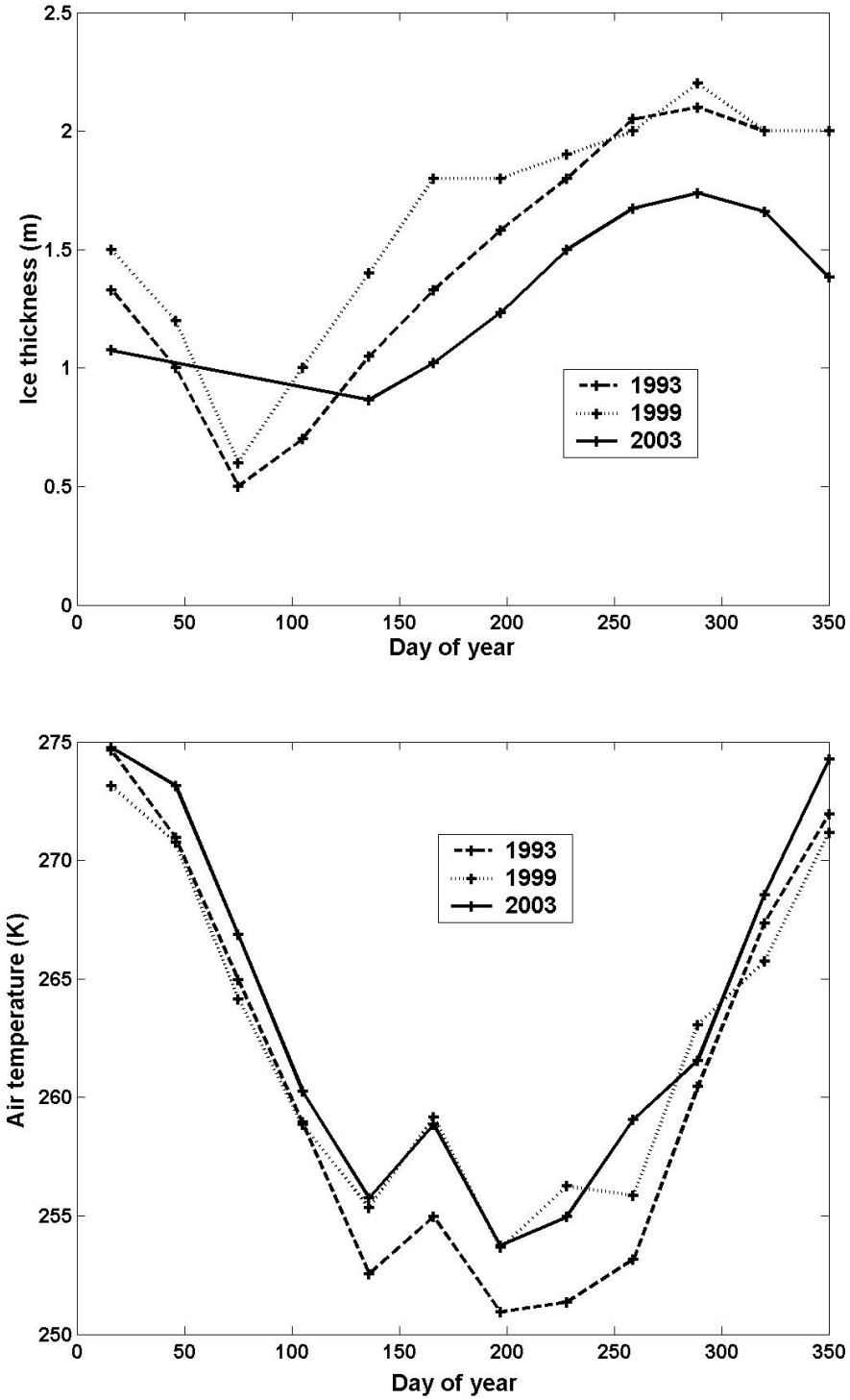

Figure 6.4: Crooked Lake monthly mean ice thickness (top) as measured by Bayliss in 1993, Henshaw in 1999 and the 2003 data, and the corresponding monthly mean air temperatures measured at Davis station (bottom).

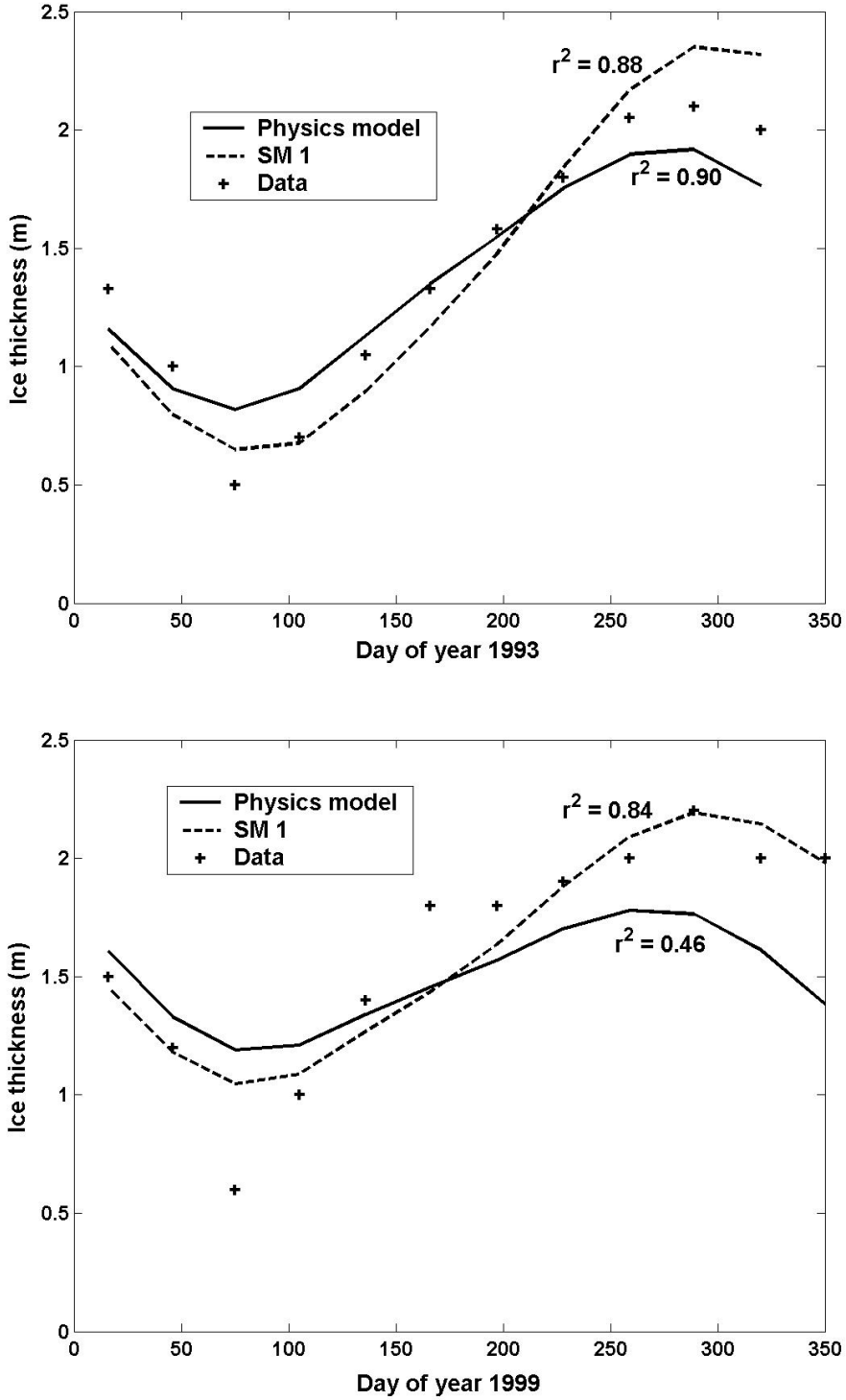

Figure 6.5: Cross-validation outputs of the physics-based model and SM 1 for 1993 (top) and 1999 (bottom). Parameter values were estimated using the high-resolution 2003 data.

thickness data for 1993 and 1999.

The monthly mean air temperature data from Davis station (Figure 6.4) was linearly interpolated to provide temperature inputs for the models. Using the parameters estimated for 2003, both models were fitted to the monthly mean ice thickness data for 1993 and 1999, by adjusting *only* the initial ice thickness $H_i(0)$ at the start of each year (Figure 6.5, Table 6.3).

Model	**Year**	χ^2	r^2	ν
Physics	1993	0.304	0.90	9
Physics	1999	1.405	0.46	10
Physics	2003	0.175	0.78	7
SM 1	1993	0.358	0.88	9
SM 1	1999	0.420	0.84	10
SM 1	2003	0.035	0.96	7

Table 6.3: Cross-validation goodness of fit of the physics-based model and SM 1 to monthly mean ice thickness for 1993, 1999 and 2003, with parameter values estimated for the high-resolution 2003 data.

The physics-based model provided a slightly better fit to the 1993 data than SM 1, while SM 1 had a much better fit to the 1999 data. So considering both years together, the definition of CV in equation 2.20 would select SM 1 over the physics model. However, given that the data is for two extra years only, which amounts to only two true samples on the 'discrete' turnover scale of the system, neither model should be ruled out. The fit for both models is comparable to or even better than the fit to the 2003 data, thus providing more statistical justification for the employment of such models in predicting the future.

6.5 Smoothing input variables

The short-term behaviour of a system may be significantly different from long-term trends, and for long-term studies one may feel inclined to ignore short-term variation as noise. For example, the shapes of the monthly mean graphs in Figure 6.2 compared to the fine-scale graphs in Figure 4.4 illustrate the dominance of the annual cycle. However, the variables are here used to predict another variable, ice thickness, which is a continuous variable affected by it's past state. The graphs also show that the size of day-to-day variations can be significantly large deviations from the annual trend, so an investigation was made into whether short-term variation has an effect on long-term behaviour, before discarding it.

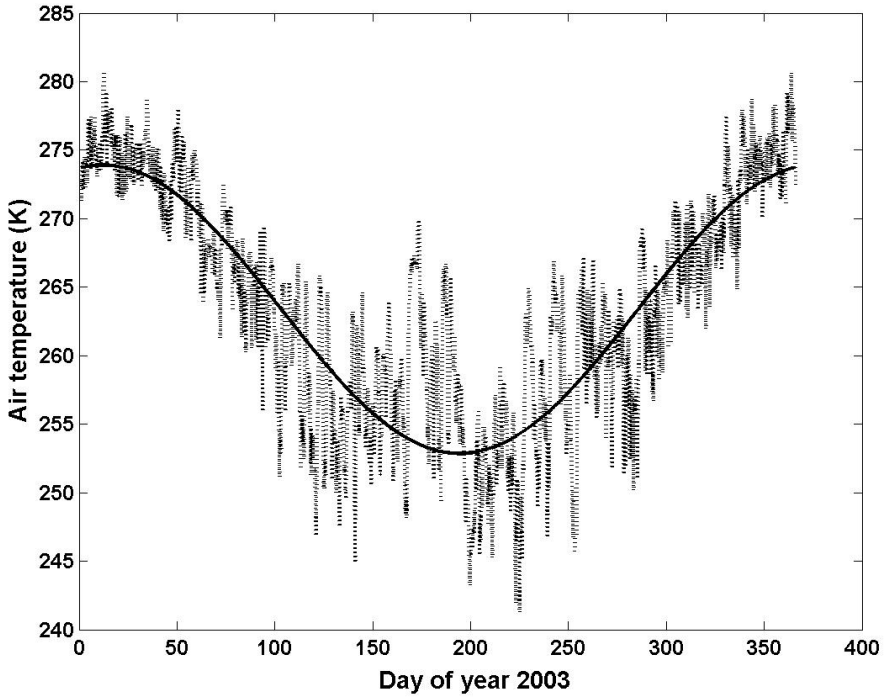

Figure 6.6: Air temperature data for 2003 (dotted line), with a best fit sine curve representing the annual cycle (solid line).

To remove noise and isolate the annual signal for each variable x_i, a cosinusoidal curve of period 365 days was fitted to the data:

$$x_i = A\cos\left(\frac{2\pi(J+\phi)}{365}\right) + C \tag{6.2}$$

where J is the Julian Day and A, ϕ and C are adjustable parameters. The parameter values for curves fitted to the 2003 T_a data (Figure 6.6), the 2003 ice thickness data and the monthly means for 1957-2003 are shown in Table 6.4.

	T_a **1957-2003**	T_a **2003**	H_i **2003**
A	9.239	10.527	0.530
ϕ	354.938	353.066	83.535
C	263.322	263.384	1.199
r^2	0.93	0.76	0.97

Table 6.4: Amplitude A, phase ϕ, offset C and the r^2 value of 365-day cosine curves fitted to the monthly mean air temperatures for 1957-2003, the 2003 air temperature and the 2003 ice thickness.

The r^2 fit was lowest for the 2003 air temperature, because it includes day-to-day noise. The parameter values were very similar to those for the 1957-2003 monthly means. The phase difference between the air temperature and ice thickness in

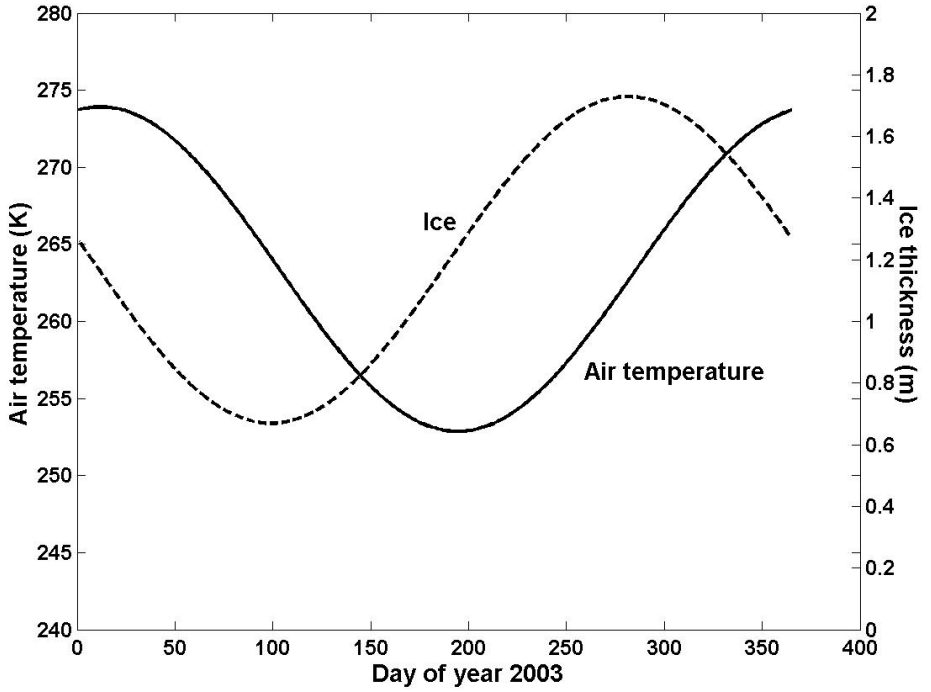

Figure 6.7: Best fit sine curves for 2003 air temperature (solid line) and ice thickness (dotted line). The ice thickness lags the air temperature by around 270^o.

2003 was 269.5 days, close to three quarters of a year (Figure 6.7), i.e. the ice thickness signal lagged behind the temperature signal by approximately 270^o. This was also true for the 1993 and 1999 datasets (not reported), and is the reason for the good fit of Model SM 1. The rate of change of a cosine curve is an inverted sine curve, and a cosine curve lags behind a sine curve by 270^o, so the analogy is:

$$\frac{dH_i}{dt} \propto -T_a \text{ versus } \frac{d\cos(J)}{dt} \propto -\sin(J) \tag{6.3}$$

where with air temperature proportional to a sine curve, the ice thickness is proportional to a cosine curve. This result may, however, be unique to the 2003 dataset, and the phase difference might be affected in years of different mean temperature.

The 2003 'T_a only' physics model was run again with T_a calculated from Equation 6.2. The fit was slightly improved from $\chi^2 = 42.98$, $r^2 = 0.74$, $\nu = 2009$ to $\chi^2 = 39.74$, $r^2 = 0.76$, $\nu = 2009$. Therefore the removal of day-to-day noise has only a small positive effect. However it provides a clearer picture, more appropriate for long-term investigations, and implies that the the annual cycle in

temperature was the only significant factor on the scale of a year. For predicting the future of the ecosystem relative to the recorded period, the historic 'smoothed' mean data was considered a suitable 'baseline' for investigating superimposed effects of climate change.

6.6 Finding a steady state model

While atmospheric variables for Davis station, and hence approximations for Crooked Lake, are available for a 45 year period, records of ice thickness on Crooked Lake are limited to 1993, 1999 and the more accurate data from 2003 (this study). However, the 5-minute data collected by the remote-sensing probe is of an unprecedentedly high temporal resolution, and when reduced to a timestep of 3 hours to relate directly to the meteorological data, the parameterisation of models may be deemed highly accurate. For this reason a 'temporally reductionist' approach can be applied; if the model accurately reproduces over 2000 datapoints over the scale of a year, where each is calculated from the previous timestep, then it must be somewhat generalisable to longer scales. This is reinforced by the fact that the models effectively treat the system as continuous. In reality the system may be treated as discrete on the timescale of a year, as the ice breaks up and disperses in summer, but it is in any case rare for the lake to be 100 % ice free. The complex processes that occur in the summer are dealt with by assuming that the physical properties of ice and water do not differ enough to have a significant effect, and that the other factors that come into play in summer, such as wind-induced mixing when open areas of water appear, have enough randomness to 'cancel themselves out'. In other words, the system is modelled as if it were a controlled laboratory experiment, with no other phenomena consistent enough to have lasting effects. This approach is given merit by Figure 5.3, where both the simple model SM 1 and the physics model were initialised with data from January 2003, and 'bridge the summer gap' to very closely reproduce the next datapoints that were recorded in May.

Some aspects of the models are specific to the year 2003. Below is a discussion of the adjustments that were made to SM 1 and the physics model to apply to a general situation. Each model was adapted to a state where the calculated ice thickness followed the same trend every year, i.e. the ice thickness was the same every successive January 1st. This gave 'steady state' models, which predict the ice thickness response if the atmosphere remains in it's mean state every year. Such models represent the 'average state' of the lake over the past 45 years.

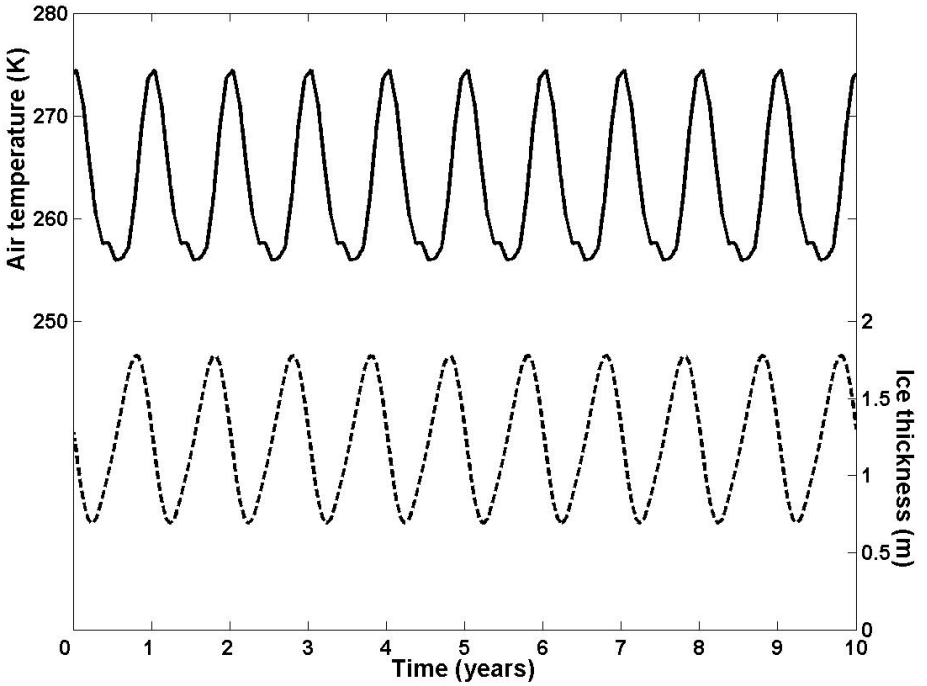

Figure 6.8: Air temperature (solid line) repeated from the monthly means for 1957-2003, and calculated ice thickness (dotted line) for 10 simulated years in a steady state version of model SM 1.

6.6.1 Model SM 1

The simple semi-mechanistic model SM 1 was generated by the equation:

$$\frac{dH_i}{dt} = c_g(T_f - T_a) \tag{6.4}$$

The right hand side of the equation is not affected by H_i. In other words, the *change* in ice thickness is not dependent on the ice thickness. For a steady state, the mean value of $\frac{dH_i}{dt}$ over time should be zero. Therefore it can immediately be inferred that for a steady state over a certain period of time, the parameter T_f must be equal to the mean value of the air temperature T_a over the same time period. The value of T_f found when the model was optimised for the 2003 data in Chapter 5 was indeed close to the mean of T_a. Therefore T_f is very specific to circumstances, providing a threshold with a value that ensures ice melts as much as it grows.

However this need not necessarily rule out SM 1 when searching for a generalisable model. The parameter values found in Chapter 5 apply to a year that had

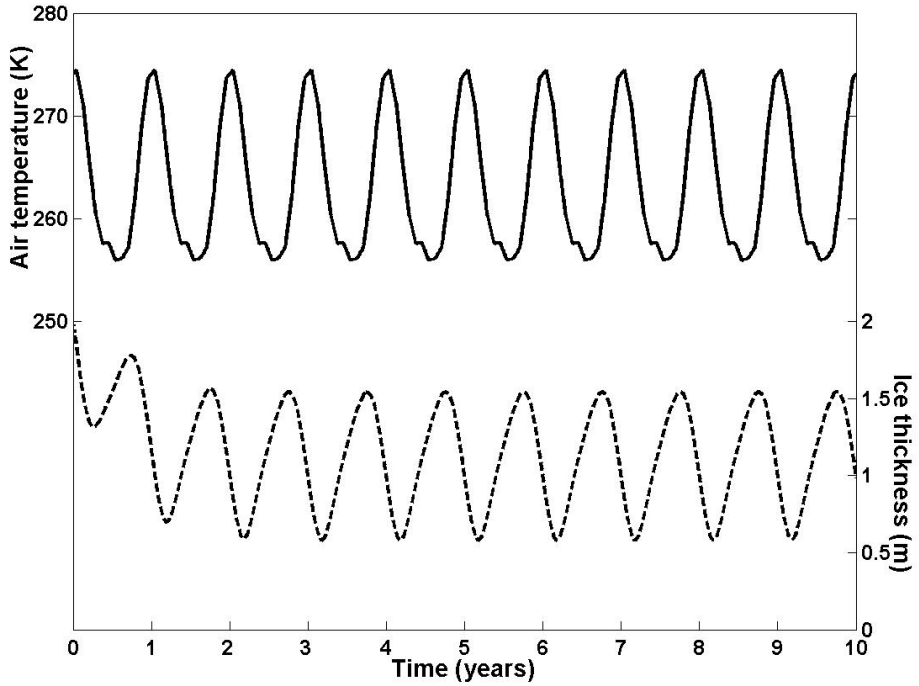

Figure 6.9: Air temperature (solid line) repeated from the monthly means for 1957-2003, and calculated ice thickness (dotted line) for 10 years, simulated by the physics-based model. Initial ice thickness was 2m, and the model predicted a steady state with maximum 1.55m, minimum 0.58m within two years.

a mean temperature (263.0 K) close to the running mean for the period since 1957 (263.4 K). Also the calibrated value for the parameter c_g, which determines the fine scale day-to-day response of the ice to air temperature changes, can be taken as generalisable given the extremely good fit to the data. Therefore to acquire a steady state model the only parameter to adjust was T_f. The mean air temperature data was repeated year-on-year for 10 complete years. The initial value of ice thickness was set equal to the mean January ice thickness across the 3 past datasets from 1993, 1999 and 2003 (= 1.3 m). The steady state model was found at $T_f = mean(T_a) = 263.4$ K (Figure 6.8). The maximum calculated ice thickness each year was 1.78m, minimum 0.69m. This illustrates that the long-term ice thickness is completely determined by the initial ice thickness, and the model is therefore completely continuous.

6.6.2 Physics-based model

The physics-based model has no freely adjustable parameters, as it is restricted to existing mechanistic theories about the system. For a steady state version

of the model, the interpolated historic monthly mean air temperature data was used as the input variable (as above), and the initial value of ice thickness was adjusted. It was found that the model evolved to a state independent of the initial conditions (Figure 6.9). For example, with initial ice thickness of 0.5 m and 2 m the same state was reached after 2 years of model run time. The steady state gave a maximum ice thickness of 1.55 m on 3 October and a minimum of 0.58 m on 6 March each year, both figures slightly lower than that suggested by SM 1.

Therefore for a steady state repeated temperature signal, the physics-based model is stable. The fact that the ice thickness is intrinsic to the calculation of the *change* in ice thickness provides the stabilising factor; for any given air temperature there is a corresponding ice thickness which provides the situation at which the total balance of heat fluxes at the top and bottom of the ice layer is zero.

6.7 Implementing climate change scenarios

The main difference between the physics model and SM 1 is that the investigation of global warming effects using the physics model comes down to an assessment of the long-term responses of the models to changes in the steady state air temperature, whereas for SM 1 the initial conditions must be very well defined for runs into the future.

According to climate sensitivity estimates and the implemented socio-economic scenarios, global climate models predict that global average temperature will increase by somewhere between 1.4 and 5.8 K over the period 1990-2100 (IPCC 2001). This in turn will affect other atmospheric parameters in ways that are hard to quantify. However some key predicted changes were approximated by varying the input signals to the model and observing model responses.

The simplest way to impose the above global warming trend on a model is to assume a linear increase over time. This was added to the input air temperature variable for Model SM 1. A conditional command was added to the model to ensure that the minimum calculated ice thickness was 0m (i.e. any negative calculated values were set to zero). It was run for a period of 100 years, with superimposed linear trends corresponding to several different values of the 'global warming per century'.

The stable-state nature of the physics model allowed a different approach. When

the mean temperature was changed, the model reached a new equilibrium state. Therefore the average response to a new average temperature was found with the input temperature expressed as a cosine curve. The temperature signal was altered by amounts between -15 and +25 K from the 1957-2003 mean (corresponding to mean temperatures of 248.33 to 288.33 K), run for 10 years to a steady state as in Figure 6.9, and the maximum, minimum and mean predicted ice thicknesses in the 10th year were noted. In addition the lengths of predicted periods of no ice were noted.

Changes in intraseasonal variation and extreme weather events due to climate change are poorly understood as they involve the interaction of several global atmospheric cycles (IPCC 2001). However some areas of the world may begin to experience colder winters at the same time as warmer summers. Such a change was approximated by altering the amplitude of the sinusoidal annual temperature signal while keeping the annual mean value the same, thus representing changes in the summer-winter difference.

Precipitation is also predicted to increase in high latitudes in winter (IPCC 2001). The effects on Crooked Lake are hard to quantify, but more snow may lead to an increase in the albedo of the ice surface. This was investigated by varying the albedo input.

6.8 Results

The 100-year outputs from SM 1 and the physics-based model with superimposed warming of 0, +1, +3 and +5 K per century were plotted against time (Figures 6.10 and Figure 6.11). With non-zero warming the predicted annual mean ice thickness from SM 1 decreased rapidly to begin with, then more slowly and approximately linearly with time. These transition points occurred in years 21, 12 and 9 for +1, +3 and +5 K respectively and corresponded to the first year in which the calculated ice thickness went to zero in summer. For the physics model the ice thickness decrease was more steady, and approximately linear.

The figures illustrate differences between the two models. SM 1 is a completely continuous model, so any decrease in ice thickness one year propagates directly to the next, and the decrease is stopped only by the built-in condition that ice thickness cannot be less than zero. Thereafter the ice only grows in periods when the air temperature is lower than the threshold parameter T_f, and such periods

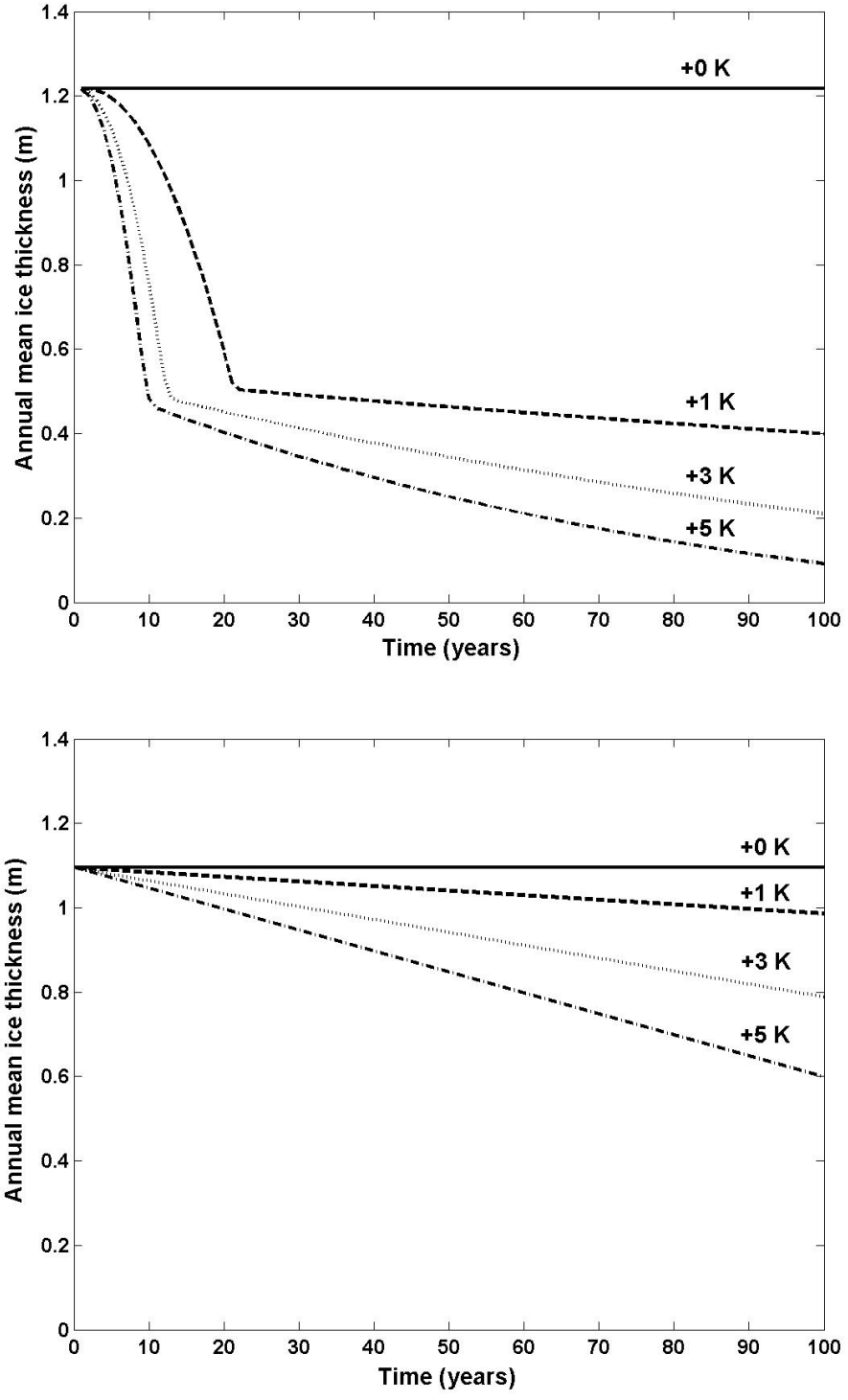

Figure 6.10: Annual mean ice thickness predicted by SM 1 (top) and the physics-based model (bottom) for model runs of 100 years, with superimposed linear temperature increases of 0, 1, 3 and 5 K per century.

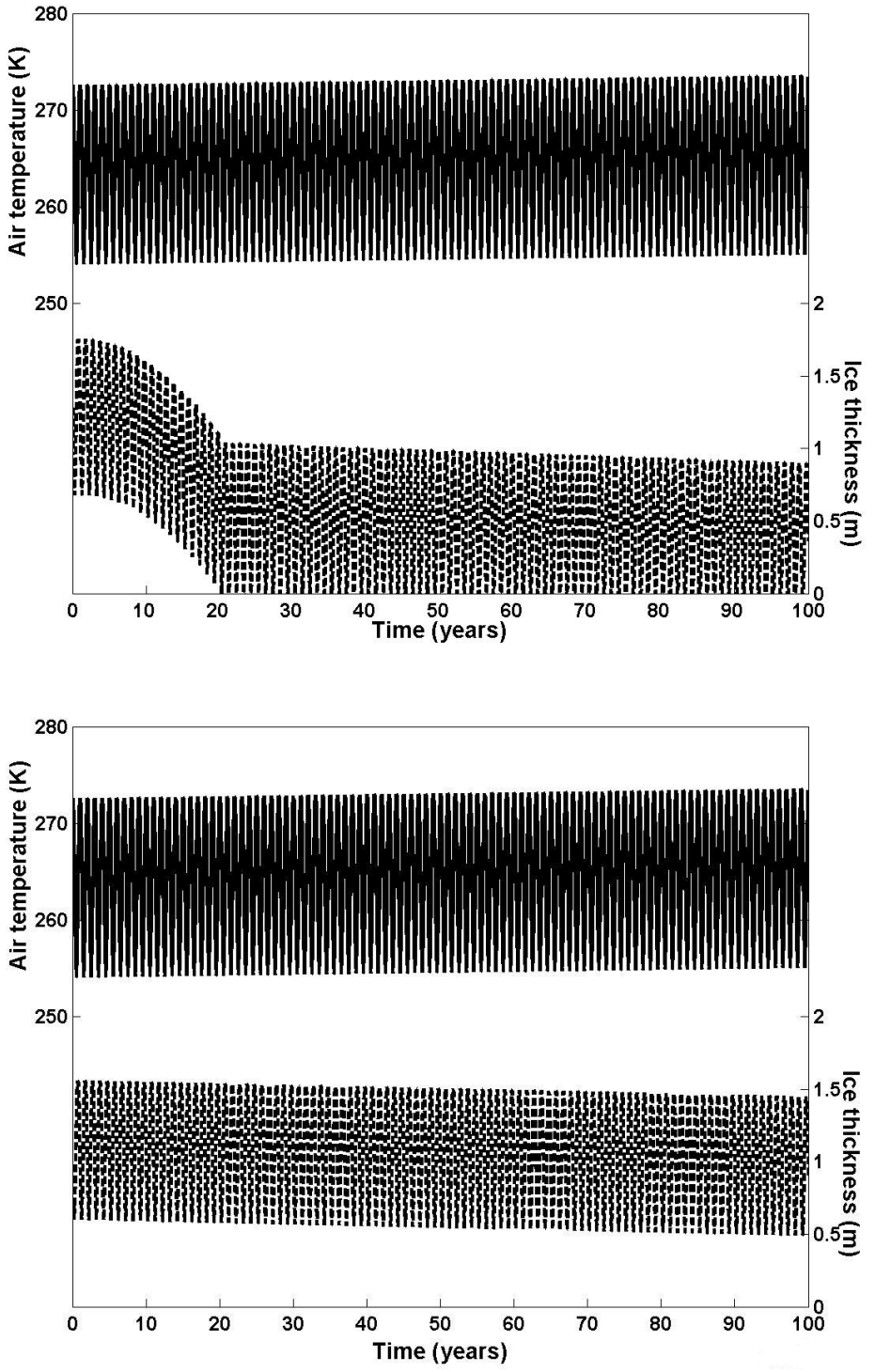

Figure 6.11: A comparison of long-term responses of SM 1 (top) and the physics model (bottom). Both were run for 100 years with a superimposed linear increase of 1 K per century on the temperature signal, and the predicted ice thickness trends are plotted.

become smaller as temperature increases.

The physics model is also continuous, however a degree of discreteness to the year in hand is indirectly introduced because any change in ice thickness is dependent on the ice thickness itself. The model automatically tends towards a stable state corresponding to the imposed temperature state, which (for a simple increasing temperature signal with no other interannual variation) is an annual oscillation steadily decreasing in amplitude. The physics model thus has the required stability for long-term predictions. It accounts far more successfully than SM 1 for summer periods when ice partly breaks up and the overall behaviour of the lake changes (which has not been explicitly modelled in this thesis). Model SM 1 can in fact be ruled out as useful for long-term predictions.

The physics-based model was therefore used for all further investigations. Firstly the mean temperature was changed and the model was run to a steady state corresponding to the new temperatures (Figure 6.12). The steady state ice thickness appeared to increase exponentially with decreasing mean temperature, and the amplitude of the annual oscillation (difference between maximum and minimum ice thickness) decreased. On increasing mean temperature, periods of no ice first occured at +5 K, where 35 days per year of no ice cover were predicted (annual minimum ice thickness was zero). The predicted number of days of no ice cover then increased approximately linearly with temperature until +23 K, where no ice was present at any point in the year.

The effects of other perturbations to input signals are shown in Figure 6.13. On increasing the amplitude of the sinusoidal temperature signal, the steady states of the model predicted larger amplitude annual oscillations in ice thickness, in an approximately linear response. The oscillation was big enough to produce periods of no ice at 6 K beyond the 1957-2003 extremes. The mean ice thickness also increased slightly with the amplitude of the temperature signal, despite the mean temperature remaining the same. This implies that the formulation of the model is slightly in favour of growth over melting, i.e. the model responds more significantly to abnormally low temperatures than to abnormally high ones.

On increasing ice albedo from 0.13 to 0.93 (corresponding to deviations of -0.3 to +0.5 on the 2003 mean value of 0.43), the predicted mean annual ice thickness increased from 1.03 to 1.27 m. This is to be expected: an increased albedo reduces the penetration of solar shortwave radiation, reducing temperatures in the ice layer and encouraging ice growth.

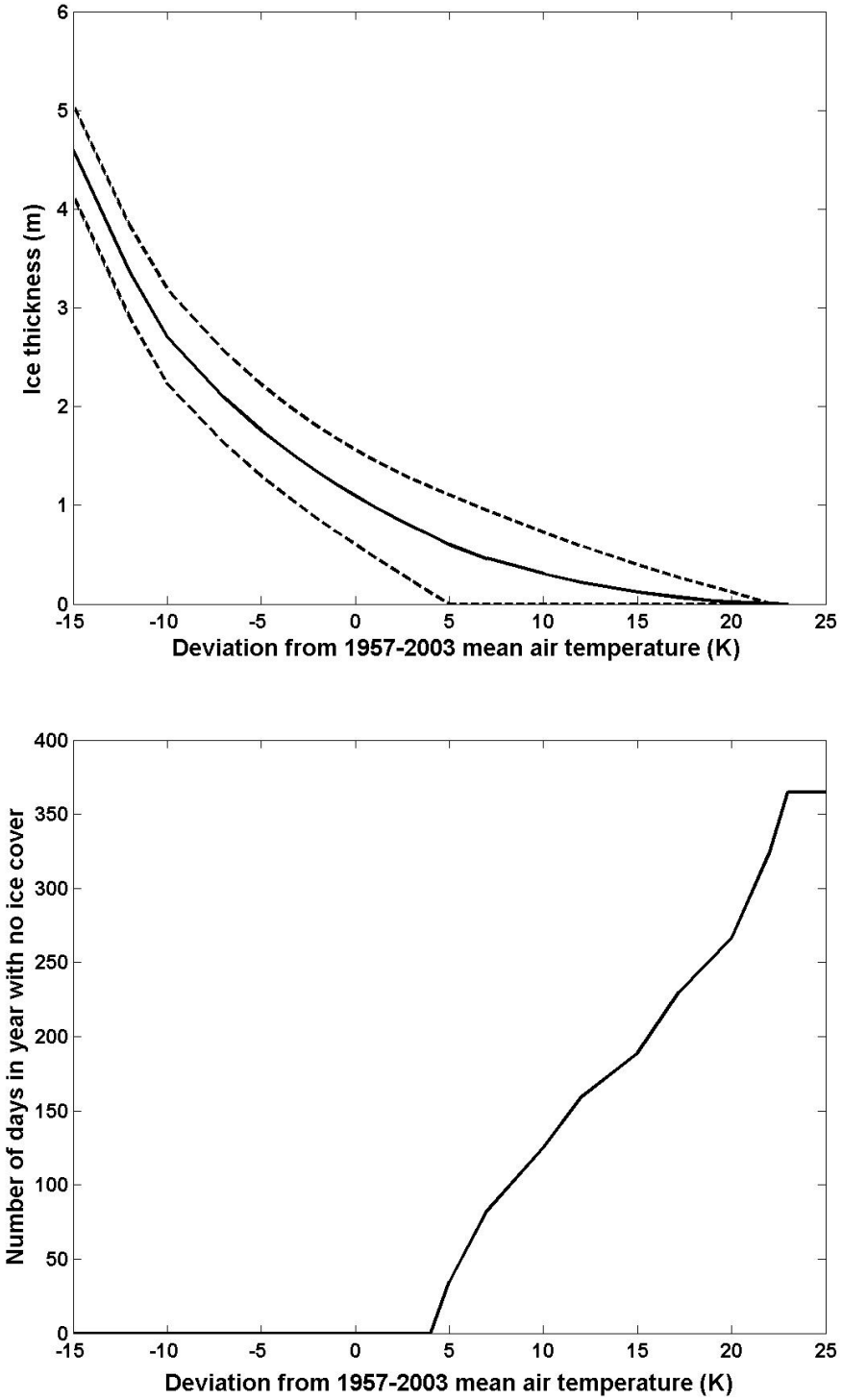

Figure 6.12: Mean (solid line) and maximum/minimum (dotted lines) ice thickness for the steady state of the physics model reached when the annual mean of the air temperature signal was deviated from the 1957-2003 average (top), and the corresponding number of days per year with no ice cover (bottom).

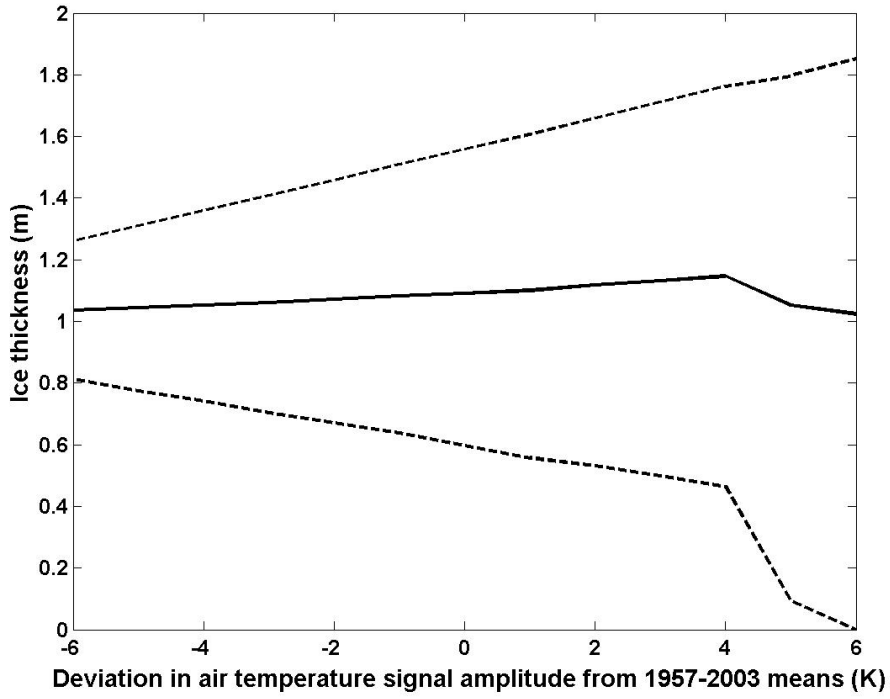

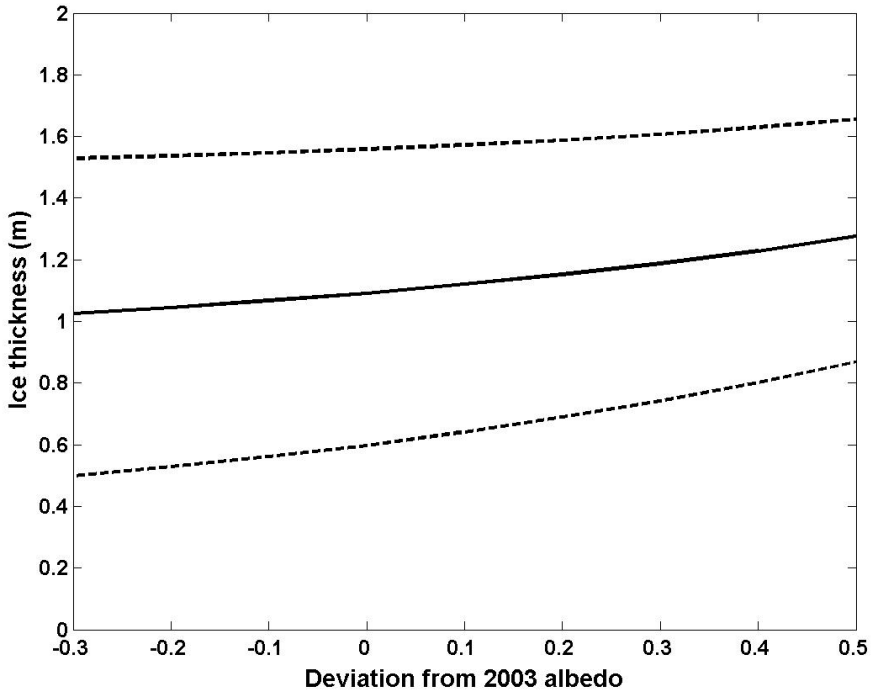

Figure 6.13: Ice thickness response of the physics model to changes in the amplitude of the input temperature signal (top) and changes in the ice albedo (bottom). This approximates the effects of changing interseasonal variability and changing precipitation, respectively. In both graphs the solid line is the annual mean at the steady state, and the dotted lines are the maximum and minimum values.

6.9 Summary

A physics-based model of lake ice has been shown to perform well with air temperature as the only input variable. Steady states were found for both the physics-based model and a simple empirical model, with a 'baseline' provided by climate averages for 1957-2003. On introducing temperature perturbations, the physics model was found to be considerably more stable in the long-term than the simple model. The simple model fitted data successfully and highlights an interesting simple relationship between ice thickness and air temperature on the scale of a year, but is meaningless in the long-term.

The physics-based model predicted an approximately exponential decay in annual mean ice thickness with increased annual mean air temperature. Completely ice free summer periods were predicted at +5 K above the 1957-2003 averages, and no ice at any point in the year at +23 K and above.

Both an increase in amplitude of the annual temperature signal and an increase in ice surface albedo produced small increases in annual mean ice thickness. This suggests that some postulated global warming 'side effects', namely more extreme weather events, increased intraseasonal variability and increased precipitation (IPCC 2001), may provide small negative feedbacks on warming effects at a local level. However such changes are poorly understood, and the impacts are in any case far less significant than an air temperature increase.

Chapter 7

Biological modelling

7.1 Overview

The physical environment on and above Crooked Lake as modelled in Chapters 3 to 6 influences the biological organisms in the water below. Changes in the ice layer affect the temperature, radiation, and wind-induced mixing of the water, which are all important for the growth and primary production of the plankton. The responses of such organisms to physical changes have been measured in lab experiments, and the general response of a whole ecosystem to large-scale anomalies such as climate change can be postulated. However, the variability in any biological system is large, and aquatic food chains involve highly complex interactions between different types of plankton and chemical resources, which are poorly understood. In addition, the amount of data available to verify models tends to be low.

In this chapter, the usefulness of biological data as an indicator of temporal change is assessed, to determine the potential benefits of adding further sensors to a device such as the Crooked Lake probe. To represent temporal change in the system, generic population dynamics models, typified by predator-prey type interactions, are investigated. A biological dataset from 1992-93 is analysed to assess whether the biomasses of carbon-based organisms display significant oscillations of wavelength one year or less, such as those predicted by plankton population models. Each modelling assessment is based on 24 datapoints over a year, so in terms of model analysis techniques it presents a marked contrast to the physical modelling in Chapters 3 to 6, where the temporal resolution was as high as several measurements per day.

In contrast, a theoretical modelling experiment was developed, which poses the question: "If we believe the system does behave according to a certain model, how much data would we need to identify it?". This was assessed for a simple sine wave model. A large number of 'simulated datasets' were created for model fitting, and the standard deviations in model parameters were plotted as a function of the sample rate and sample error. The procedure provides a prototype tool analogous to a power analysis for scientists who believe they may observe a certain type of behaviour in a system, and need to estimate how much data they should collect.

7.2 Analysis of past data

The longest continuous limnological study of Crooked Lake to date was undertaken in the years 1992 to 1993 by Laybourn-Parry et al. (1995). This produced data that covered an entire year for the numbers and biomasses of bacteria, phototrophic nanoflagellates (PNAN), heterotrophic nanoflagellates (HNAN) and ciliates, as well as the concentrations of dissolved organic carbon (DOC) and inorganic nutrients. Each was sampled at depths of 0, 2, 5, 10, 15, 20, 30 and 40 m on 24 dates in total, giving an average of two datapoints per month with the first on 21 December 1992 and the last on 29 November 1993. Only one replicate was counted for each depth, but for considering changes over time this gives an 8-point sample for calculating the average concentration in the whole water column.

For the investigation of predator-prey type oscillations in Crooked Lake, the cycling of carbon is the most important factor, so only the measurements of plankton and DOC are considered here. HNAN consume bacteria, while ciliates may feed on all smaller plankton, and all types of plankton are believed to exploit the DOC pool as a resource to some extent (Laybourn-Parry and Parry 2000). Therefore as the abundance of one type of plankton increases, another may be decreasing. Considering only the DOC and plankton biomass measurements (all in μg l^{-1}) allows direct investigation of temporal changes in the carbon distribution.

A discrete Fourier transform was used to obtain a spectrum of frequencies in the data. This required an evenly spaced time series, and given the sporadic sampling dates this was approximated by calculating a mean value for each of the 12 months. For a sampling interval Δt the maximum frequency that can be observed is given by the Nyquist critical frequency, $f_c = \frac{1}{2\Delta t}$, so for monthly data $f_c = 0.5$ month^{-1}. This corresponds to a wavelength of around 60 days. The

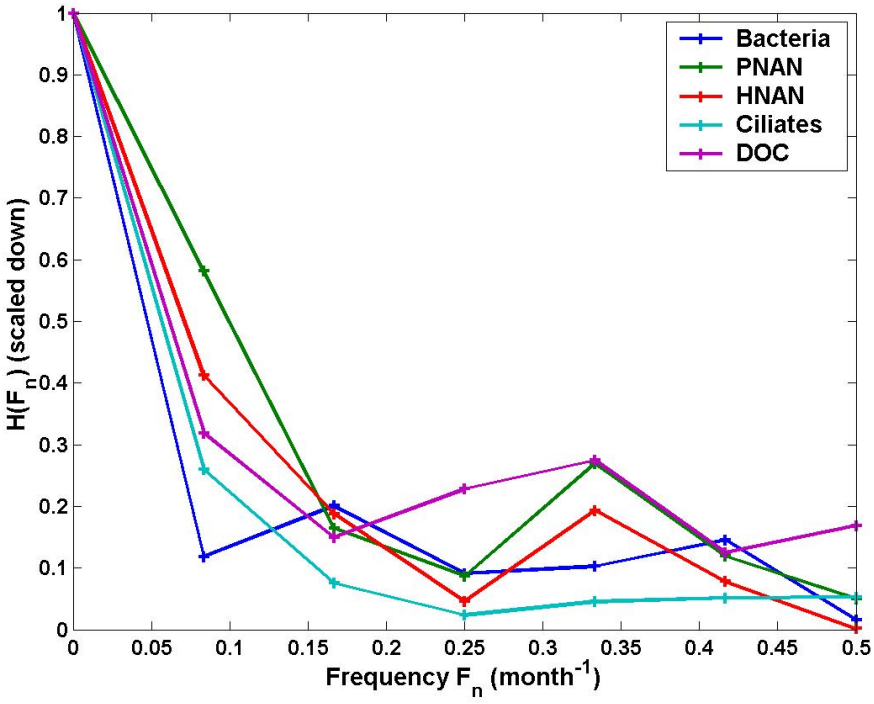

Figure 7.1: Discrete Fourier Transform spectra of plankton and DOC in Crooked Lake, based on 12 monthly datapoints extrapolated from the work of Bayliss in 1992-93. $H(F_n)$ is scaled down to fit all on the same graph.

discrete Fourier transform was approximated by:

$$H(f_n) \approx \Delta t \sum_{k=0}^{n_d-1} h_k \exp\left(\frac{2\pi i k n}{n_d}\right) \tag{7.1}$$

where h_k represents the kth datapoint in the time series and n_d is the total number of datapoints ($n_d = 12$). $H(f_n)$ was calculated for the discrete frequencies $f_n = \frac{n}{n_d \Delta t}$, where $n = 0, 1, ..., \frac{n_d}{2}$. The values of $H(f_n)$ were scaled by dividing by $H(0)$, to allow plotting on the same graph (Figure 7.1). $H(f_n)$ represents the strength of the 'signal' at frequency f_n. This is highest at $f_n = 0$, corresponding to the null signal, and tails off at higher frequencies. There are small peaks in the DOC, HNAN and PNAN spectra at 0.33 month^{-1} (wavelength of 3 months), which corresponds to a population oscillation of comparable size to the oscillations of 50-100 days calculated in the plankton models of Edwards and Brindley (1999) or Huisman and Weissing (1999). However, a Fourier transform with such a small amount of data is far from conclusive, and there is a high probability that any signals are just a result of the error variation in the data.

To gain insight into how significant any existing oscillations may be, the system

was modelled using a simplified form of spectral analysis, with two superimposed cosine oscillations dependent on time alone - one with a fixed period of 365 days to represent the seasonal cycle, and another with an adjustable period parameter representing the population oscillation. The model had 6 parameters in total to model the 24 datapoints and was formulated as follows:

$$Biomass = A_1 \cos\left(\frac{2\pi(t+\phi_1)}{365}\right) + A_2 \cos\left(\frac{2\pi(t+\phi_2)}{T_2}\right) + C \qquad (7.2)$$

where t is the time in days, A_1 and ϕ_1 are respectively the amplitude and phase of the seasonal cycle, A_2, ϕ_2 and T_2 are respectively the amplitude, phase and period of the population oscillation, and C is an offset parameter. The model was first run with A_2 set to zero, representing the annual oscillation alone. Then A_2 was given a non-zero value, with T_2 given an initial value of 80 days to approximately represent the oscillations suggested in the Fourier spectra. The significance of adding the new oscillation was assessed using the ANOVA test as described in Chapter 2. As an example, the model output for ciliates is plotted with the data in Figure 7.2, and it's ANOVA assessment is in Table 7.1. Table 7.2 summarises the results for all the series.

	n_p	df	WSS	MS	F	P
Annual cycle	3	2	0.22	0.11	25.04	< 0.001
+ oscillation	+3	+3	0.02	0.007	1.75	0.193
Residual		18	0.07	0.004		
Total		23	0.31			

Table 7.1: ANOVA table assessing the model from Equation 7.2 with only an annual cycle, and the improvement in fit on adding a superimposed population oscillation.

The values of P(annual) in Table 7.2 are very low for all the measurements except the bacteria, therefore there is a significant sinusoidal annual cycle in all the quantities except bacteria. The phase ϕ_1 for the DOC indicates that it was almost completely out of phase with the plankton populations, as may be expected - the DOC pool is higher in winter because there is less light for growth and reproduction in the food web, and hence less uptake of DOC by organisms and higher contribution to the DOC from dead organisms. The phase ϕ_1 for bacteria indicates that the annual cycle peaks slightly ahead of the HNAN, suggesting a predator-prey type time-lag on the scale of a year.

The estimated periods of the population oscillations (T_2) were all between 80 and 90 days. However the values of P(oscillation) are all higher than the usual

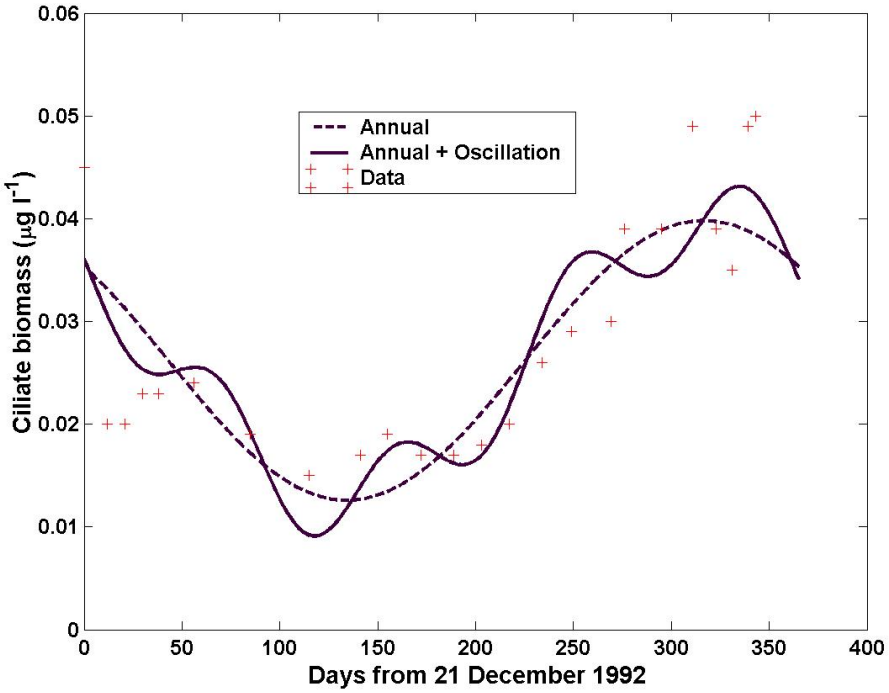

Figure 7.2: Superimposed sine waves model (Equation 7.2) optimised for ciliate biomass data (crosses), with only the annual cycle (dotted line), and with an added population oscillation (solid line). Goodness of fit of the solid line is $\chi^2 = 0.07$, $r^2 = 0.77$, $\nu = 18$.

maximum significance level desired in a statistical test (0.05). Therefore the analysis gives no confidence that oscillations on scales of less than a year are occurring. Also the results of optimisation appeared to be sensitive to initial conditions and produced some different values of T_2 when the procedure was started with values other than $T_2 = 80$ days. Therefore it seems that when the average time between measurements (around 15 days) is high relative to the period of oscillation, there may be several local minima relating to oscillations of different sizes.

In conclusion, considerably more data, and more accurate data, would be required to demonstrate the existence of population oscillations in Crooked Lake. Moreover, the balance of requirements between a higher sampling rate and more accurate data is a point which needs careful consideration.

	Bacteria	**PNAN**	**HNAN**	**Ciliates**	**DOC**
A_1	1.36	0.98	0.53	0.014	448.50
ϕ_1	19.39	-14.05	-15.18	48.36	-156.55
A_2	1.72	0.23	0.21	0.004	349.49
ϕ_2	17.80	36.56	42.56	19.86	23.78
T_2	83.04	80.13	84.43	89.56	87.05
C	5.16	0.81	0.60	0.026	714.86
r^2(annual)	0.13	0.72	0.52	0.71	0.31
r^2(both)	0.37	0.76	0.60	0.77	0.49
P(annual)	0.688	< 0.001	< 0.001	< 0.001	0.006
P(both)	0.031	< 0.001	0.002	< 0.001	0.010
P(oscillation)	0.112	0.420	0.328	0.193	0.141

Table 7.2: Estimated parameters found when using Equation 7.2 to model the 1992-93 plankton biomass measurements in Crooked Lake, the r^2 fit without and with the superimposed population oscillation, and the P values corresponding to the annual cycle, both cycles and the oscillation as an 'improvement'.

7.3 Identifying oscillations in simulated data

A modelling procedure was developed to estimate how much data may be needed to verify the existence of oscillations in a plankton population. This simulates the hypothetical situation where the behaviour of the observed system is dominated by an underlying 'true model', with a certain amount of random variation superimposed. The question is then focussed on what sample rate may be required to produce sufficient data for the underlying model to 'shine through the noise', and be adequately identified through parameter estimates.

The procedure considers an arbitrary population P with an underlying sinusoidal oscillation of amplitude A, period T, phase ϕ and offset (mean value) C:

$$P_{model} = A\cos\left(\frac{2\pi(t+\phi)}{T}\right) + C \tag{7.3}$$

It was not considered necessary to simulate the annual oscillation as in Equation 7.2. Equation 7.3 was used to create 'simulated datasets', using the initial parameter values shown in Table 7.3. Firstly a value of P for every day of an arbitrary year (0,1...365) was calculated. The data was generated by defining an experimental sample rate and taking the value of the model at each discrete time when samples were made. For example, to represent a sample rate of once a week, every seventh value was extracted. Random variation was superimposed to approximate more realistic data.

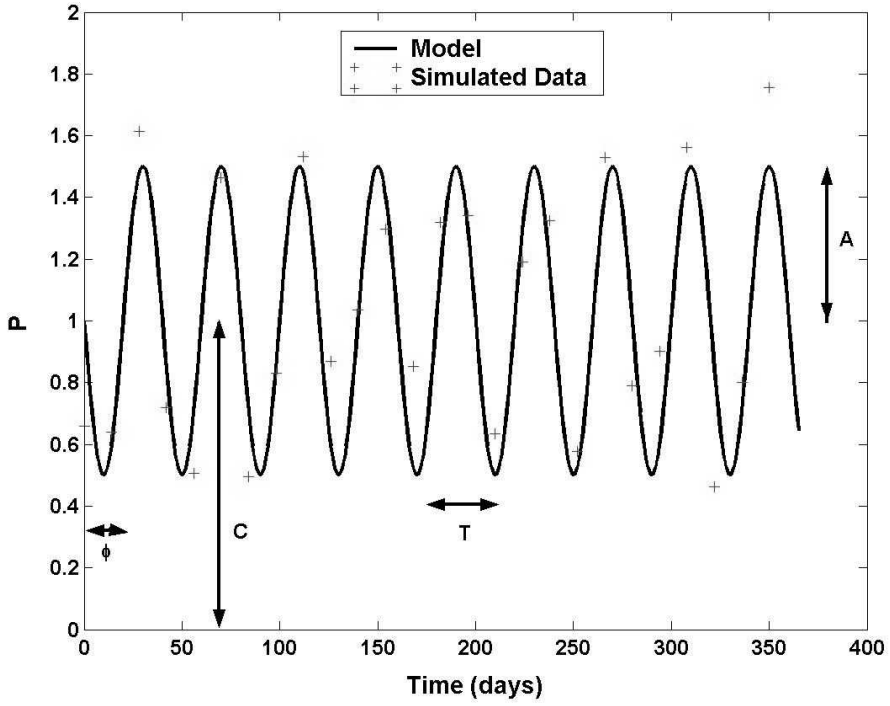

Figure 7.3: Simulated data (crosses) created from the underlying model (solid line) using a sample rate of one sample every 14 days and added random variation with a standard deviation of $\sigma_r = 0.2$.

Parameter	Initial value
A	0.5
T	40
ϕ	20
C	1

Table 7.3: Initial parameter values used for all simulations involving Equation 7.3.

The first method used to add realistic variation to the simulated datasets was to add a normally distributed random number to each datapoint, with a mean of zero and standard deviation σ_r (Figure 7.3). To do this the *randn* function in MatLab was used, such that $P_{simulated} = P_{model} + \sigma_r \times randn$. This represents the random variability that may be expected in a natural system, and the random nature of a sample mean versus the true population mean. MatLab code was used to run the following procedure:

1. Choose a standard deviation σ_r to try.

2. Choose a 'time between sample' value to try (t_s, corresponding to sample frequency $f_s = 1/t_s$).

3. Run the model (Equation 7.3) to get a value of P_{model} for every day of an arbitrary year.

4. Extract every t_sth model value and add random variation (dictated by σ_r) to get simulated dataset.

5. Estimate the model parameters for the simulated dataset using Levenberg-Marquardt optimisation.

6. Repeat steps 3 to 5 many times (Between 100 and 500 repeats were used).

7. Calculate the standard deviations of the parameter values across all the simulated datasets.

8. Go back to 2 and repeat all for another value of t_s.

Given that the period of the underlying oscillation was 40 days, the maximum value of t_s that could be used was 19 (to stay below the Nyquist frequency where $t_s = 20$). The procedure was run for $t_s = 1, 2...19$, and three different values of σ_r (Figure 7.4).

The mean values of all the parameters over the 500 simulated datasets were equal or very close to the initial values used in generating the datasets, irrespective of the sampling rate (Table 7.3). The coefficient of variation (standard deviation expressed as a percentage of the initial parameter value) of each parameter increased as the time between samples increased (sample frequency decreased), following approximately exponential curves. It also increased with σ_r. The amplitude parameter A had the highest standard deviation across the 500 simulated datasets. This is connected to the way in which the random variation was added on; A determines the vertical height of the oscillation, and hence is the parameter that compensates most for 'vertical' changes in the population. The period parameter T had the lowest standard deviation, because it related to the 'horizontal' size of the oscillation, to which no random variation was added.

In general the standard deviations of parameters were low. Even at the lowest sample rate of 1/19 day^{-1} and with $\sigma_r = 0.3$, the highest standard deviation (on A) was less than 20 %. In this case $\sigma_r = 0.3$ approximately represents the highest end of sample standard deviation which occurs in plankton sampling, which may be reduced further by taking more replicates. One may tentatively conclude at this point that in a system dominated by one strong underlying signal with only random noise added, sampling frequency can be reduced to just below the Nyquist

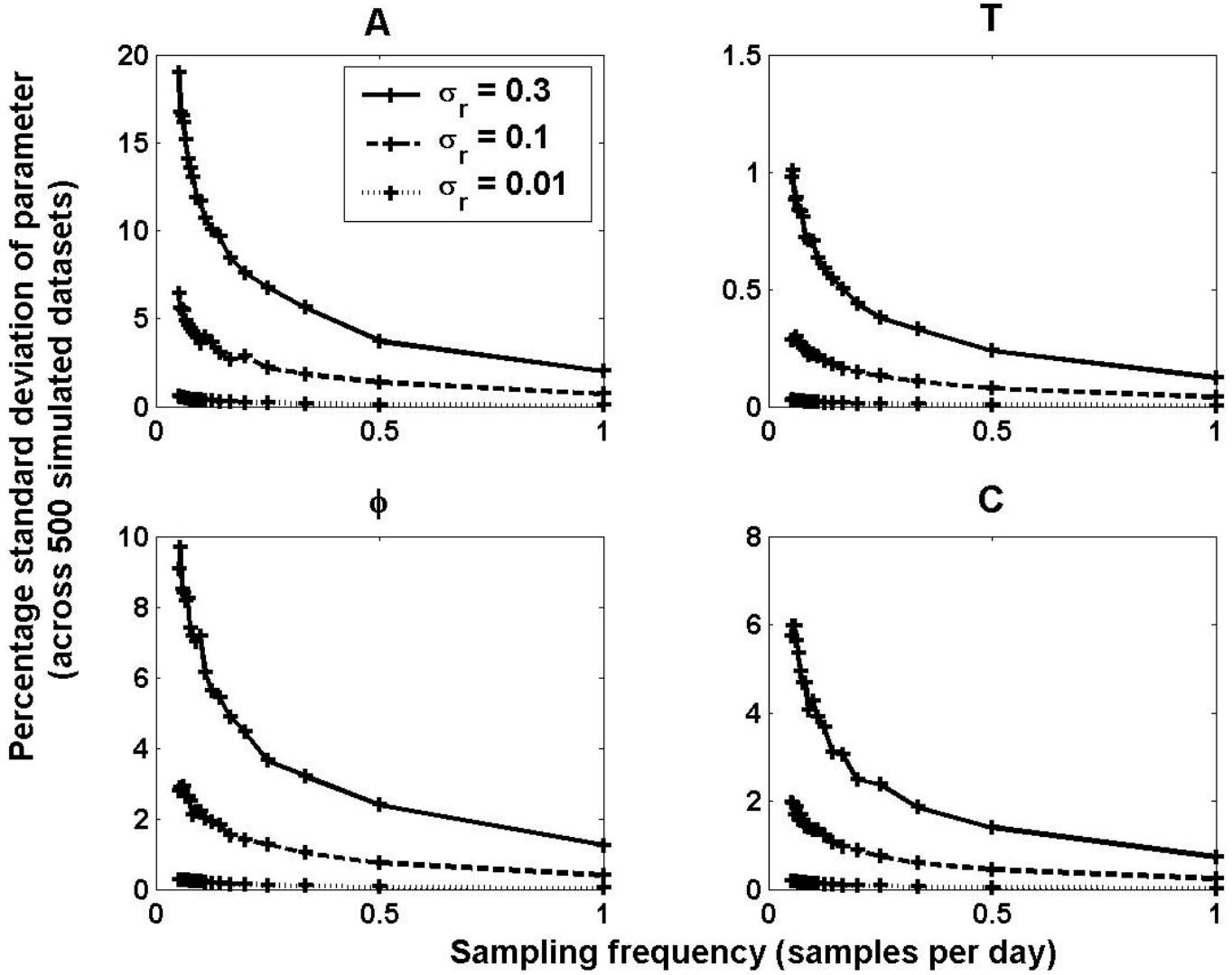

Figure 7.4: Percentage standard deviation of four sine wave parameters A, T, ϕ and C across 500 repeats, plotted against sample frequency. Equation 7.3 was used to create 500 simulated datasets, with added random variation created by adding a random number with mean 0 and standard deviation $\sigma_r = 0.01$ (dotted line), $\sigma_r = 0.1$ (dashed line) and $\sigma_r = 0.3$ (solid line).

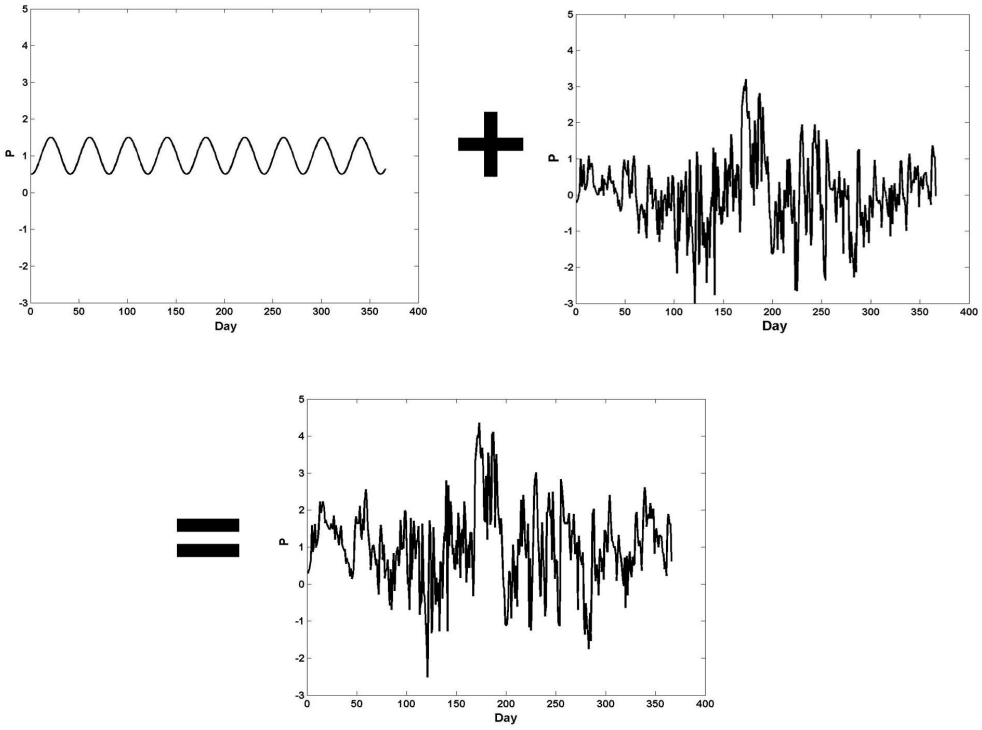

Figure 7.5: Addition of non-random variation to an oscillating model, for creating simulated data with an underlying oscillatory trend. Normalised temperature data from Crooked Lake in 2003 was used as an example of a non-random signal.

frequency of an oscillation and still detect such an oscillation to a high degree of statistical significance.

However the result is rather false, as it assumes that the oscillation is the only significant signal present in the population dynamics. Random noise can effectively cancel out over several datapoints. In reality some smaller, non-random but unquantifiable signals may be present, and the analysis may have difficulty identifying out the underlying signal when it is one of many. For example, the atmosphere provides many signals that affect the population, and although some simple relationships can be postulated (e.g. greater light and temperature increase photosynthesis and growth rates), they are poorly quantified (e.g. growth is limited by other factors such as nutrients).

Atmospheric signals are dominated by the annual cycle, with shorter-scale changes related to shifting weather patterns. For the investigation in hand, the variations in air temperature recorded at Davis station were used as an example of the sort of non-random signal that may be superimposed on population data and obscure an underlying oscillation. Daily temperature data for 2003 was used. The annual cycle was removed from the temperature data by subtracting the best fit annual sine curve (of period 365 days), and the data was normalised. This provided a

non-random signal T_a with mean zero, which was added to the simulated data (Figure 7.5):

$$P_{simulated} = P_{model} + \sigma_r \times randn + T_a \tag{7.4}$$

The exercise was repeated using Equation 7.4 with the same three values of σ_r as above (Figure 7.6). The standard deviations on all the parameters increased at all sampling frequencies, and was again highest for A and ϕ. The period T again had a standard deviation of less than 5 %. The plots were considerably less smooth than in Figure 7.4, implying that the addition of a non-random signal added more variation in the responses to changing sampling frequency. Increasing the number of repeats from 500 would show the response more accurately, but would be more computationally expensive.

In practice there is unlikely be such a consistent underlying oscillation as has been simulated above. The optimisation procedure has very biased initial conditions, given by the parameters which generated the data in the first place. There is also no random variation added in the 'horizontal' of the signal, which results in the low standard deviations on the period parameter. The period of a population oscillation may be variable as a result of external factors, and may be affected by atmospheric signals. There is also the issue of success; several factors can hinder work in the Antarctic such as extreme weather, logistics and lack of ice cover for travel, so it may not always be feasible to reach the study site on the day planned.

Improvements on the usefulness of such a technique would require the simulation of more realistic data. This could involve more superimposed non-random signals, and the addition of stochastic elements to both the day on which sampling can be made and the period of the underlying population oscillation.

7.4 Summary

A Fourier analysis and ANOVA tests were used to assess the significance of oscillations in plankton populations in Crooked Lake, using data from 24 sample dates in 1992-93 on bacteria, heterotrophic nanoflagellates, phototrophic nanoflagellates, ciliates and dissolved organic carbon. Oscillation models were successfully fitted to the datasets, but the statistical significance was too low to prove the existence of oscillations of wavelength less than one year. However all the measured

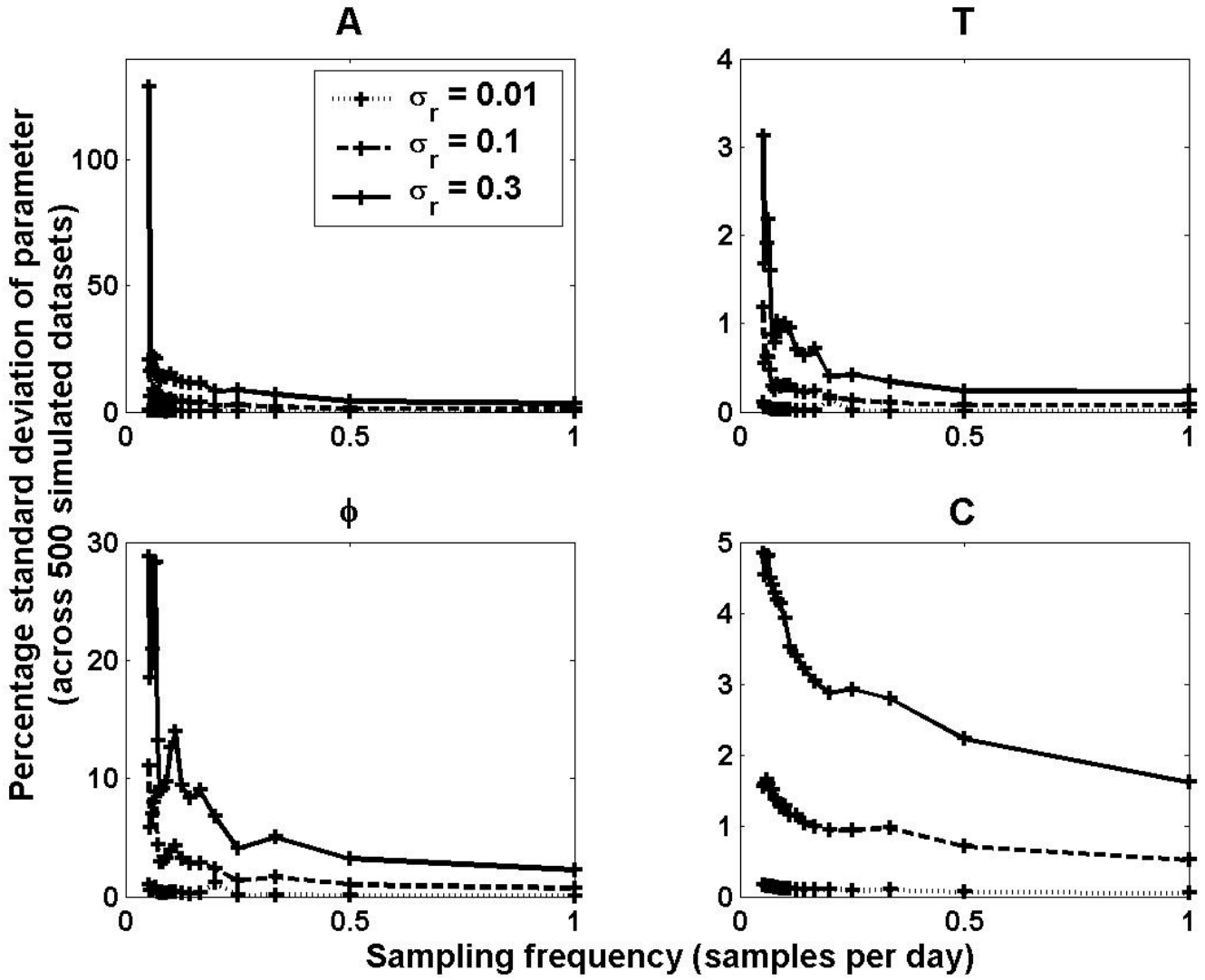

Figure 7.6: Results for the same exercise as Figure 7.4, but with a normalised non-random signal superimposed on the simulated data. 500 simulated datasets were used.

quantities except bacteria exhibited a significant 365-day oscillation in line with the annual cycle.

A prototype technique has been developed to assist in the development of sampling strategies when the aim is to identify an underlying model behaviour. For the specific case of a sine wave model, several datasets were generated from a model with a given sample rate, with both random and non-random variation superimposed. On fitting the original model for each dataset, model parameters were found to have significant values at low sample rates, just greater than the Nyquist frequency of the underlying oscillation. However the technique has several flaws, and generation of truly realistic data for such a purpose would require a greater quantity of relevant real data from the field, for an assessment of its statistical characteristics. In addition, models of different systems may have different relative responses to data sample rate and data error. It may be more worthwhile to rely on the simple philosophy that one should always collect as much data, and as accurate data, as possible. That said, with a truly plausible model, especially one that has been verified using data from similar systems, the procedure could provide a good picture of the accuracy of parameter estimates one may expect. The experimenter could overcompensate where possible to account for unpredictable natural variability.

For Antarctic plankton, complex population dynamics models have not been verified due to the lack of data; research into these systems is still at a relatively early stage and progress is slow due to the logisitics of working in such an environment. Hence most studies thus far have been building up a general catalogue of the organisms present across large areas like the Vestfold Hills, rather than rigorously analysing any one system. The 1992-93 data in particular highlights the fact that for population modelling purposes it may be informative to conduct an intensive study of one aspect of a system as well as spreading time across several. For example, on a device such as the Crooked Lake probe, the addition of a fluorimeter to estimate chlorophyll content in the water on high temporal resolution would give a better indication of whether such models can be applied to Antarctic microbial systems.

This chapter has highlighted a number of important differences between physical and biological systems, in particular with regard to long-term climate change predictions. Physical data is generally better understood and exhibits less complex natural variability than biological data. In the previous chapters, it was shown that the responses of ice to changes in temperature are both fast and significant, and thus the good fit to the 2003 data may be taken as justification that the

model will be at least approximately applicable in future years. However the climate is only one of many factors which may affect an individual organism or a food chain over the course of a year, particularly in a system which is so limited in terms of light and nutrients. Therefore data from one day in the field cannot be taken as a generic sample with regard to climate change, and to establish strong correlations between atmospheric and biological quantities the system would have to be studied over a far longer time period. For this purpose, the temporal coherence supplied by a sampling strategy similar to that in 1992-93 may be enough to allow 'averaging-out' of any unpredictable shorter scale changes, but may provide only one accurate datapoint per year.

Chapter 8

General discussion

8.1 Overview

This chapter provides a summary of the main findings in this project, the limitations of the work, and how it can be related to similar present and future work.

8.2 Main findings and achievements

This thesis has described the development, analysis and comparison of data and models related to an Antarctic freshwater lake ecosystem. It has also provided a forum for testing and developing some new and emerging model assessment techniques.

A Levenberg-Marquardt optimisation procedure was developed for MatLab, and was used successfully throughout the project. Unlike some existing optimisation software tools, it can be applied to models of any given complexity or linearity, and allows the user to change certain accuracy settings, so may be of use to mathematically literate scientists who wish to monitor exactly how their parameter search is carried out. In addition, the procedure calculates five common model selection criteria.

A technique termed 'model trimming' has been introduced, which is intended for assessing the relative importance of input variables in a complex model. It has proven useful for identifying variables that introduce 'more noise than signal' to

a model, and thus for informing the development of parsimonious models.

A physics-based model of freshwater lake ice has been developed using data from an automatic probe on Crooked Lake, Antarctica. The large amounts of data allowed considerable detail to be included, such as variations in ice albedo and the radiation extinction coefficient, which are often assumed to be constants. All parameters were kept within constraints concordant with well-established physical laws and empirical relationships. The model was fitted to ice thickness data, and an analysis revealed that air and water temperature were the most important driving input variables.

Several empirical models were also developed by considering simple relationships between input and output variables. On comparing these to the physics-based model, some model selection criteria 'chose' the empirical models while the ICOMP criteria 'chose' the physics-based model. However, the large amount of data and the more mechanistic nature of the physics-based model were shown to reduce the usefulness of these techniques. It may be that only models with completely free adjustable parameters should be meaningfully compared using model selection criteria.

A danger of accepting parsimonious models was highlighted when running long-term simulations. A simple empirical model was shown to be unstable in its response to a long-term temperature signal, whereas the physics-based model adopted a steady state independent of initial conditions. This is the most acute example of a failure of model selection criteria - they did not point out the problems with the simple model, but a long-term model run and mathematical common sense did.

The physics-based model predicted summer periods of no ice at +5 K above the 1957-2003 mean temperatures, and no ice at all at +23 K. It also exhibited small positive responses of ice thickness to increased air temperature signal amplitude (representing increased interseasonal variability) and increased ice albedo (representing increased precipitation).

To complement the physical description of Crooked Lake, an investigation was made into the potential of biological data from the area to be an effective indicator of climate change. To gain insight into what sort of changes could be observed in such a simple system, the common phenomena of predator-prey oscillations was considered. Some plankton biomass data collected at Crooked Lake in 1992-93 were analysed and shown to exhibit no significant oscillations, suggesting that more data is required to identify such phenomena. This is in stark contrast to

the ice modelling situation where vast amounts of data were available, and highlights a common difference in temporal resolution between physical and biological datasets which is generally unavoidable due to the logistics of data collection. For these reasons a procedure was developed using simulated data to develop sampling strategies which could identify an expected underlying behaviour. However the technique relies on a strong belief in the model, and given the limitations and uncertainties on plankton data for the area, no conclusions can be made. In reality the limiting factors of nutrients, light and temperature may suppress growth and species interactions, such that any existing dynamics on scales of less than a year are below the detection limit.

8.3 Limitations

The temperature data collected at Crooked Lake is very specific to one year in the lake's history, and will not be collected on a regular basis. For these reasons the models in Chapters 3 to 6 were developed using meteorological data from Davis station, which have been measured on a regular basis since 1957, and will be as long as the station exists. However for most of the analyses the models were fitted to the ice thickness data from 2003, which although of high temporal resolution is still only representative of one year. The successful cross-validation with 1993 and 1999 data improves the generalisability of the physics model, but does not remove the possiblility that the model could fail to reproduce data from a less typical year.

Lake ice is difficult to define as either a discrete or continuous system. One may define a discrete 'turnover time' of a year as the longest cycle affecting the system, but ice thickness is certainly dependent on the value the previous day and (unless the ice has melted completely in summer) the previous year. The physics model solves this problem to some extent by including the ice thickness value in the calculation of ice thickness change, thereby adjusting itself to whatever new temperature state is imposed. A successful linear relationship between mean annual air temperature and ice thickness may prove the system is discrete on the scale of a year, but would require many years of data to verify it.

It has been shown that it is impossible to be entirely 'mechanistic' in modelling such a system. The physics model is only mechanistic in the sense that no equations were 'made up from scratch' - all were reproduced from existing theories and literature. However many of those concepts arose from empirical studies

themselves. In addition, the model was 'tweaked' to fit the data by adjusting the parameter k_w - it is highly unlikely that a model of a natural system will fit data without some degree of adjustment. It seems likely that the best possible model has not been discovered in this thesis, and may have complexity somewhere between the physics model and the simple models - for example, a model using the same ice layer solution of the physics model, but with all the heat flux calculations replaced with a simple equation in one input variable, air temperature.

However, the physics-based model in this thesis provides a good description of the response of lake ice to meteorological variables, at least at values close to those in 2003. If adapted the model may provide insight into larger scale responses of, for example, sea ice or continental ice sheets, but would require far more information to rule out extreme events; ice sheets may respond to climate change in a non-linear way, for example there may be thresholds which, once crossed, lead to unstable behaviour, sudden growth or collapse (Sugden 1991).

Finally, it is difficult to make any judgement on links between the physical and biological components of the Crooked Lake ecosystem without considerably more data collection and modelling work. Climate change effects on the water column can be inferred from lake ice models - lake water temperature will increase in proportion to air temperature, while radiation levels and wind-induced mixing will be greater due to reduction in ice cover. There may be little or no response of the organisms to increased light or temperatures if the main limiting factor is nutrients, but in a shallow lake, increased mixing may slightly increase nutrient concentrations by disturbing the lake bed. Whether any resulting change will be noticeable is difficult to answer - Stonehouse (1991) suggests that despite their relative simplicity, polar ecosystems are remarkably complex, and the air temperatures recorded by climatologists often bear only a superficial relationship to the microclimates experienced by organisms.

8.4 Ongoing and future work

There is considerable potential for current and future work to expand on the work presented in this thesis. This could involve further analysis of the Crooked Lake probe data or generalisation of models for use in other situations. For example, the effects of changing physical properties of ice such as roughness, albedo and opacity across the year have been mentioned, but could be further investigated in terms of their significance on larger scales, e.g. sea ice or continental ice sheets.

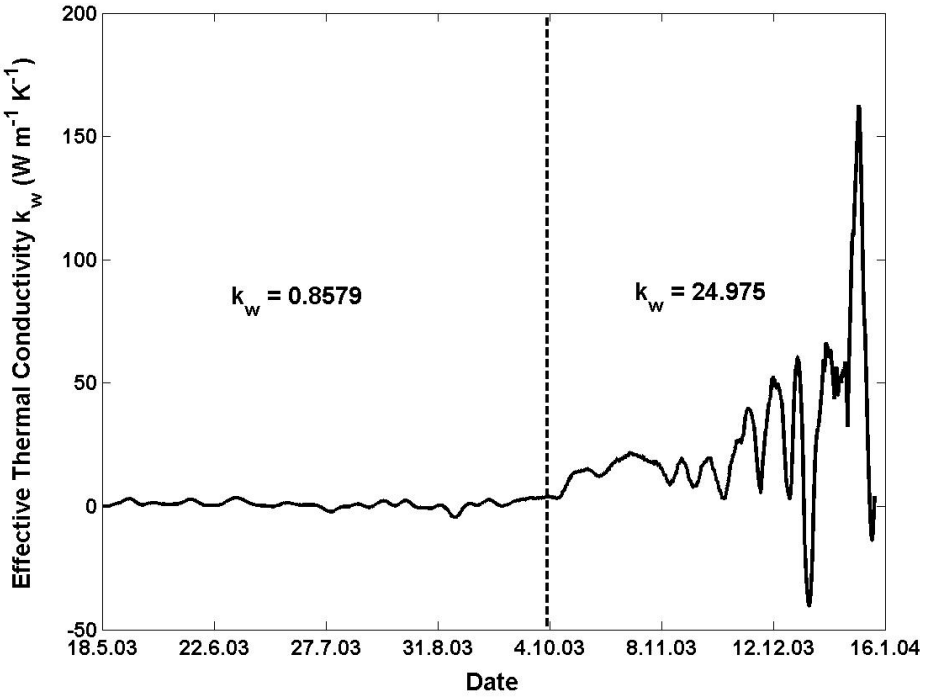

Figure 8.1: Effective conductivity k_w of water in Crooked Lake in 2003, calculated by Foster (2005, unpublished) using Equation 8.1. k_w was relatively constant with time up until October 1st (vertical dotted line), suggesting that the growing ice layer could be modelled using only the conductive fluxes at the ice bottom.

An analysis not reported in this thesis showed that imposing annual sinusoidal variation in these three physical parameters in place of constant values improved the goodness of fit to ice thickness data from $\chi^2 = 16$, $r^2 = 0.90$, $\nu = 2005$ to $\chi^2 = 8$, $r^2 = 0.95$, $\nu = 2002$ (Reid and Crout 2004).

The ice temperature data recorded by the Crooked Lake probe were acquired using thermistors separated by 5 cm on a profiling stick reaching from the air above the ice to the water below. This data has not been thoroughly investigated in this thesis, but can provide further insights into the physics of the ice layer. Current work by Foster (2005, unpublished) related to this project uses the data to calculate temperature gradients close to the ice-water boundary. This allows the ice layer to be modelled using only the conductive fluxes at the ice bottom:

$$\frac{dH_i}{dt} = \frac{1}{\rho_i L_f}\left(k_i \frac{dT_i}{dz} - k_w \frac{dT_w}{dz}\right) \tag{8.1}$$

where k_w is an 'effective conductivity' of water, i.e. the water is treated like a solid and sensible heat transfer due to fluid motion is not explicitly modelled.

This is analogous to Equation 3.61, but is a model in its own right with ice and water temperatures as the only input variables. Such an approach is consistent with Figure 4.8, which shows that the majority of melt and growth occurs at the ice bottom (using the ice temperature data effectively skips a stage in the physics model, such that surface fluxes need not be considered). On differentiating the ice thickness data to find $\frac{dH_i}{dt}$, Equation 8.1 can be solved to give values of k_w across 2003 (Figure 8.1). For the period from May to September (winter), k_w was relatively constant with a mean value of 0.86 W m^{-1} K^{-1}, which is of the same magnitude as values given in the literature (around 0.6 W m^{-1} K^{-1}). This implies that with a constant value of k_w, Equation 8.1 could be an accurate model of the ice layer for the winter period; indeed using a value of $k_w = 0.6$ the model fitted the winter ice thickness data with $r^2 = 0.8$. However, from October onwards the values of k_w become erratic, so the increased solar shortwave radiation or sensible heat from the water may be taking effect and the model loses its usefulness.

In terms of responses to climate change such a model is not useful without finding a quantitative link between ice temperature and air temperature, as is provided in the physics-based model in this thesis. However, it highlights an issue that should be taken into consideration when developing future equipment - a temperature measuring stick such as the one deployed may be all that is required for monitoring the state of an ice layer. As shown in this thesis, the effects of other atmospheric variables are considerably less significant than temperature. If carefully positioned a temperature profiling stick can measure air, ice and water temperatures, and ice thickness can be estimated by identifying discontinuities in the temperature profile at the top and bottom ice surfaces. In addition, thermistors are very inexpensive compared to other sensors, so it may be practical and affordable to have several measurement sites scattered across a lake, with wireless connection to a datalogger on dry land. This would allow observation of any existing horizontal variability in the ice.

With unlimited funds, other useful additions to an automatic probe would include micrometeorological sensors to directly measure sensible and latent heat flux, and profiles of humidity, temperature and wind speed on a fine scale near the surface, to build up a detailed picture of atmosphere-surface interactions. A fluorimeter in the water could provide regular measurements of chlorophyll concentrations and hence an indication of the primary productivity in the water column, allowing direct assessment of relationships between the physics and biology of the lake.

8.5 Final remarks

One of the most important observations in this thesis is that air temperature is the dominant variable in the dynamics of Antarctic lake ice, and therefore such ecosystems may be noticeably affected by global warming. Climate change is one of the greatest scientific and sociological challenges of the 21st century, and although this thesis has concentrated on a specific effect rather than causes, it is connected to some related ethical issues.

For example, with current data the only conclusion that can be made about the biological ecosystem in Crooked Lake is that it will change somehow with changing climate (whether or not we can identify the change), and that may be enough reason for concern. Warmer temperatures and less ice cover will be generally preferential for organisms in the Antarctic to flourish. However this may not be advantageous for the world as a whole. McKibben (1989) somewhat dramatically defines climate change as "the end of nature", or at least the end of "the thing that has, at least in modern times, defined nature for us - its separation from human society". If we are even slightly altering the life cycle of a bacteria in Antarctica, he may be right.

Working in Antarctica presents its own moral dilemmas. Are the results one may obtain worth the inevitable human impact of going there and setting up a research base? It is difficult for a scientist to avoid hypocrisy on this issue, but the spirit of exploration is an inevitable human trait. In the long term it could be argued that any direct human impact will be very small compared to climate change. The aesthetic quality of Antarctica can be cited as another reason why we shouldn't alter it, but in the anthropocentric worldview there may be no point in such beauty if no-one goes there to observe it.

Since the concept of climate change first arose, the most significant question has been over the amount that can be attributed to human activity. The issue of identifying significant change in the face of natural variability is highly complex. Scientists are faced with a dilemma whereby they must present their work with adequate statistics, which can be easily misinterpreted by policymakers and the public to under-represent the scale of the problem. The concept of modelling exemplifies this problem, if (as in this thesis) scientists must always confess that theirs is only one of several possible explanations. It is rare to find a model that is so convincing it becomes part of any 'standard model'. Sir Martin Rees, the current Astronomer Royal, claims that Newton (arguably one of the scientific world's first great 'modellers') was lucky to find, in planetary orbits, one of the

few aspects of nature that is highly predictable (Rees 2001). He therefore warns against scientific 'triumphalism', wherein one may exaggerate how much we can ever really understand of nature's intricacies. Modern tools such as model selection criteria are attempts to introduce objective quantities that measure the limitations of our knowledge, and it could be argued that failure to use proper model tests is akin to failing to use replicates in scientific fieldwork (Stapleton 2004).

With model testing now focussing on the best choice between several explanations, one may conclude that any hopes of stumbling across a 'true model' of nature have been all but abandoned. George Box's famous claim that "All models are wrong, but some are useful" is a good maxim. The idea of being 'close enough for all practical purposes' may at least satisfy some engineers, but if it seems disheartening to some of the more idealistic scientists among us, it may be necessary to turn to the wisdom of a poet for inspiration:

> All nature is but art, unknown to thee;
> All chance, direction, which thou canst not see.
>
> *- from "An Essay on Man" (1733-34)*
> *by Alexander Pope*

References

AHRENS C.D. (1994) *Meteorology today: an introduction to weather, climate, and the environment.* West Publishing Company, St. Paul, MN, U.S.A.

ANDREAS E.L. (1986) A theory for the scalar roughness and the scalar transfer coefficients over snow and sea ice. *Boundary-Layer Meteorology* 38, 159-184.

ANDREAS E.L. (1996) *The atmospheric boundary layer over polar marine surfaces.* Cold Regions Research and Engineering Laboratory, U.S. Army Corps of Engineers, Hanover, NH, U.S.A.

ANDREAS E.L. (2002) Parameterizing scalar transfer over snow and ice: a review. *Journal of Hydrometeorology* 3, 417-432.

ANDREAS E.L. and MAKSHTAS A.P. (1985) Energy exchange over Antarctic sea ice in the spring. *Journal of Geophysical Research* 90, 7199-7212.

ANTARCTIC AND SOUTHERN OCEAN COALITION (1998) *Why protect Antarctica?* Factsheet online at http://www.asoc.org/general/whyprotect.htm

BAK P. (1997) *How nature works: the science of self-organized criticality.* Oxford University Press, Oxford, U.K.

BANKE E.G., SMITH S.D. and ANDERSON R.J. (1980) Drag coefficient at AIDJEX from sonic anemometer measurement. In: *Sea-ice processes and models*, pp. 430-442 (Ed. R.S. Pritchard) University of Washington Press, Seattle, U.S.A.

BAYLISS P., ELLIS-EVANS J.C. and LAYBOURN-PARRY J. (1997) Temporal patterns of primary production in a large ultra- oligotrophic Antarctic freshwater lake. *Polar Biology* 18, 363-370.

BENNETT T.J. (1982) A coupled atmosphere-sea-ice model study of the role of sea ice in climatic predictability. *Journal of Atmospheric Science* 39, 1456-1465.

BETY J., GAUTHIER G., GIROUX J.F. and KORPIMAKI E. (2001) Are goose nesting success and lemming cycles linked? Interplay between nest density and predators. *Oikos* 93, 388-400.

BITZ C.M. and LIPSCOMB W.H. (1999) An energy-conserving thermodynamic model of sea ice. *Journal of Geophysical Research* 104, 15669-15677.

BLOMQVIST S., HOLMGREN N., AKESSON S., HEDENSTROM A. and PETTERSON J. (2002) Indirect effects of lemming cycles on sandpiper dynamics: 50 years of counts from southern Sweden. *Oecologia* 133, 146-158.

BOHMER L. and HILDEBRANDT G. (1998) Variance analysis of bacterial counts in milk 1. Communication: characterization of total variance and the components of variance random sampling error, methodical error and variation between parallel errors during storage. *Berliner und Munchener Tierarztliche Wochenschrift* 111(1), 13-20.

BROWNE M.W. (2000) Cross-validation methods. *Journal of Mathematical Psychology* 44, 108-132.

BRUNT D. (1932) Notes on radiation in the atmosphere. *Quarterly Journal of the Royal Meteorological Society* 58, 389-420.

CAMPBELL J.W. and AARUP T. (1989) Photosynthetically available radiation at high-latitudes. *Limnology and Oceanography* 34, 1490-1499.

CHENG B. (2002) *On the modelling of sea ice thermodynamics and air-ice coupling in the Bohai Sea and the Baltic Sea.* PhD thesis, Finnish Institute of Marine Research, Helsinki, Finland.

CHENG B. and LAUNIAINEN J. (1998) A one-dimensional thermodynamic air-ice-water model: technical and algorithm description report. *Report Series of the Finnish Institute of Marine Research* 37, 15-35.

CHENG B., LAUNIAINEN J., VIHMA T. and UOTILA J. (2001) Modelling sea-ice thermodynamics in BALTEX-BASIS. *Annals of Glaciology* 33, 243-247.

COOK A.J., FOX A.J., VAUGHAN D.G. and FERRIGNO J.G. (2005) Retreating glacier fronts on the Antarctic Peninsula over the past half-century. *Science* 308(5721), 541-544.

DAWKINS R. (1986) *The blind watchmaker: why the evidence of evolution reveals a universe without design.* Penguin, London, UK.

DE LA MARE W.K. (1997) Abrupt mid-twentieth-century decline in Antarctic sea-ice extent from whaling records. *Nature* 389(6646), 57-60.

DENBY B. and SNELLEN H. (2002) A comparison of surface renewal theory with the observed roughness lengths for temperature on a melting glacier surface. *Boundary-Layer Meteorology* 103, 459-468.

DRAKE F. (2000) *Global warming: the science of climate change.* Oxford University Press, Oxford, UK.

EDWARDS A.M. (2001) Adding detritus to a nutrient-phytoplankton-zooplankton model: a dynamical-systems approach. *Journal of Plankton Research* 23, 389-413.

EDWARDS A.M. and BEES M.A. (2001) Generic dynamics of a simple plankton population model with a non-integer exponent of closure. *Chaos Solitons & Fractals* 12, 289-300.

EDWARDS A.M. and BRINDLEY J. (1999) Zooplankton mortality and the dynamical behaviour of plankton population models. *Bulletin of Mathematical Biology* 61, 303-339.

EFIMOVA N.A. (1961) On methods of calculating monthly values of net longwave radiation. *Meteorol. Gidrol.* 10, 28-33.

ELTON C. and NICHOLSON M. (1942) The ten year cycle in numbers of the Lynx in Canada. *Journal of Animal Ecology* 11, 215-244.

FANG X., ELLIS C.R. and STEFAN H.G. (1996) Simulation and observation of ice formation (freeze-over) in a lake. *Cold Regions Science and Technology* 24, 129-145.

FANG X. and STEFAN H.G. (1996) Long-term lake water temperature and ice cover simulations/measurements. *Cold Regions Science and Technology* 24, 289-304.

FLEMING R.A., BARCLAY H.J. and CANDAU J.N. (2002) Scaling-up an autoregressive time-series model (of spruce budworm population dynamics) changes its qualitative behavior. *Ecological Modelling* 149, 127-142.

FOSTER M. (2005) Personal communications.

FRENOT Y., CHOWN S.L., WHINAM J., SELKIRK P.M., CONVEY P., SKOT-

NICKI M. and BERGSTROM D.M. (2005) Biological invasions in the Antarctic: extent, impacts and implications. *Biological Reviews* 80(1), 45-72.

FRITSEN C.H. and PRISCU J.C. (1999) Seasonal change in the optical properties of the permanent ice cover on Lake Bonney, Antarctica: consequences for lake productivity and phytoplankton dynamics. *Limnology and Oceanography* 44(2), 447-454.

GAMARRA J.G.P., SOLE R.V. (2000) Bifurcations and chaos in ecology: lynx returns revisited. *Ecology Letters* 3, 114-121.

GILL A.E. (1982) *Atmosphere-ocean dynamics.* Academic Press, Inc. (London) Ltd., London, U.K.

GRENFELL T.C. and MAYKUT G.A. (1977) The optical properties of ice and snow in the Arctic Basin. *Journal of Glaciology* 18, 445-463.

GRÜNWALD P. (2000) Model selection based on minimum description length. *Journal of Mathematical Psychology* 44, 133-152.

GUEST P.S. (1998) Surface longwave radiation conditions in the eastern Weddell Sea during winter. *Journal of Geophysical Research* 103(C13), 30761-30771.

HANDORF D., FOKEN T. and KOTTMEIER C. (1999) The stable atmospheric boundary layer over an Antarctic ice sheet. *Boundary-Layer Meteorology* 91, 165-189.

HANSKI I., HENTTONEN H., KORPIMAKI E., OKSANEN L. and TURCHIN P. (2001) Small-rodent dynamics and predation. *Ecology* 82, 1505-1520.

HART D.R. (2002) Intraguild predation, invertebrate predators, and trophic cascades in lake food webs. *Journal of Theoretical Biology* 218, 111-128.

HART J.D. and LEE C.L. (2005) Robustness of one-sided cross-validation to autocorrelation. *Journal of Multivariate Analysis* 92, 77-96.

HENNEMAN H.E. and STEFAN H.G. (1999) Albedo models for snow and ice on a freshwater lake. *Cold Regions Science and Technology* 29, 31-48.

HENSHAW T. (2001) *Seasonal microbial dynamics in two ultra-oligotrophic Antarctic freshwater lakes.* PhD thesis, The University of Nottingham, Nottingham, U.K.

HENSHAW T. and LAYBOURN-PARRY J. (2002) The annual patterns of photosynthesis in two large, freshwater, ultra-oligotrophic Antarctic lakes. *Polar Biology* 25(10), 744-752.

HOLLAND J. (1999) *Emergence: From Chaos to Order.* Perseus Books, Philadelphia, U.S.A.

HOLLAND D.M. and JENKINS A. (1999) Modeling thermodynamic ice-ocean interactions at the base of an ice shelf. *Journal of Physical Oceanography* 29, 1787-1801.

HOLT R.D. and POLIS G.A. (1997) A theoretical framework for intraguild predation. *American Naturalist* 149, 745-764.

HORNBERGER G.M. and SPEAR R.C. (1981) An approach to the preliminary analysis of environmental systems. *Journal of Environmental Management* 12, 7-18.

HOWARD-WILLIAMS C., SCHWARZ A.M., HAWES I. and PRISCU J.C. (1998) Optical properties of the McMurdo dry valley lakes, Antarctica. In: *Ecosystem dynamics in a polar desert: the McMurdo Dry Valleys, Antarctica*, pp. 189-203 (Ed. J.C. Priscu) Antarctic Research Series 72, American Geophysical Union, Washington, D.C., U.S.A.

HUISMAN J. and WEISSING F.J. (1999) Biodiversity of plankton by species oscillations and chaos. *Nature* 402, 407-410.

HUISMAN J. and WEISSING F.J. (2001) Biological conditions for oscillations and chaos generated by multispecies competition. *Ecology* 82, 2682-2695.

INTERGOVERNMENTAL PANEL ON CLIMATE CHANGE (2001) *Climate change 2001: the scientific basis: contribution of Working Group I to the third assessment report of the Intergovernmental Panel on Climate Change.* Cambridge University Press, Cambridge, UK.

JACOBS J.D. (1978) Radiation climate of Broughton Island. In: *Energy budget studies in relation to fast-ice breakup processes in Davis Strait: occasional paper 26*, pp. 105-120 (Eds. R.G. Barry and J.D. Jacobs) Institute of Arctic and Alpine Research, The University of Colorado, Boulder, CO, U.S.A.

JENSEN A.L. and MILLER D.H. (2001) Age structured matrix predation model for the dynamics of wolf and deer populations. *Ecological Modelling* 141, 299-305.

KADANE J.B. and LAZAR N.A. (2004) Methods and criteria for model selection. *Journal of the American Statistical Association* 99(465), 279-290.

KARENTZ D. and BOSCH I. (2001) Influence of ozone-related increases in ultraviolet radiation on Antarctic marine organisms. *American Zoologist* 41, 3-16.

KENDALL B.E. (2001) Cycles, chaos, and noise in predator-prey dynamics. *Chaos Solitons & Fractals* 12, 321-332.

KEY J.R., SILCOX R.A. and STONE R.S. (1996) Evaluation of surface radiative flux parameterisations for use in sea ice models. *Journal of Geophysical Research* 101(C2), 3839-3849.

KIRK J.T.O. (1986) *Light and photosynthesis in aquatic ecosystems.* Cambridge University Press, Cambridge, U.K.

KÖNIG-LANGLO G. and AUGSTEIN E. (1994) Parameterization of the downward long-wave radiation at the Earth's surface in polar regions. *Meteorologische Zeitschrift* 3, 343-347.

LAUNIAINEN J. and CHENG B. (1998) Modelling of ice thermodynamics in natural water bodies. *Cold Regions Science and Technology* 27, 153-178.

LAYBOURN-PARRY J. and BAYLISS P. (1996) Seasonal dynamics of the planktonic community in Lake Druzhby, Princess Elizabeth Land, Eastern Antarctica. *Freshwater Biology* 35, 57-67.

LAYBOURN-PARRY J., BAYLISS P. and ELLIS-EVANS J.C. (1995) The dynamics of heterotrophic nanoflagellates and bacterioplankton in a large ultra-oligotrophic Antarctic lake. *Journal of Plankton Research* 17, 1835-1850.

LAYBOURN-PARRY J., HENSHAW T., JONES D.J. and QUAYLE W. (2004) Bacterioplankton production in freshwater Antarctic lakes. *Freshwater Biology* 49, 735-744.

LAYBOURN-PARRY J., HOFER J.S. and SOMMARUGA R. (2001) Viruses in the plankton of freshwater and saline Antarctic lakes. *Freshwater Biology* 46, 1279-1287.

LAYBOURN-PARRY J. and MARCHANT H.J. (1992) Daphniopsis-studeri (Crustacea, Cladocera) in lakes of the Vestfold-Hills, Antarctica. *Polar Biology* 11, 631-635.

LAYBOURN-PARRY J., MARCHANT H.J. and BROWN P.E. (1991) The plankton of a large oligotrophic freshwater Antarctic lake. *Journal of Plankton Research* 13, 1137-1149.

LAYBOURN-PARRY J., MARCHANT H.J. and BROWN P.E. (1992) Seasonal cycle of the microbial plankton in Crooked Lake, Antarctica. *Polar Biology* 12, 411-416.

LAYBOURN-PARRY J. and PARRY J. (2000) Flagellates and the microbial loop. In: *The flagellates - unity, diversity and evolution*, pp. 216-239 (Eds. B.S.C Leadbetter and J.C. Green) Taylor and Francis Ltd., London, U.K.

LETELLIER C., AGUIRRE L.A., MAQUET J. and AZIZ-ALAOUI M.A. (2002) Should all the species of a food chain be counted to investigate the global dynamics? *Chaos Solitons & Fractals* 13, 1099-1113.

LUMB F.E. (1964) The influence of cloud on hourly amounts of total radiation on the sea surface. *Quarterly Journal of the Royal Meteorological Society* 90, 43-56.

MAGNUSSON J.J., ROBERTSON D.M., BENSON B.J., WYNNE R.H., LIVINGSTONE D.M., ARAI T., ASSEL R.A., BARRY R.G., CARD V., KUUSISTO E., GRANIN N.G., PROWSE T.D., STEWART K.M. and VUGLINSKI V.S. (2000) Historical trends in lake and river ice cover in the Northern Hemisphere. *Science* 289(5485), 1743-1746.

MAKSHTAS A.P., ANDREAS E.L., SVYASHCHENNIKOV P.N. and TIMACHEV V.F. (1999) Accounting for clouds in sea ice models. *Atmospheric Research* 52, 77-113.

MALCHOW H., PETROVSKII S. and MEDVINSKY A. (2001) Pattern formation in models of plankton dynamics. A synthesis. *Oceanologica Acta* 24, 479-487.

MASON R.L., GUNST R.F. and HESS J.L. (2003) *Statistical design and analysis of experiments: with applications to engineering and science (2nd edition).* Wiley, Hoboken, N.J., U.S.A.

MAYKUT G.A. and CHURCH P.E. (1973) Radiation climate of Barrow, Alaska. *Journal of Applied Meteorology* 12, 620-628.

MAYKUT G.A. and UNTERSTEINER N. (1971) Some results from a time dependent thermodynamic model of sea-ice. *Journal of Geophysical Research* 76(6), 1550-1575.

MCCANN K., HASTINGS A. and HUXEL G.R. (1998) Weak trophic interactions and the balance of nature. *Nature* 395, 794-798.

MCKAY C.P., CLOW G.D., ANDERSEN D.T. and WHARTON R.A. (1994) Light transmission and reflection in perennially ice-covered Lake Hoare, Antarctica. *Journal of Geophysical Research - Oceans* 99, 20427-20444.

MCKAY C.P., CLOW G.D., WHARTON R.A. and SQUYRES S.W. (1985) Thickness of ice on perennially frozen lakes. *Nature* 313, 561-562.

MCKIBBEN B. (1989) *The end of nature.* Random House, New York, U.S.A.

MCLAUGHLIN J.F., HELLMANN J.J., BOGGS C.L. and EHRLICH P.R. (2002) The route to extinction: population dynamics of a threatened butterfly. *Oecologia* 132, 538-548.

MOONEY D.D. and SWIFT R.J. (1999) *A course in mathematical modelling.* The Mathematical Association of America, U.S.A.

MORIN P. (1999) Productivity, intraguild predation, and population dynamics in experimental food webs. *Ecology* 80, 752-760.

MORITZ R.E. (1978) A model for estimating global solar radiation. In: *Energy budget studies in relation to fast-ice breakup processes in Davis Strait: occasional paper 26*, pp. 121-142 (Eds. R.G. Barry and J.D. Jacobs) Institute of Arctic and Alpine Research, The University of Colorado, Boulder, CO, U.S.A.

MYUNG I.J. (2000) The importance of complexity in model selection. *Journal of Mathematical Psychology* 44, 190-204.

NATIONAL RESEARCH COUNCIL (1999) *Global environmental change: research pathways for the next decade.* National Academy Press, Washington, D.C., U.S.A.

NIEMELA S.I. (2003) Measurement uncertainty of microbiological viable counts. *Accreditation and Quality Assurance* 8(12), 559-563.

NORRDAHL K. and KORPIMAKI E. (2000) Do predators limit the abundance of alternative prey? Experiments with vole-eating avian and mammalian predators. *Oikos* 91, 528-540.

NORRDAHL K. and KORPIMAKI E. (2002) Changes in individual quality during a 3-year population cycle of voles. *Oecologia* 130, 239-249.

PALETHORPE B., HAYES-GILL B., CROWE J., SUMNER M., CROUT N., FOSTER M., REID T., BENFORD S., GREENHALGH C. and LAYBOURN-PARRY J. (2004) Real time physical data acquisition through a remote sensing platform on a polar lake. *Limnology and Oceanography Methods* 2, 191-201.

PARKINSON C.L. and WASHINGTON W.M. (1979) A large-scale numerical model of sea ice. *Journal of Geophysical Research* 84(C1), 311-337.

PASCUAL M., ROY M., GUICHARD F. and FLIERL G. (2002) Cluster size distributions: signatures of self-organization in spatial ecologies. *Philosophical Transactions of the Royal Society of London Series B - Biological Sciences* 357, 657-666.

PEETERS F., LIVINGSTONE D.M., GOUDSMIT G.H., KIPFER R. and FORSTER R. (2002) Modeling 50 years of historical temperature profiles in a large central European lake. *Limnology and Oceanography* 47, 186-197.

PERES L.F. and DACAMARA C.C. (2004) Land surface temperature and emissivity estimation based on the two-temperature method: sensitivity analysis using simulated MSG/SEVIRI data. *Remote Sensing of Environment* 91(3-4), 377-389.

PEROVICH D.K. (2003) Complex yet translucent: The optical properties of sea ice. *Physica B - Condensed Matter* 338(1-4), 107-114.

PETROVSKII S.V. and MALCHOW H. (2001) Wave of chaos: New mechanism of pattern formation in spatio- temporal population dynamics. *Theoretical Population Biology* 59, 157-174.

PITT M.A. and MYUNG I.J. (2002) When a good fit can be bad. *Trends in Cognitive Science* 6(10), 421-425.

POLIS G.A. and HOLT R.D. (1992) Intraguild predation - the dynamics of complex trophic interactions. *Trends in Ecology and Evolution* 7, 151-154.

PRATA A.J. (1996) A new long-wave formula for estimating downward clear-sky radiation at the surface. *Quarterly Journal of the Royal Meteorological Society* 122, 1127-1151.

PRESS W.H., TEUKOLSKY S.A., VETTERLING W.T. and FLANNERY B.P. (2002) *Numerical recipes in C++ (2nd edition).* Cambridge University Press, Cambridge, U.K.

QUINN G.P. and KEOUGH M.J. (2002) *Experimental design and data analysis*

for biologists. Cambridge University Press, Cambridge, U.K.

RAE R. and VINCENT W.F. (1998) Effects of temperature and ultraviolet radiation on microbial foodweb structure: potential responses to global change. *Freshwater Biology* 40, 747-758.

RAFTERY A.E. and ZHENG Y. (2003) Discussion: performance of Bayesian model averaging. *Journal of the American Statistical Association* 98(464), 931-938.

REES M. (2001) *Just six numbers: the deep forces that shape the universe.* Basic Books, Abingdon, U.K.

REID T.D. and CROUT N.M.J. (2004) Selecting appropriate models of Antarctic lake ice dynamics. *Proceedings of the IASTED International Conference on Environmental Modelling and Simulation* Electronic paper 432-078.

REIJMER C.H., VAN MEIJGAARD E. and VAN DEN BROEKE M.R. (2004) Numerical studies with a regional atmospheric climate model based on changes in the roughness length for momentum and heat over Antarctica. *Boundary-Layer Meteorology* 111, 313-337.

REVILLA T. (2002) Effects of intraguild predation on resource competition. *Journal of Theoretical Biology* 214, 49-62.

RISSANEN J.J. (1996) Fisher information and stochastic complexity. *IEEE Transactions on Information Theory* 42(1), 40-47.

ROBERTS E.C., LAYBOURN-PARRY J., MCKNIGHT D.M. and NOVARINO G. (2000) Stratification and dynamics of microbial loop communities in Lake Fryxell, Antarctica. *Freshwater Biology* 44, 649-661.

SHINE K.P. (1984) Parameterization of shortwave flux over high albedo surfaces as a function of cloud thickness and surface albedo. *Quarterly Journal of the Royal Meteorological Society* 110, 747-764.

SHIRIHAI H. (2002) *The complete guide to Antarctic wildlife: birds and marine mammals of the Antarctic continent and the Southern Ocean.* Princeton University Press, Princeton, U.S.A.

SMITH G.D. (1985) *Numerical solution of partial differential equations: finite difference methods.* Oxford University Press, Oxford, U.K.

SMITH J.T. and ELDER D.G. (1999) A comparison of models for characterizing the distribution of radionucleides with depth in soil. *European Journal of Soil Science* 50, 295-307.

SOLE R.V., MANRUBIA S.C., BENTON M., KAUFFMAN S. and BAK P. (1999) Criticality and scaling in evolutionary ecology. *Trends in Ecology and Evolution* 14, 156-160.

STAPLETON L. (2004) *Modelling Carbon and Nitrogen fluxes for two terrestrial ecosystems on Svalbard.* PhD thesis, The University of Nottingham, Nottingham, U.K.

STEELE J.H. and HENDERSON E.W. (1981) A simple plankton model. *American Naturalist* 117, 676-691.

STONEHOUSE B. (1991) Polar ecosystems, management and climate modelling. In: *Antarctica and global climate change*, pp. 147-154 (Eds. C.M. Harris and B. Stonehouse) Belhaven Press, London, U.K.

TETENS, O. (1930) Uber einige meteorologische Begriffe. *Zeitschrift fur Geophysik* 6, 297.

TRATHAN P.N., CROXALL J.P. and MURPHY E.J. (1996) Dynamics of Antarctic penguin populations in relation to interannual variability in sea ice distribution. *Polar Biology* 16(5), 321-330.

TURCHIN P. and HANSKI I. (2001) Contrasting alternative hypotheses about rodent cycles by translating them into parameterized models. *Ecology Letters* 4, 267-276.

TURCHIN P., OKSANEN L., EKERHOLM P., OKSANEN T. and HENTTONEN H. (2000) Are lemmings prey or predators? *Nature* 405, 562-565.

VINCENT W.F., LAURION I. and PIENITZ R. (1998) Arctic and Antarctic lakes as optical indicators of global change. *Annals of Glaciology* 27, 691-696.

VINCENT W.F., RAE R., LAURION I., HOWARD-WILLIAMS C. and PRISCU J.C. (1998) Transparency of Antarctic ice-covered lakes to solar UV radiation. *Limnology and Oceanography* 43(4), 618-624.

WADHAMS P. (1991) Atmosphere-ice-ocean interactions in the Antarctic. In: *Antarctica and global climate change*, pp. 65-81 (Eds. C.M. Harris and B. Stonehouse) Belhaven Press, London, U.K.

WANGBERG S.A., SELMER J.S. and GUSTAVSON K. (1998) Effects of UV-B radiation on carbon and nutrient dynamics in marine plankton communities. *Journal of Photochemistry and Photobiology B - Biology* 45, 19-24.

WASSERMAN L. (2000) Bayesian model selection and model averaging. *Journal of Mathematical Psychology* 44, 92-107.

WETTLAUFER J.S. (1999) Ice surfaces: macroscopic effects of microscopic structure. *Philosophical Transactions of the Royal Society of London Series A - Mathematical Physical and Engineering Sciences* 357, 3403-3425.

WHARTON JR. R.A., MCKAY C.P., CLOW G.D., ANDERSEN D.T., SIMMONS JR. G.M. and LOVE F.G. (1992) Changes in ice cover thickness and lake level of Lake Hoare, Antarctica: implications for local climatic change. *Journal of Geophysical Research* 97, 3503-3513.

YOUNG P. (1998) Data-based mechanistic modelling of environmental, ecological, economic and engineering systems. *Environmental Modelling and Software* 13, 105-122.

ZILLMAN J.W. (1972) *A study of some aspects of the radiation and heat budgets of the southern hemisphere oceans.* Meteorological Studies Report 26, Bureau of Meteorology, Department of the Interior, Canberra, Australia.